

# ACI CRC 2019 P0027: Effective Characterization of Recycled Concrete Aggregate (RCA) for Concrete Applications

Final Report

May 4, 2022

**PI: Jiong Hu**

*Associate Professor*

*University of Nebraska-Lincoln*

*Ph. 402.937.2863 | E. [jhu5@unl.edu](mailto:jhu5@unl.edu)*

**Co-PI: Tara Cavalline**

*Associate Professor*

*University of North Carolina Charlotte*

*Ph. 704.687.5035 | E. [tcavalline@uncc.edu](mailto:tcavalline@uncc.edu)*

**Miras Mamirov**

*Graduate Research Assistant*

*University of Nebraska-Lincoln*

**Arindam Dey**

*Graduate Research Assistant*

*University of North Carolina Charlotte*



University of Nebraska-  
Lincoln  
1400 R St, Lincoln, NE 68588



UNC CHARLOTTE

University of North  
Carolina at Charlotte  
9201 University City Blvd,  
Charlotte, NC 28223



ACI Foundation  
38800 Country Club Drive  
Farmington Hills, MI  
48331USA

# TABLE OF CONTENTS

List of Figures .....	v
List of Tables .....	viii
EXECUTIVE SUMMARY .....	xi
ACKNOWLEDGEMENTS .....	xii
CHAPTER 1. Introduction .....	1
1.1 Background .....	1
1.2 Research Significance and Methodology .....	3
1.3 Organization of Report .....	3
CHAPTER 2. Literature review .....	4
2.1 RCA Production .....	4
2.2 RCA Characteristics .....	6
2.2.1 Residual mortar content .....	6
2.2.2 Physical and mechanical properties .....	7
2.2.3 Chemical composition .....	10
2.2.4 Potential contaminants .....	10
2.3 Test Methods .....	10
2.3.1 Geometrical properties .....	11
2.3.2 Physical and mechanical properties .....	13
2.3.3 Chemical compositions .....	20
2.4 RCA Specifications .....	23
2.4.1 United States .....	23
2.4.2 State Departments of Transportation (DOT) .....	24
2.4.3 Japan .....	25
2.4.4 RILEM .....	25
2.4.5 Germany .....	26
2.4.6 Other countries .....	26
2.5 Recycled aggregate concrete mix design methodologies .....	27
2.5.1 Direct replacement methods .....	27
2.5.2 Methods that consider RCA as a two-phase material .....	28
2.5.3 Particle packing methods .....	29
2.5.4 Empirical (experimental) methods .....	29

CHAPTER 3. Experimental program .....	30
3.1 Aggregates Collection.....	30
3.2 Test methods for aggregates .....	31
3.2.1 Specific gravity and absorption .....	32
3.2.2 Void content.....	33
3.2.3 Shape and texture .....	33
3.2.4 Aggregate crushing value .....	36
3.2.5 Residual mortar content .....	40
3.2.6 Freeze-thaw resistance .....	49
3.2.7 Handheld XRF for chemical characterization.....	51
3.3 Test methods for concrete.....	62
3.3.1 Fresh concrete properties .....	62
3.3.2 Specimen casting and curing .....	64
3.3.3 Hardened concrete properties .....	64
3.3.4 Durability tests .....	65
CHAPTER 4. RCA characteristics .....	67
4.1 Residual Mortar Content.....	67
4.2 Physical and Mechanical Properties .....	70
4.2.1 Specific gravity and absorption .....	70
4.2.2 Aggregate crushing value .....	73
4.2.3 Freeze-thaw resistance .....	74
4.2.4 Shape and surface texture .....	76
4.2.5 Void content.....	80
4.2.6 Absorption rate.....	81
4.3 Chemical compositions .....	83
4.3.1 Control Sample .....	83
4.3.2 Statistical analysis to determine optimal particle size for PHXRF characterization of RCA .....	86
4.3.3 Development of models to predict mortar content using PHXRF .....	92
4.3.4 Prediction of the chemical composition of RCA using PHXRF data.....	97
4.3.5 Recommendation for particle size for PHXRF analysis .....	99
4.3.6 Summary, limitations, and recommendations for future work of PHXRF .....	100
4.4 Summary .....	103

CHAPTER 5. Concrete MixTure Design and Results .....	104
5.1 Mixture design and concrete performance based on RCA geometry and gradation .....	104
5.1.1 Testing matrix development .....	104
5.1.2 Mixture proportions .....	107
5.1.3 Results.....	108
5.2 Mixture design nomograph development based on RCA mechanical properties .....	118
5.2.1 Testing matrix development .....	119
5.2.2 Mixture proportions .....	119
5.2.3 Results.....	120
CHAPTER 6. Conclusions and Recommendation for Future Work.....	131
6.1 Conclusions.....	131
6.2 Recommendations for future studies .....	132
References .....	133
Appendix A. Details Summary of NA and RCA Characteristics .....	147
Appendix B. Details of Statistical Analysis from PHXRF Results .....	150
Appendix C. Recommended Test Method with PHXRF .....	162
Appendix D. Use of the Mixture design nomograph.....	166

## List of Figures

Figure 1 Different types of crushers (Hiller et al. 2011).....	5
Figure 2 Interfacial transition zone in RCA (Verian et al. 2018) .....	7
Figure 3 Particle size vs RMSD % curve (Cerato et al. 2017) .....	22
Figure 4 Aggregate identification .....	30
Figure 5 Images of collected RCA specimens .....	31
Figure 6 Aggregate absorption rate test setup.....	33
Figure 7 Aggregate Image Measurement System setup .....	34
Figure 8 Aggregate angularity rankings (adapted from the AIMS2 Manual) .....	34
Figure 9 Aggregate texture rankings (adopted from AIMS2 Manual) .....	35
Figure 10 Displacement of RCA samples at different procedures .....	38
Figure 11 Displacement comparison for different RCA sizes during crushing value test.....	39
Figure 12 Aggregate crushing value test setup .....	40
Figure 13 Example of RCA mortar disintegration after temperature shock .....	41
Figure 14. RMC measurement by thermal shock method .....	43
Figure 15 Residual mortar removal over grinding time.....	44
Figure 16 Aggregate surface texture change over grinding time.....	46
Figure 17 Effect of grinding on RCA texture .....	46
Figure 18 Effect of thermal shock and grinding on the material loss of NA.....	47
Figure 19 Impact of soaking water amount on the residual mortar removal rate .....	48
Figure 20 Example of natural aggregate becoming too brittle .....	48
Figure 21 FT resistance of aggregates test setup .....	50
Figure 22 Approach utilized to evaluate accuracy and precision of PHXRF for chemical characterization of RCA .....	52
Figure 23 Bruker Tracer III-SD PHXRF .....	55
Figure 24 PHXRF sample preparation.....	56
Figure 25 Quadrant scanning technique .....	57
Figure 26 Sample cup dimension.....	59
Figure 27 PHXRF connected to a vacuum pump .....	61
Figure 28 Yellow filter for trace element analysis .....	62
Figure 29 Slump test setup.....	62

Figure 30 Type B air meter (pressure meter).....	63
Figure 31 Box Test setup .....	64
Figure 32 Compressive strength test setup .....	64
Figure 33 Static modulus of elasticity test setup .....	65
Figure 34 Resistivity test setup .....	66
Figure 35 Length comparator used for shrinkage measurement.....	66
Figure 36 Variation of RMC with source .....	68
Figure 37 Relationship between ACV and residual mortar content .....	70
Figure 38 Correlation between absorption and specific gravity, and other RCA characteristics .	72
Figure 39 Variation of ACV with source.....	73
Figure 40 Total freeze-thaw mass loss comparison.....	75
Figure 41 Percentages of residual mortar loss comparison .....	76
Figure 42 RM loss-to-ACV ratio comparison .....	76
Figure 43 Variation of angularity with source.....	77
Figure 44 Variation of surface texture with source .....	78
Figure 45 Variation of flat and elongated particles with source.....	79
Figure 46 Effect of shape and texture parameters on particle packing.....	81
Figure 47 Relative absorption rate over time.....	82
Figure 48 Absolute absorption rate over time.....	83
Figure 49 Sieve size vs. RMSD (NC_AP1 RCA sample-major and trace elements .....	90
Figure 50 Sieve size vs. RMSD (NC_CT1 RCA sample-major and trace elements).....	90
Figure 51 Sieve size vs. RMSD (NC_HW1 RCA sample-major and trace elements) .....	91
Figure 52 Sieve size vs. RMSD (NC_CT2 RCA sample-major and trace elements).....	91
Figure 53 Proposed mixture design procedure for pavement concrete by Mamirov et al. (2021) .....	105
Figure 54 Theoretical packing degrees from the Modified Toufar Model .....	106
Figure 55 Correlation between theoretical and experimental packing degrees of optimum blends .....	107
Figure 56 Mix identification system.....	108
Figure 57 Box test results .....	110
Figure 58 Compressive strength results.....	112

Figure 59 Splitting tensile strength results.....	113
Figure 60 Example of visual examination of fractured surface.....	114
Figure 61 Relationship between the percentage of fractured aggregates and aggregate ACV...	114
Figure 62 Elastic modulus and Poisson's ratio results.....	115
Figure 63 Results from resistivity test .....	116
Figure 64 Results from drying shrinkage tests .....	117
Figure 65 Effect of concrete mixture design and RCA ACV on compressive strength of concrete .....	123
Figure 66 Effect of concrete mixture design and RCA ACV on splitting tensile strength of concrete .....	125
Figure 67 Effect of concrete mixture design and RCA ACV on modulus of elasticity of concrete .....	127
Figure 68 Effect of concrete mixture design and RCA ACV on surface resistivity of concrete	128
Figure 69 Developed nomograph with different aggregate .....	130
Figure 70 Example of utilizing the developed nomograph.....	166

## LIST OF TABLES

Table 1. Summary of key RCA characteristics.....	11
Table 2. Summary of residual mortar measurement tests through mortar disintegration.....	18
Table 3. Physical properties criteria of RCA per AASHTO M 43 .....	24
Table 4. Summary of deleterious substances criteria of RCA per AASHTO MP16.....	24
Table 5 Summary of RCA criteria for different classes per JIS 5021-5023 .....	25
Table 6 Summary of RCA criteria for different types per RILEM TC 121-DRG.....	26
Table 7 Summary of RCA criteria for different types per DIN 4226-100.....	26
Table 8 Summary of RCA criteria for different types/classes .....	27
Table 9 Sources and information of collected RCA specimens .....	30
Table 10 Proposed tests for RCA characteristics.....	32
Table 11 Summary of the procedure comparison for crushing value test .....	37
Table 12 Vibration time requirement for separating crushed RCA samples. ....	38
Table 13 Residual mortar removal at different heating temperatures.....	44
Table 14 Major elements and trace elements quantified by the PHXRF for this study.....	57
Table 15 Mudrock/Ceramic analysis depth (from Bruker).....	58
Table 16 Effects of particle size on XRF STDEV, $COV_{stdev}$ , RMSD, $COV_{RMSD}$ .....	60
Table 17 Instrument settings .....	60
Table 18 Linear regression analysis summary for RMC prediction .....	68
Table 19 Linear regression analysis summary for ACV prediction .....	74
Table 20 Element weight % obtained via whole rock analysis .....	84
Table 21 Control sample Composition .....	85
Table 22 Average element concentrations in weight % from PHXRF .....	85
Table 23 ANOVA test for RCA samples- No.4, No.12, No.50.....	87
Table 24 ANOVA test for NC_API1/NC_CT1/NC_CT2/NC_HW1 RCA sample- No.4, No.12 & No.50.....	88
Table 25 Regression equations for No. 4, No. 12, No. 50 .....	93
Table 26 Percent difference between predicted and actual mortar content for No.4 size .....	94
Table 27 Percent difference between predicted and actual mortar content for No.12 size .....	94
Table 28 Percent difference between predicted and actual mortar content for No.50 size .....	94
Table 29 Average element concentrations in weight % from PHXRF .....	95



Table 30 Model to predict mortar content using No. 4 PHXRF data from seven sources .....	96
Table 31 Percent difference between predicted and actual mortar content for No. 4 size using improved model .....	97
Table 32 $R^2$ values for major and trace elements.....	99
Table 33 Summary of theoretical and experimental packing degrees of different aggregate blends .....	107
Table 34 Mixture proportions based on RCA geometry and gradation.....	108
Table 35 Fresh concrete properties .....	109
Table 36 Summary of factors affecting concrete compressive strength .....	112
Table 37 Estimated % of fractured aggregates along the fracture surface .....	114
Table 38 Expansion of samples during the curing period.....	118
Table 39 Selected aggregates for mixture design nomograph development .....	119
Table 40 Mixture design for mixture adjustment study.....	120
Table 41 Fresh concrete properties of mixtures in mixture adjustment.....	121
Table 42 Influence of w/c, ACV, and cement content on concrete mechanical properties and surface resistivity .....	129
Table 43 Summary of NA and RCA characteristics.....	147
Table 44 Standard deviation, $COV_{STD\ DEV}$ , RMSD & $COV_{RMSD}$ values for No.4 NC_AP1 sample .....	150
Table 45 Standard deviation, $COV_{STD\ DEV}$ , RMSD & $COV_{RMSD}$ Values for No.12 NC_AP1 RCA sample .....	151
Table 46 Standard Deviation, $COV_{STD\ DEV}$ , RMSD & $COV_{RMSD}$ Values for No.50 NC_AP1 RCA sample.....	152
Table 47 Standard Deviation, $COV_{STD\ DEV}$ , RMSD & $COV_{RMSD}$ Values for No.4 NC_CT1 sample .....	153
Table 48 Standard deviation, $COV_{STD\ DEV}$ , RMSD & $COV_{RMSD}$ values for No.12 NC_CT1 RCA sample .....	154
Table 49 Standard deviation, $COV_{STD\ DEV}$ , RMSD & $COV_{RMSD}$ values for No.50 NC_CT1 RCA sample .....	155
Table 50 Standard deviation, $COV_{STD\ DEV}$ , RMSD & $COV_{RMSD}$ values for No.4 NC_HW1....	156
Table 51 Standard deviation, $COV_{STD\ DEV}$ , RMSD & $COV_{RMSD}$ values for No.12 NC_HW1..	157

Table 52 Standard deviation,  $COV_{STD\ DEV}$ , RMSD &  $COV_{RMSD}$  values for No.50 NC\_HW1.. 158

Table 53 Standard deviation,  $COV_{STD\ DEV}$ , RMSD &  $COV_{RMSD}$  values for No.4 NC\_CT2 ..... 159

Table 54 Standard deviation,  $COV_{STD\ DEV}$ , RMSD &  $COV_{RMSD}$  values for No.12 NC\_CT2 .. 160

Table 55 Standard deviation,  $COV_{STD\ DEV}$ , RMSD &  $COV_{RMSD}$  values for No.50 NC\_CT2 ... 161

## **EXECUTIVE SUMMARY**

Concrete waste contributes to the majority of 230-530 million tons of Construction and Demolition wastes produced in the US each year, yet only a small proportion of which is recycled. Recycling waste concrete and producing recycled concrete aggregate (RCA) is one of the crucial topics in civil engineering as it promotes sustainability by reducing the demand for natural resources and consumption of landfill space and lowering the production costs. Major obstacles that hinder the use of RCA in concrete construction are the lack of specifications and procedures for qualifying an RCA source and the unclear impact of RCA on concrete performance. A more comprehensive study focused on RCA characterization, and its use in concrete mixture design is needed.

Most of the current practices and standard specifications use only gradation, specific gravity, and absorption to characterize and classify RCA, as they are easily accessible and generally considered to be related to the strength and residual mortar content of RCA. However, it is unclear if these parameters can sufficiently characterize RCA for concrete applications. The proposed study considers and evaluates various parameters that can be used to describe the physical, mechanical, and durability characteristics of RCA. Besides, with the more effective characterization, a more rational mixture design of concrete that incorporates RCA has been developed. There is a misconception that the properties of concrete are definitely compromised with the incorporation of RCA. However, the study showed that with an effective characterization of the geometrical and physical properties of RCA, and particle packing-based mixture design approach, concrete with workability and mechanical properties comparable to normal concrete could be achieved. This study provides a concrete mixture design method that incorporates key RCA characteristics, focusing on pavement concrete.

## **ACKNOWLEDGEMENTS**

The authors would like to thank the ACI Foundation for funding the research project. In particular, the authors thank the Advisory Panel members Mark Snyder, Karthik Obla, Cecil Jones, and Matthew Adams for their technical support and valuable inputs and assistance throughout the project. The authors would also like to thank the recycled concrete aggregate, and cement producers for the kind donation of materials for this research. Finally, the authors would like to thank the lab managers and students at both the University of Nebraska-Lincoln and the University of North Carolina at Charlotte for their valuable assistance throughout the project.

# CHAPTER 1. INTRODUCTION

## 1.1 Background

Recycling, being one of the strategies for minimizing waste, offers three benefits: a) lessens the demand for new resources; b) reduces transportation and production energy costs; and c) beneficially reutilizes waste, which would otherwise be lost in landfill sites. The recycling of construction waste materials is highly attractive compared to using non-renewable natural resources, promoting environmental protection, or allowing the development of new raw materials. The beneficial reuse of these wastes, such as aggregates for concrete production, especially those obtained from the crushing of old concrete, is one of the most prominent means to improve the sustainability of the built environment worldwide.

While the cement and concrete industries can help reduce some environmental issues associated with solid waste (for example, by burning hazardous waste as cement kiln fuel and by using fly ash in concrete mixtures), one cannot overlook the fact that concrete is the largest and most widespread component of Construction and Demolition (C&D) waste. According to estimates presented in the American Institute of Architects Environmental Resource Guide, concrete accounts for up to 67% by weight of C&D waste (53% by volume), with only 5% currently recycled. Concrete recycling conserves not only virgin aggregate resources but also reduces unnecessary consumption of limited landfill space, saves energy, reduces greenhouse gas emissions, and removes CO<sub>2</sub> from the atmosphere.

According to a Federal Highway Administration (FHWA) study (FHWA 2004), 38 states recycle concrete as an aggregate base; 11 states recycle it into new portland cement concrete. While the states that do use Recycled Concrete Aggregate (RCA) in new concrete report that concrete with RCA performs equal to concrete with natural aggregates (NA), most of the agencies specify limitation of the quantity of RCA in the concrete as only 10 to 20% (PCA n.d.). Of the concrete that is recycled, most is used in low-profile applications, such as a highway substrate or as clean fill around buildings. However, in transportation applications, RCA has been used in new concrete pavements in several states, and with a few exceptions, has generally performed well over several decades (Snyder et al. 2018).

While the use of coarse portions of RCA, i.e., Coarse Concrete Recycled Aggregate (CRCA) has been well documented, due to concerns of unsatisfactory properties (especially high

fine content and absorption), use of Fine Recycled Concrete Aggregates (FRCA) in new concrete is restricted or even prohibited (Lauritzen 1998, Evangelista and de Brito 2007; 2010; Kou and Poon 2009a; Khatib 2005; Yaprak et al. 2011), which may result in up to 40% to 60% of RCA turn into landfills or different forms of solid wastes.

Most concrete on a project can be recycled if adequately matched to the quality of material needed for a specific application. Ultimately, if the potential quality of RCA produced from a demolished structure can be reliably linked to the quality of the source concrete before production, stakeholders can have confidence in using RCA or other recycling options. Typically, concrete sourced from transportation agency infrastructure is of known (and often, good) quality, having met previous QA requirements. For concrete of unknown quality or sourced from non-highway agency projects, testing to determine characteristics such as compressive strength, abrasion resistance, and susceptibility to materials-related distress (such as alkali-aggregate reactivity (AAR) and D-cracking) is recommended (Snyder et al. 2018). If RCA is to be used for new PCC applications, additional QA measures are typically implemented (Cavalline 2017). Once the material characteristics of RCA have been confirmed, the candidate uses for the RCA can be identified.

While there has been a limited amount of research carried out on the influence of RCA quality and proportioning criteria on concrete properties (Lopez-Gayarre et al. 2009; Kwan et al. 2012; Gonzalez-Taboada et al. 2016; Omary et al. 2016), a more comprehensive study focused on RCA characterization is needed to assist practitioners in understanding the influence of the quality of the RCA on the performance of different concrete mixtures. Due to a wide range of variability of engineering properties for RCA, a large number of trial batches are often required to determine an RCA concrete mixture with suitable properties. An effective characterization protocol for RCA, as well as specification guidance, are therefore essential to promote greater use of RCA in concrete construction. A reliable, effective characterization protocol will include suitable existing test methods, along with emerging test protocols to determine the geometry, physical and mechanical properties, chemical contents, and composition of RCA from different sources and to confirm the suitability of RCA for use in new concrete. While RCA is more complicated compared to natural aggregate (primarily due to its residual mortar fraction), characterization is currently focused primarily on gradation, specific gravity, and absorption. Additional testing to characterize the RCA

could reduce stakeholder concerns and encourage use. However, it is not practical to include all different characterization methods. Research is needed to identify the most effective and practical RCA characterization methods and procedures.

## **1.2 Research Significance and Methodology**

While most concrete on a project can be recycled if properly matched to the quality of material needed for a specific application, major obstacles that hinder the use of RCA in concrete construction are the lack of specifications/procedures for qualifying an RCA source and the unclear impact on concrete performance. An accurate characterization of RCA can resolve many of these problems. The success of the study will greatly encourage the use of RCA in daily concrete production.

## **1.3 Organization of Report**

The report is divided into six chapters. Chapter 1 is an introduction, where the general background and research significance are provided. A literature review is presented in Chapter 2, which includes a summary of different RCA characteristics, test methods, existing RCA specifications, and available recycled aggregate concrete (RAC) mixture design procedures. Chapter 3 includes an experimental program, namely RCA collection, RCA characterization methods, and concrete test methods. Chapter 4 presents RCA characteristics and the feasibility of recommended test methods. Experimental design and results of the performance of concrete that incorporates RCA are discussed in Chapter 5. Chapter 6 summarizes all conclusions and provides recommendations for future studies.

## **CHAPTER 2. LITERATURE REVIEW**

### **2.1 RCA Production**

Humankind is affected by issues of sustainability due to the large-scale consumption of natural resources and other contributing factors. Sustainability considerations will soon become a part of decision-making across various industries (Hiller et al. 2011). The construction industry is one of the largest consumers of natural resources due to rapid industrialization and urbanization. It produces a large amount of construction waste in the form of bricks, wood, steel, concrete, and other materials. Of all the construction materials, the concrete industry is the largest consumer of natural resources (Behera et al. 2014). The consumption of natural resources can have a negative impact on the environment, energy, and economies. Since concrete is approximately 75% aggregates, the use of recycled aggregate instead of virgin aggregates is an economically viable and sustainable decision. New concrete mixtures can be produced with aggregates obtained from construction and demolition (C&D) waste materials by either partial or complete replacement of virgin aggregates (Van Dam et al. 2015).

The aggregates obtained by crushing existing or “parent” concrete from construction wastes such as demolished buildings, highways, and other structures are called RCA. At present, the applications of RCAs primarily extend to unbound applications such as pavement base course, fill material, and soil stabilization, although increasingly, RCA is being used as aggregates in hot-mix asphalt or portland cement concrete (Snyder et al. 2018). The underutilization of RCA in new concrete is primarily due to its material properties that can negatively affect the fresh and hardened properties of concrete (Abbas et al. 2009). The presence of residual mortar in RCA affects the mechanical and durability properties of RAC, which is why special consideration and adequate QC are required when producing concrete using RCAs (Snyder et al. 2018). The variability of RCA, particularly when produced from crushed concrete obtained from two or more sources, can also be a barrier to increased use in new concrete (ACPA 2008a).

The process to produce RCA begins with breaking or fracturing the original structure, then reduction of the source concrete into smaller fragments and removing contaminants such as plastic, wood, reinforcing steel, and other components, followed by different stages of crushing, screening, and sorting (Behera et al. 2014). The concrete structures are broken apart and reduced to smaller sizes by chipping tools, impact breakers, or resonant breakers to prepare them for crushing. Breaking is also done to ensure debonding of reinforcing steel from existing concrete. Additional



contaminants such as dowel bars, wire mesh, steel reinforcements, joint sealant, patching material, and other undesirable materials are removed by electromagnetic separators, air blowers, or liquid separation methods. The broken concrete might be subjected to further manual screening in case the contaminants are not completely eliminated (Fick 2017).

After the breaking operation, the fractured concrete is crushed using three different types of crushers (jaw, cone, and impact crushers, shown in Figure 1). These crushers typically reduce the size of concrete to a level that can be used as concrete. The concrete is first subjected to a primary crusher (often a jaw or a cone crusher) followed by secondary crushing (typically by a cone or impact crushers), which reduces the size of the concrete, which is uniformly distributed. Occasionally, to meet gradation requirements, final crushing is performed with an impact crusher which removes a significant percentage of adhered mortar from the original aggregates (Hiller et al. 2011).

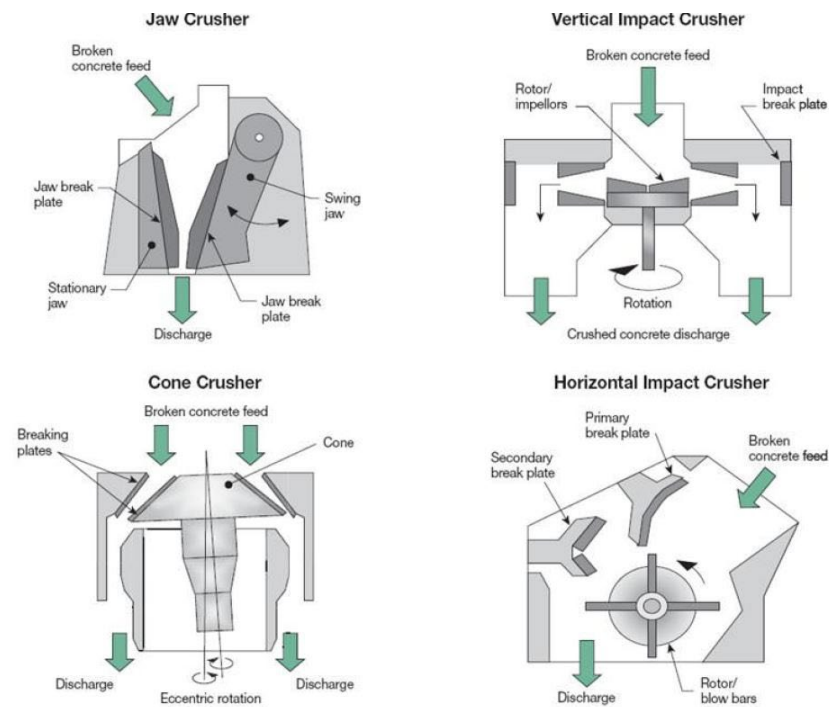


**Figure 1 Different types of crushers (Hiller et al. 2011)**

The crushing operation usually leads to the production of a large amount of top-sized aggregate and fine material. The dearth of mid-sized materials can often cause difficulty in achieving gradation specifications and can be overcome by additional sieving (Hiller et al. 2011).

## **2.2 RCA Characteristics**

The quality of the original concrete sourced for use as RCA has a strong influence on the properties of RCA, and the characteristics and composition of RCA affect the performance of the bound and unbound systems it is reused in. Understanding the composition and characteristics allows the user to assess the RCA quality and its fitness for potential use in lower-grade applications (such as unbound base materials) and in higher-grade applications (such as new concrete) to be determined.

It is important to determine the composition and characteristics of RCA, particularly when the history and properties of the source concrete are unknown (Silva et al. 2014). The key differences between the RCA and virgin aggregates are primarily a result of the residual mortar attached to the RCA. Sometimes, particularly with RCA sourced from non-state highway agency sources or from local crushing and grading facilities (which may blend material from multiple uses and sites), there is a lack of information about the original quality standards met by the concrete, and about the environment and conditions to which the original concrete structure was exposed (Snyder et al. 2018). Therefore, a thorough understanding of RCA's physical/geometrical properties and chemical composition is vital (Hiller et al. 2011).

### **2.2.1 Residual mortar content**

The presence of residual mortar on the surface of the original aggregates is known to affect the properties of RCA. The mortar content of RCA is partially dependent on the type of the original aggregates. When concrete is crushed into RCA, rounded, less porous aggregates tend to have less adhered residual mortar compared to porous or crushed aggregates that do not solely rely on shear resistance for bond (Hiller et al. 2011). The absorption capacity increases while the specific gravity of RCA decreases due to the adhered mortar (Verian et al. 2018). When RCAs are used in a concrete system, two types of interfacial transition zones (ITZ) (i.e., between the aggregate and residual mortar and between new mortar and the aggregate) are created (Figure 2). They are responsible for affecting the properties of RAC. The ITZ in new concrete produced using RCA tends to be weaker in nature due to the crushing process, which causes the formation of continuous cracks and fissures inside the aggregate and the pores present in the adhered mortar (Behera et al. 2014).

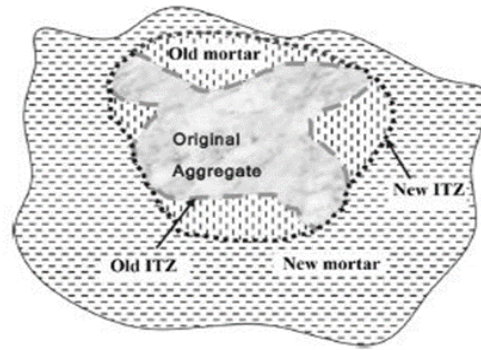


**Figure 2 Interfacial transition zone in RCA (Verian et al. 2018)**

The most distinguishing difference between RCA and NA is the presence of two different materials in RCA. RCA is composed of coarse aggregate and cement mortar attached to its surface, originating from the parent concrete (de Juan and Gutiérrez 2009). The mortar clinging to the surface of RCA is generally composed of fine aggregate, hydrated cement particles, and unhydrated cement particles, along with the hardened pore and void system from the original source concrete (Behera et al. 2014). Most of the detrimental effects on concrete properties and performance associated with RCA have been attributed to the presence of the adhered mortar and RCA particles comprised only of mortar. The mortar can have a negative influence on some of the aggregate's important properties like density, absorption, and specific gravity. Of these, the increased absorption of the RCA is often cited as the most problematic use of RCA in new concrete (Snyder et al. 2018). The presence of RCA in a concrete mixture results in a lower unit weight due to the high porosity and less dense nature of the mortar adhered to the aggregate matrix (Verian et al. 2018).

### **2.2.2 Physical and mechanical properties**

RCA's have several physical similarities and dissimilarities compared to virgin aggregates. Important physical and mechanical properties affecting performance in reuse applications include, but are not limited to, mortar content, specific gravity, absorption capacity, strength, freeze-thaw resistance, and soundness. A brief description of each of these properties, along with some supporting information, is presented below.

Particle shape and texture: Due to the crushing operation, RCA generally tends to have a poorer particle size distribution than conventional aggregates (Behera et al. 2014). The presence of adhered cement mortar and the crushing operations result in RCA particles tending to have

irregular, angular shapes with a very rough surface texture. The mortar content can vary from 30 to 60%, depending on the aggregate size. Generally, the amount of finer fraction material in RCA is greater, and finer RCA tends to include a greater portion of mortar (Safiuddin et al. 2013). The shape and size of RCAs are largely influenced by the type of crushing devices used. Jaw crushing (typically used as the primary stage crusher) has been known to provide a well-graded grain-size distribution of RCA, often exhibiting an angular shape, whereas cone crushers (often used in the secondary crushing stage) tend to produce RCA with more spherical shaped particles. The presence of pores in the adhered mortar also leads to the development of cracks and fissures inside the aggregates during the crushing operation (Snyder et al. 2018).

Specific Gravity: The specific gravity of RCA is lower than that of the natural aggregate because of the attached mortar's lower density and greater porosity (Verian et al. 2018). Finer RCA particles in concrete can increase its water demand which will reduce its workability. It can also lead to other issues such as low modulus of elasticity, low fracture resistance, and high drying shrinkage in new concrete (Hiller et al. 2011).

Absorption Capacity: The absorption capacity of RCA is higher than that of NA due to the adhered mortar on its surface (Hiller et al. 2011). As the adhered mortar content increases, the porosity of the RCA also increases, causing an increase in the absorption capacity. When RCA is used in new concrete, the higher absorption increases the water demand of the mixture, which (if unaddressed using other methods such as water-reducing admixtures) can lead to a higher w/c ratio, a weaker ITZ, poor fracture resistance, and lower strength (Snyder et al. 2018).

Mechanical properties: Depending on the amount of RCA used in concrete (often expressed as a replacement percentage of conventional aggregates), the strength of RCA has a direct impact on the mechanical properties of concrete. The mechanical properties of RCA are generally expected to be lower than those of natural aggregate, largely due to the negative influence of the residual mortar fraction of the RCA. Under load, the residual mortar can break off easily at the ITZ, which is the typically weak area of concrete. Thus, the strength of concrete with RCA is typically lower than that of conventional concrete (Chen et al. 2003, Etxeberria et al. 2007, Padmini et al. 2009). Due to the softer nature of RCA, the elastic modulus of RAC is also typically lower compared to normal concrete d (Etxeberria et al. 2007, Chen et al. 2003). Studies performed by multiple researchers demonstrated the reduction in strength and abrasion resistance through the LA abrasion test (Shayan and Xu 2003; Tavakoli and Soroushian 1996) and the crushing value test

(Limbachiya et al., 2004, Butler et al., 2011). However, the study from Hansen and Narud (1983) showed that the compressive strength of recycled concrete is largely controlled by the water-to-cement ratio of the original concrete, and using common mixture design strategies such as lowering the water-to-cement ratio and use of water-reducing admixtures, RCA has been used to produce concrete mixtures with adequate strength and other mechanical properties.

**Freeze-thaw resistance:** Freeze-thaw (F/T) resistance of RCA is a crucial property when it comes to designing concrete that is expected to experience F/T cycles. If used in new concrete mixtures, RCA produced from non-entrained concrete results in new concrete with a poor F/T resistance despite the amount of AEA dosage added (Gokce et al., 2004, Lofty et al., 2015, Liu et al., 2016). The addition of an extra air-entrainment agent does not help to provide better resistance, since it only provides protection to the new mortar component of the RCA concrete, but not the residual mortar fraction introduced with the RCA. However, when RCA crushed from air-entrained concrete is used, new concrete has excellent F/T resistance, comparable to or sometimes even better than the concrete with NA (Gokce et al. 2004, Liu 2016).

**Soundness:** Several types of soundness tests exist to assess aggregate durability, but the durability of RCA is often assessed by subjecting it to repeated cycles of freezing and thawing in a sodium chloride solution (Verian et al. 2013). The mass loss is calculated after every cycle, which provides an indication of the aggregate's resistance to disintegration by freezing and thawing. The level of deterioration of RCA tends to be higher than virgin aggregates due to higher mass loss when subjected to freezing and thawing cycles (Verian et al. 2018). Sodium and magnesium sulfate soundness testing of RCA can produce unreliable results not representative of the actual durability of RCA, and should not be used (Snyder et al. 2018).

A concern about using RCA from some sources is its alkali-silica reaction (ASR) potential. In the ASR reaction, an amorphous gel is formed when alkalis present in cement react with reactive silica present in the aggregates. This gel is known to produce cracks in concrete as it absorbs water and expands, which results in the development of tensile forces, which eventually lead to cracking and deterioration of the concrete structure (Johnson and Shehata 2016). RCA produced from ASR-affected or ASR-susceptible source concrete may also exhibit these characteristics. Guidance for the assessment of RCA for ASR potential is presented in Snyder et al. (2018).

### **2.2.3 Chemical composition**

The chemical composition of the RCA will be highly dependent on the chemical composition of the materials used in the aggregates and paste of the source concrete. Therefore, most are calcium and silica-rich (primarily from aggregate sources), with aluminates, alkalis, and ferrous materials contributed by the cement. Other chemical contaminants may also be present, depending on the use and exposure of the source concrete. These can include organic chemicals from automobiles (hydrocarbons, other automobile fluids) and inorganic chemicals (from deicers, spilled materials, and other sources). Other larger contaminants may be present, such as joint filler, patching material, construction debris, or other materials – these may be present as entire particles from the crushing process or as contaminants on particles primarily consisting of RCA (Snyder et al. 2018).

### **2.2.4 Potential contaminants**

The presence of deleterious chemicals such as alkalis, sulfates, chlorides, organic impurities, etc., greatly influences the chemical properties of RCA concrete and its durability. Sulfates may be present in RCA produced from C&D waste in the form of water-soluble sulfates sourced mostly from gypsum plaster (Silva et al. 2014). The presence of sulfates in RCA may lead to reactive expansion. According to de Juan and Gutierrez (2009), the sulfate content in RCA is higher than NA due to the presence of cement in the adhered mortar. Alkalis can contribute to alkali-silica reaction (ASR). Another deleterious contaminant that affects the durability of concrete is chloride which may be found in RCA due to long-term exposure to de-icing chemicals containing chloride. The chloride causes corrosion of the steel reinforcement, which affects the durability of concrete (Anderson et al. 2009). Lastly, RCA may also contain organic impurities like paper, wood, textile fabrics, joint seals, plastics, rubber, and other polymeric materials. The presence of these materials can cause instability in concrete when exposed to freezing/thawing or drying/wetting conditions (Khalaf and DeVenny 2004).

## **2.3 Test Methods**

Information regarding the quality of the parent concrete of RCA, such as water-to-cement ratio (w/c), type and amount of cement, cementitious materials and chemical admixtures, aggregate origin and gradation, etc., is often unknown. Additionally, even if the quality of the concrete at the time of construction is known, the properties of concrete may have degraded during its time in service. Therefore, the key characteristics and test methods to characterize RCA are typically

grouped into three categories: a) Geometrical properties; b). Physical and mechanical characteristics; and c) Chemical characteristics and compositions, summarized in Table 1.

**Table 1. Summary of key RCA characteristics**

	Characteristics
Geometrical properties	Particle size distribution
	Particle shape and surface texture
	Clay content
Physical and mechanical properties	Specific gravity and absorption
	Abrasion resistance
	Aggregate strength
	Residual mortar content
Chemical properties and compositions	Chloride and sulfate content
	ASR potential

The section below summarizes potential test methods and procedures for RCA characterization, along with supporting information identified through a comprehensive literature review of test methods for both natural aggregate and RCA.

### **2.3.1 Geometrical properties**

#### *Particle size distribution*

Particle size distribution can be obtained by performing a sieving analysis according to ASTM C136. The ASTM C33 specification defines the requirements of gradation of fine and coarse aggregates to be used in concrete.

#### *Particle shape and texture*

The aggregate shape is an important characteristic that has a direct impact on paste demand, workability, and strength, primarily due to the influence of particle shapes on particle packing and bonding with paste. The shape of an aggregate is mainly described by its sphericity, flatness, angularity, and roundness (Quiroga et al. 2004). According to Kwan (2002), the two factors affecting particle packing the most are shape and convexity factors. The aggregate texture is primarily related to the roughness of a particle. According to Kosmatka et al. (2008), aggregate shape and texture have more impact on fresh concrete rather than on hardened concrete. RCA typically has a more irregular shape and rougher texture than NA due to the attached mortar (Ravindrarajah 1987, Topcu 1997, Limbachiya et al. 2004, Butler et al. 2011)

ASTM D 3398 (2006) is sometimes used to quantitatively measure the particle index value by means of estimating void contents in bulk material under different compaction methods. An

aggregate sample is sieved into different sizes, and bulk density is obtained for individual size fractions. Cylindrical molds of a known volume are filled in three layers, and each layer is tamped 10 or 50 times. The particle index value is computed using Equation 1,

$$I_a = 1.25V_{10} - 0.25V_{50} - 32.0 \quad (\text{Eq. 1})$$

where,  $I_a$  = particle index value;  $V_{10}$  = void content in aggregate sample compacted at 10 drops per layer in %; and  $V_{50}$  = void content in aggregate sample compacted at 50 drops per layer in %.

ASTM D4791 (2019) can be used to evaluate aggregate shape by means of proportional calipers. Particles can be characterized as cubical, flaky, elongated, or flaky and elongated according to their dimension ratios (ICAR 2003).

BS 812-105.1 (1989) and BS 812-105.2 (1990) are widely used to characterize particle flakiness and elongation, respectively. Flaky particles are differentiated from non-flaky particles by determining whether the thickness (smallest dimension) of a particle is less than 60% of its mean sieve size. A particle is considered elongated when its length (greatest dimension) is more than 180% of its mean sieve size.

The uncompacted void content (determined per ASTM C29 or AASHTO T19, and C1252 or AASHTO TP33 test for coarse and fine aggregate, respectively) can be used to indirectly measure aggregate shape and texture, since these parameters primarily influence the particle packing of coarse and fine aggregate, respectively.

Aggregate Image Measurement System (AIMS2) equipment can also be used to determine particle shape and texture properties directly. The AIMS2 is an integrated machine that contains image acquisition hardware and computer software for data analysis. The equipment can provide information that includes angularity, texture, and sphericity, as well as the distribution of flat and elongated particles. The software can also provide weighted stockpile properties, which is the weighted characterization of an entire aggregate source based on every data from each aggregate size obtained individually.



### 2.3.2 Physical and mechanical properties

#### *Specific gravity and absorption*

Due to the relatively porous matrix of the adhered and included mortar fraction, RCA typically has a higher absorption capacity and lower specific gravity compared to NA (ACPA 2009, Olorunsogo et al. 2002). Moreover, according to de Juan et al. (2009), the adhered mortar content increases with the decrease in particle size, which typically leads to even higher absorption and lower specific gravity of fine RCA, compared to coarse RCA. ASTM C127 and C128 can be used to obtain the specific gravity and absorption values of coarse and fine fractions of aggregates, respectively.

Kim et al. (2017) developed a new method to measure water absorption of very fine particles based on the percolation threshold defined by the electrical resistivity. Tam et al. (2006) proposed a new approach called real-time assessment of water absorption, in measuring water absorption of recycled aggregates. In this test, an oven-dried aggregate sample was placed in a pycnometer, followed by completely filling the container with water. As RCA starts to absorb water, the water level drop is noticeable. By adding water to the original level, the water absorption rate in real-time can be determined. Besides allowing monitoring absorption speed, this new test method eliminates two issues that could be particularly important to the evaluation of RCA with traditional test methods. The method does not require using a cloth towel to dry aggregates, which is believed to introduce a human error. Also, the test does not require drying aggregates at  $105 \pm 5$  °C, which can remove water within the crystal structures of compounds present in the residual mortar of RCA.

#### *Abrasion resistance*

The standard L.A. abrasion test per AASHTO T 96 evaluates aggregate's resistance to abrasion by grinding it in a rotating steel drum with a specified number of steel balls as grinding media. This test is often performed on the size fraction of aggregate retained on the No.12 sieve. After 500 revolutions of the steel drum, the percentage of the particles broken down and passed No.12 is recorded and reported as sieve mass loss.

The abrasion resistance can also be determined using the Micro-Deval method, which is similar to the LA abrasion test, but a much smaller drum is used. The test is carried out in accordance with ASTM D6928. Approximately 1500g (mass of fine aggregate, or  $M_F$ ) of washed and oven-dried samples are re-sieved to a specific gradation (50% of 14 to 20 mm size and 50%

of 10 to 14 mm size). After 120 minutes in the Micro-Deval apparatus, the abrasion loss is calculated using the following equation:

$$\text{Abrasion Loss} = \frac{M_F - M_{OD}}{M_F} * 100\% \quad (\text{Eq. 2})$$

Where  $M_{OD}$  is the oven-dry mass of the aggregate after mass loss and sieving.

#### *Crushing strength*

One of the test methods to characterize RCA strength is the evaluation of the resistance of aggregate to crushing under static compressive load. Typically the higher the resistance of RCA to crushing, the higher splitting tensile strength, modulus of rupture, and reinforcement bond of the concrete produced with the RCA (Butler 2012). Various standards have been used for this test, including a British Standard (BS 812-110 and BS 812-111), a Chinese standard (JGJ 52-2006), and a European standard for lightweight aggregates (EN 13055).

The BS 812-110 standard, which is the method for the determination of aggregate crushing value (ACV), is a very widely used method among researchers (Hansen et al. 1983, Ravindrarajah 1987, Limbachiya et al. 2004, Butler et al. 2011). The standard test is generally conducted for the aggregate portion that passes 14 mm sieve and retains on 10 mm sieve. If the specified size is not available, the standard includes recommendations for the testing of larger or smaller-sized aggregates. The test includes subjecting compacted aggregates to a gradually increasing compressive load, so the load of 90 kips reaches 10 min  $\pm$  30 sec. Afterward, the specimen is sieved using a 2.36 mm sieve, and the mass of particles passed the sieve is recorded. ACV is calculated as follows:

$$ACV = \frac{\text{Mass of the material passed 2.36 mm}}{\text{Initial mass of the specimen}} \times 100 \quad (\text{Eq. 3})$$

The higher the ACV, the weaker the aggregate. BS 812-110 states that this method can be used for aggregates with ACV no higher than 30. In the case of ACV higher than 30, another method (BS 812-111) is applicable, which is used to determine the ten percent fines value (TFV) of the RCA sample. The aggregate sample and apparatus used are similar to the ACV test, but the main difference is that rather than controlling the maximum load to be reached, the targeted percent of material passing No. 8 sieve is controlled to be within 7.5-12.5%. Once that is obtained, the following equation is used to determine the TFV:

$$TFV = \frac{14 \times \text{Maximum load}}{\text{Mass of the material passed 2.36 mm} + 4} \quad (\text{Eq. 4})$$

Chinese standard JGJ 52-2006 is similar to BS 812-110, with the difference between the target maximum load and the loading rate. This method requires reaching the load of 45 kips at a 225 lb/s rate, holding the maximum load for 5 sec, and then releasing it. The crushing index ( $Q_e$ ) can be calculated as follows:

$$Q_e = \frac{\text{Mass of the material passed 2.36 mm}}{\text{Initial mass of the specimen}} \times 100 \quad (\text{Eq. 5})$$

EN 13055 was developed for lightweight aggregates with specific gravity not exceeding 2.00. Instead of having a particular maximum load as a target, in this method, the maximum deformation of 20 mm has to be reached within approximately 100 seconds. The following equation is used to determine the crushing resistance ( $C_a$ ):

$$C_a = \frac{\text{Load exerted by the piston} + \text{Maximum load}}{\text{Area of the piston}} \quad (\text{Eq. 6})$$

Some researchers do not follow a specific standard and use different test configurations. Nagataki et al. (2004) used the maximum load of 22.5 kips to obtain the crushing value of RCA. Saravanakumar et al. (2016) used the maximum load of 9 kips and sieved the crushed specimen using a No. 12 sieve instead of the standard No. 8 sieve per BS 812-110 to determine ACV.

Li et al. (2019) proposed a completely different approach by testing one RCA particle at a time. The compressive load is applied at a 1mm/min rate, and the maximum load at the initial crack is recorded. The surface area of each RCA particle was derived as follows:

$$\text{Surface area} = \pi \times \frac{(\text{Width} + \text{Height}) \times \text{Length}}{2} \quad (\text{Eq. 7})$$

Consequently, the stress can be calculated:

$$\text{Crushing stress} = \frac{\text{Maximum load}}{\text{Surface area}} \quad (\text{Eq. 8})$$

### *Impact strength*

Impact resistance of aggregate is another test method to characterize aggregate strength (Limbachiya et al. 2004, Saravanakumar et al. 2016). BS 812-112 is a standard method to determine aggregate impact value (AIV). The test is based on subjecting compacted aggregates to

the 15 blows of a 13.5-14.0 kg metal hammer freely dropped from a height of  $380 \pm 5$  mm and then measuring mass loss.

#### *Residual mortar content*

To obtain the residual mortar content (RMC) of RCA, chemical solutions can be used to dissolve the adhered mortar leaving behind the original aggregate only. By knowing the original mass of RCA and the mass of virgin aggregate left after mortar disintegration, the RMC can be calculated as follows:

$$\% \text{ Residual mortar} = \frac{\text{Mass of RCA} - \text{Mass of RCA after mortar removal}}{\text{Mass of RCA}} \quad (\text{Eq. 9})$$

Abbas et al. (2008) investigated the effect of chemical stresses on the removal of residual mortar by comparing sodium sulfate, magnesium sulfate, and magnesium chloride solutions. The concentration of the solutions was 26% (by mass). RCA samples were submerged in the solutions for 15 days. It was found that the samples immersed in the sodium sulfate solution experienced significant mortar degradation, whereas samples immersed in the other two solutions did not respond to the test, with almost no mortar disintegrated. Butler et al. (2011) immersed RCA in a 20% (by volume) nitric acid solution, followed by heating to dissolve the residual mortar for two hours. Despite the significant mass loss, there was a substantial amount of adhered mortar remained. Additional measures such as subjecting the RCA to mechanical friction for 15 minutes were not successful.

It is possible to use a more aggressive environment in terms of both chemical solution, and exposure time; however, care should be taken, so the original aggregate itself does not dissolve. The hydrochloric solution is another option to dissolve residual mortar (Nagataki et al. 2000, Nagataki et al. 2004, Afroughsabet et al. 2017). However, it can also dissolve original carbonate aggregates (e.g., limestone). Therefore, Nagataki et al. (2000) used a correction factor to compensate for original aggregate dissolution. A study by Tam et al. (2007) included soaking RCA in 0.1 molar acidic solutions (HCl hydrochloric acid, H<sub>2</sub>SO<sub>4</sub> sulfuric acid, and H<sub>3</sub>PO<sub>4</sub> phosphoric acid) for 24 hours. With the sulfuric and hydrochloric acids being the most efficient reagents, the mortar removal resulted in the decrease of water absorption by 7-12%, from which the conclusion can be drawn that the removed mortar content is low. Since the goal of the study was to improve RCA by reducing the RMC, and not completely removing it, it seems that a relatively low

aggression environment was used. Studies conducted by Akbarnezhad et al. (2011) have shown that immersing RCA in a sulfuric acid concentration of at least 2M for five or more days can completely remove the residual mortar.

Another method used to disintegrate residual mortar is a thermal treatment method, where RCA is subjected to large temperature variations (De Juan et al. 2009, Butler et al. 2011, Pepe et al. 2014). The method includes soaking RCA samples in water for 24 hours and then subjecting the samples to a temperature of 500°C using a muffle furnace for 2 hours, then quickly immersing in cold water to provide a sudden and significant reduction in aggregate temperature, which creates internal thermal stresses. Once the RCA samples are cooled, adhered mortar becomes extremely brittle and easy to be removed with additional efforts, such as hammering the particles with a rubber mallet or scratching the surface of individual particles. Based on the visual observation, this method seems to remove nearly 100% of the residual mortar (Butler et al. 2011).

Some researchers use combined methods to enhance the removal rate of residual mortar. Abbas et al. (2008) investigated the combined effect of the chemical attack and freeze-thaw stresses on the removal of residual mortar. RCA was soaked in three solutions, magnesium sulfate, magnesium chloride, and sodium sulfate, for 6 hours, followed by 12 hours (overnight) of freezing at -18°C and thawing at room temperature during the day. The cycle was repeated five times. RCA that was soaked in sodium sulfate showed extensive removal of the mortar, while the other two solutions seem to be ineffective. Compared to either chemical treatment or freeze-thaw method alone, research showed that the combination of these two methods will result in a higher mortar disintegration rate and will more effectively characterize the RMC in RCA (Salas et al. 2013). It should be noted that although this method can provide complete removal of mortar, it is not time efficient due to the required multiple F/T cycles.

Akbarnezhad et al. (2013, 2011) adopted multiple methods to identify a more time-efficient way to determine the RMC of RCA. The first method was to soak RCA in the sulfuric acid solution for 24 hours and then wash the sample on a No. 4 sieve (Akbarnezhad et al. 2011). The second method included washing away the mortar and replacing the acidic solution with the fresh one after 8 hours, and then continuing soaking for the remaining 16 hours. The two other methods used by Akbarnezhad et al. were similar to the first two methods, but with a continuous rotary agitation introduced. Besides the different procedures and chemicals used, acid concentration and

$V_{\text{acid}}/V_{\text{RCA}}$  were varied within each method. The results showed that the method that included continuous rotary agitation and acid replacement at 8 hours was the most efficient in removing the mortar fraction. With the acid concentration of 3M and  $V_{\text{acid}}/V_{\text{RCA}}$  of 5, almost 100% of residual mortar can be removed after 24 hours. Table 2 provides a summary of the removal and time efficiencies of different residual mortar characterization methods.

**Table 2. Summary of residual mortar measurement tests through mortar disintegration**

Method	Mechanism	Removal efficiency	Time efficiency	Need of large and/or expensive equipment
Thermal treatment	Large temperature drops	High	High	Yes
Chemical dissolution	Sodium sulfate	Medium	Low	No
	Magnesium sulfate	Low	Low	No
	Magnesium chloride	Low	Low	No
	Hydrochloric solution	High	Low	No
	Nitric acid	Low	Low	No
	Sulfuric acid	High	Low	No
Combinations	Sulfuric acid + rotary agitation + acid replacement	High	High	Yes
	Sodium sulfate + freeze/thaw	High	Low	Yes

Unlike the above-mentioned methods that focused on mortar disintegration, the following test procedures implement image analysis by differentiating colors of virgin aggregate, residual mortar, and new binder. Ravindrarajah et al. (1985) used white cement to produce concrete in order to provide a clear color difference between the new paste and old (residual) mortar of RCA. 150 mm cube specimens of RCA concrete were cut into three slices, and four exposed surfaces were analyzed using an electronic digital planimeter to obtain areas of the original aggregate and residual mortar. Abbas et al. (2009) adopted the same idea of using white cement but proposed a computer software for image analysis to determine the RMC. 4in×4in×16in prisms were cast and cut into 1.2 in thick slides and then polished using three different methods. Results showed that the grinding method using a single-row cup wheel to remove cutting grooves is sufficient, and no additional polishing using grit pads is necessary. It was also recommended to wet the surface before obtaining photographs. Once the photographs were obtained, computer software was used for image analysis, where multiple steps were performed to determine the areas of each RCA particle, virgin coarse aggregate in RCA, and residual mortar, respectively. Afterward, following

the equations from Abbas et al. (2009), the obtained surface area results were converted to weight-based quantities using specific gravity measurements.

Verian (2012) used an approach similar to Abbas et al. (2009), but instead of embedding RCA in white cement paste, RCA was embedded in epoxy to prepare the specimen for microscopic analysis using a low magnification optical microscope. The point count method used was similar to the ASTM C457, where the percentages of mortar-free aggregates surface and mortar present on the surface were calculated by dividing the number of stops on the clean (mortar free or mortar covered) aggregate surface by the total number of stops in the aggregate. These numbers were determined by linearly transverse the sawn surface of the puck (in 0.1 in increments) and recording the aggregate surface characteristics (e.g., clean or covered with mortar) positioned directly under the index point (crosshair of the microscope eyepiece) at each of the stops. Pepe et al. (2016) used Computer Tomography and image analysis conducted according to ASTM E1570 to determine the RMC.

#### *Freeze-thaw resistance of RCA*

Gokce et al. (2011) used the F/T soundness loss test to evaluate if the test can determine frost susceptible RCA. The test seems to clearly differentiate air-entrained and non-air-entrained parent concretes. However, only one level of air-entrained parent concrete RCA (at approximately 4.5% of air content) was used, and it is difficult to state if the test is sensitive enough to differentiate between other levels of air-entrainment (such as higher 6-8% or lower 2-4%).

The Canadian Standards Association (CSA) has a similar test (CSA A23.2-24A) to assess the resistance of unconfined coarse aggregate to F/T cycles. The procedure consists of placing aggregate samples in frost-resistant containers filled with 3% sodium chloride solution to completely immerse aggregate particles and keeping them sealed at room temperature for 24 hours. The solution was then drained by inverting a container over a screen smaller than 5 mm mesh. Containers were then sealed and placed in a freezer at -18°C for 16 hours. After that duration of freezing, containers were removed from the freezer, and aggregate samples were allowed to thaw at room temperature for 8 hours. The procedure was repeated for five cycles, and aggregates were then washed over a screen smaller than 5 mm to obtain mass loss.

Some researchers have also used Mercury Intrusion Porosimetry (MIP) to evaluate the pore size distribution of RCA (Pepe et al., 2016), which is related to the freeze-thaw resistance of RCA.

### 2.3.3 Chemical compositions

#### *RCA Characterization Using PHXRF*

XRF is an elemental analysis technique where a material excited by high-energy X-rays emits secondary X-rays of characteristic energy or wavelength (Brouwer 2006). XRF is used to determine the elemental composition of materials and has been used in a wide range of applications, including archaeology (Shugar and Mass 2012, Calparsoro et al. 2019, Sánchez De La Torre et al. 2018), mining and geology, metallurgy (Marucco 2004), medical, food science (Chailapakul et al. 2008, Ali et al. 2004), environmental, and construction (Steiner 2011) sectors. The portable handheld X-ray fluorescence (PHXRF) devices are relatively simple to use and provide accurate analyses of a range of elements.

Recently, several studies have focused on geotechnical material analysis using PHXRF. Many transportation projects use stabilizers to improve the mechanical properties of soil. Previous research studies for Oklahoma DOT have concluded PHXRF can be used to determine the stabilizer content in the subgrade, aiding geotechnical inspections by detecting irregularities (Ferraro 2016, Cerato et al. 2017). Procedures developed by Cerato et al. (2017) were used to guide work on the use of PHXRF on RCA are presented here in some detail to support the comparison of findings from this work.

The research study by Cerato et al. (2017) was conducted on five sites where soils were stabilized with quicklime or high calcium fly ash (Class C). Two PHXRF devices were used, and the stabilizer content readings of these devices were compared to laboratory readings using the “Whole Rock Analysis” technique to identify sample preparation and analysis techniques producing accurate PHXRF results. Whole Rock Analysis is a geochemical technique commonly used to analyze rock samples to determine the composition of major and trace elements. Widely used in the mining and geochemical fields, this technique involves tests including inductively coupled plasma mass spectrometry (ICP-MS), inductively coupled plasma atomic emission (ICP-AES), infrared spectroscopy (IR), and loss on ignition (LOI). Samples are pulverized to the size of few microns and are fused using a fusion flux (Twelker et al. 2017). Using this technique, major and trace elements are quantified on a weight % basis.

Cerato et al. (2017) used statistical techniques including ANOVA and regression analysis to evaluate the accuracy of the PHXRF on determining sample composition. The influence of



variables including scan duration, scan technique, particle size, and the type of sampling on PHXRF results, was also evaluated. A 60-second scan duration was determined to be appropriate for stabilized soil materials since longer scanning durations did not yield significant benefits in terms of precision. Two types of scanning techniques (standard and quartering) were also evaluated to assess the homogeneity of the sample (Cerato et al. 2017). The researchers found that particle size played a prominent role in the accuracy of PHXRF in measuring stabilizer contents. Two types of soils were mixed with three stabilizing agents at different concentrations, which were milled to pass sieve sizes of No. 4, No. 40, No. 100, and No. 200, creating a matrix with a total of 56 total samples. The effect of particle size on the root mean standard deviation (RMSD) and the coefficient of variation of the RMSD ( $COV_{RMSD}$ ) of the samples revealed that milling samples to smaller particle sizes improved the accuracy of PHXRF readings. Field samples were milled to pass a No. 40 sieve because the accuracy of PHXRF begins to level off after they are reduced past the No. 40 sieve (Figure 3).

The study by Cerato et al. (2017) demonstrated that with a certain level of sample preparation, the PHXRF could be a useful tool to improve QA and QC capabilities in future roadway inspections. More importantly, for the present work on RCA characterization, this study demonstrated the capability of PHXRF to successfully characterize granular, silicate, and calcareous materials (Cerato et al. 2017).

With lesser success, PHXRF was used to estimate the mixture proportions of concrete (Taylor et al. 2012). The individual chemical composition of cementitious materials (slag cement, silica fume, Class C fly ash, Class F fly ash, and type I portland cement) used in concrete mixtures were initially tested using the PHXRF. Paste mixtures with different combinations of cementitious materials and mortar samples (1:3 ratio of cement to sand by mass) were prepared and tested using the PHXRF. The results were averaged after testing three samples from each mixture. The researchers determined the PHXRF was reasonably accurate in determining the SCM dosages of paste mixtures, but the inhomogeneity of the mortar samples affected the analysis of mortar, which significantly increased errors.

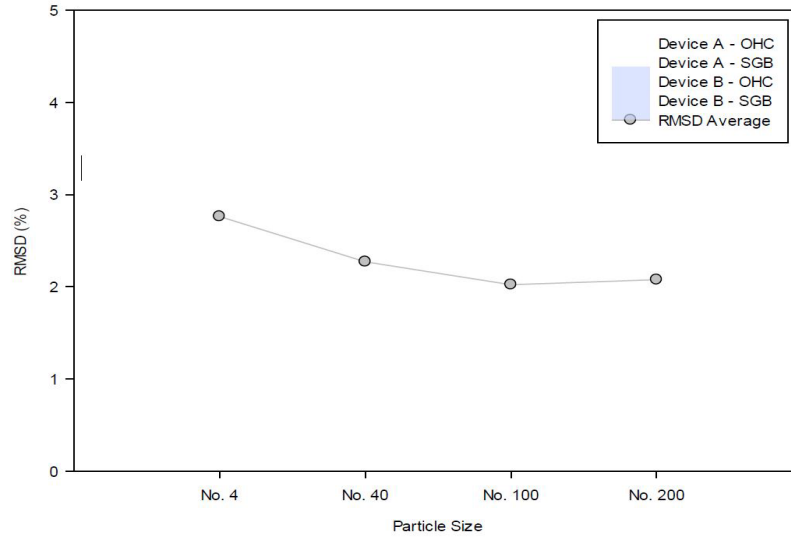


**Figure 3 Particle size vs. RMSD % curve (Cerato et al. 2017)**

With its successful use in construction applications, including the analysis of granular soil materials and cementitious/pozzolan binders (Dey 2020), PHXRF shows promise for use in the analysis and characterization of RCA. However, there is not an established testing protocol to support the use of PHXRF for the characterization of RCA. Several variables must be considered to obtain accurate PHXRF measurements of RCA:

1. *Duration of each scan*: The effect of duration of each scan with respect to variables, including sample type, particle size of the sample, thickness of sample, and scanning technique, should be considered to obtain the desired level of accuracy and precision (Cerato et al. 2017).

2. *Scanning Technique*: Cerato et al. (2017) noted that the scanning technique influenced the precision of PHXRF measurements more than the accuracy. Hence, the scanning technique should be selected from an efficiency standpoint.

3. *Sample Thickness*: PHXRF intensities are influenced by the thickness of the sample. Therefore, the minimum thickness should be carefully evaluated because the minimum thickness for each element is correlated to its characteristic x-ray energy (Padilla et al. 2019).

4. *Particle Size*: As discussed previously, Cerato et al. (2017) noticed significant drops in RMSD and  $COV_{RMSD}$  when the particles were reduced to smaller sizes. When the particle size was compared against the RMSD values, it was observed that with the size reduction beyond the No.

40 sieve, the RMSD values leveled off, indicating no noteworthy reduction in the accuracy of XRF measurements.

5. *Sample Type*: Different sample preparation approaches, such as loose powder, pressed pellets, loose aggregates, or unprepared samples, can be used for XRF analysis. Inaccurate results may be obtained if the sample is non-homogenous, and therefore, some amount of sample preparation should be done to obtain accurate results. The practicality of preparation should also be considered, since some types of preparation may require a significant amount of time, cost, and effort, or may not be feasible in field applications (Cerato et al. 2017).

If a testing protocol to support the use of PHXRF in construction applications can be developed, it could be used to provide confidence to stakeholders considering the use of RCA, since the characteristics of RCA could be rapidly determined and assessed. Benefits of successful development of this protocol would include the ability for stakeholders to perform rapid QA or QC analysis of RCA, and identify appropriate reuse applications for RCA materials based on characteristics. If successful and subsequently utilized in the field, the long-term benefit of this research could be the promotion of sustainability through the greater use of RCA in construction.

## **2.4 RCA Specifications**

### **2.4.1 United States**

ACI 555R-01 covers demolition methods, types, and degrees of removal, as well as RCA quality and effects of RCA on concrete properties. However, no specific information on RCA classification is included in this document. Although ASTM C33 allows using RCA, it does not present any specific criteria for them in concrete use, implying that they should be evaluated in the same manner as NA. However, the ASTM C33 standard contains a note with some additional precautions when RCA is used, such as a possible increase in the mixing water requirement, a potential decrease in freeze-thaw resistance, an influence on air void structure, and the potential presence of chemical constituents that might result in ASR, sulfate and chloride attacks. AASHTO MP 16-13 (2015) includes the criteria for coarse recycled aggregate to be used in normal concrete applications. This standard cannot be used when lightweight, high-density, or other specialty concretes are used. In terms of grading, coarse RCA must conform to the coarse aggregate gradation requirements as described in AASHTO M 43 (2015) or ASTM C33 (2018). Regarding

the physical properties, there is a criterion for Los Angeles abrasion loss and soundness loss only. Table 3 summarizes the requirements for physical properties included in AASHTO M 43.

**Table 3. Physical properties criteria of RCA per AASHTO M 43**

Property	Maximum allowable loss (%)
LA abrasion	50
Soundness (sodium sulfate)	12
Soundness (magnesium sulfate)	18

AASHTO MP 16 contains a detailed list of criteria for deleterious substances in RCA. Table 4 presents limits for deleterious substances for three classes of aggregates based on the weathering exposure, where class A is for severe exposure, class B is for moderate exposure, and class C is for negligible exposure. Additionally, the amount of particles finer than 75 microns in recycled aggregates shall not exceed 1.5% by mass. RCA shall not contain chloride ions at an amount of more than 0.6 lb/yd<sup>3</sup> of concrete.

**Table 4. Summary of deleterious substances criteria of RCA per AASHTO MP16**

Class designation	Maximum allowable %				
	Clay lumps and friable particles	Chert (<SG <sub>SSD</sub> =2.4)	Sum of clay lumps, friable particles, and chert	Other deleterious substances	Coal and lignite
A	2.0	3.0	2.0	0.3	0.2
B	3.0	5.0	3.0	0.3	0.2
C	3.0	8.0	5.0	0.3	0.2

#### **2.4.2 State Departments of Transportation (DOT)**

Texas DOT allows the use of recycled crushed hydraulic cement concrete in PCC as long as it passes the performance criteria set for coarse aggregate in general. Minnesota DOT allows the use of recycled aggregates in PCC, and the Engineer is responsible for determining the suitability of using recycled aggregates as well as concrete proportioning. Illinois DOT permits the use of crushed concrete aggregates provided they have the quality matching the best quality of aggregates (class A). Michigan DOT limits the use of crushed concrete coarse aggregates in new concrete to such applications as curb and gutter, valley gutter, sidewalk, concrete barriers, driveways, temporary pavements, concrete shoulders, and interchange ramps with a commercial average daily traffic (ADT) less than 250. For other applications such as mainline pavements or ramps with ADT higher than 250, bridges, pre-stressed concrete, and heavily reinforced concrete,

the use of crushed concrete is prohibited. Michigan DOT emphasized that for each project, the freeze-thaw durability of crushed concrete coarse aggregates has to be tested. Virginia DOT permits the use of crushed hydraulic cement concrete in new concrete other than reinforced cement concrete. West Virginia DOT allows the use of recycled pavement but emphasizes removing any asphaltic resurfacing, reinforcing steel to limit the contamination. Most of the DOTs characterize coarse aggregates for concrete in terms of LA abrasion resistance, soundness loss, and the amount of deleterious materials. Some of the states (TX, IL) mention that the soundness loss criterion does not apply to recycled crushed concrete.

### 2.4.3 Japan

Japanese specifications contain criteria for both coarse and fine RCA. JIS 5021, JIS 5022, and JIS 5023 specifications include requirements for three classes of RCA, i.e., high (H), medium (M), and low (L), respectively. Class H RCA has no limitations in concrete use, whereas class M RCA can only be used when concrete is not subjected to drying or freezing-thawing cycles, and class L RCA can be used in such applications as backfill concrete, blinding concrete, and leveling concrete. Table 5 summarizes recycled aggregate criteria for use in concrete per JIS 5021-5023.

**Table 5 Summary of RCA criteria for different classes per JIS 5021-5023**

RCA Class	Min SG <sub>OD</sub>	Max AC (%)	Max LA abrasion loss (%)	Max amount of particles < 75µm (%)	Max Cl content (%)	Maximum SO <sup>2-</sup> content (%)	Min. solid volume for shape determination (%)
Class H coarse	2.5	3.0	35	1.0	0.04	NA	55
Class H fine	2.5	3.5	NA	7.0	0.04	NA	53
Class M coarse	2.3	5.0	NA	NA	NA	NA	NA
Class M fine	2.2	7.0	NA	NA	NA	NA	NA
Class L coarse	NA	7.0	NA	NA	NA	NA	NA
Class L fine	NA	13.0	NA	NA	NA	NA	NA

### 2.4.4 RILEM

A European standard specification for concrete with RCA is presented in RILEM TC 121-DRG recommendation report. This specification defines three types of RCA, which are Type I demolished masonry rubble, Type II demolished concrete rubble, and Type III blend of recycled and NA (>80% of NA, <10% of Type I aggregate). All three types of aggregates can be used in both dry and wet environments. However, Type I RCA is not allowed to be used when water is exposed to frost. RILEM criteria for RCA to be used in concrete are summarized in Table 6.

**Table 6 Summary of RCA criteria for different types per RILEM TC 121-DRG**

Criteria	RCA Type I	RCA Type II	RCA Type III
Minimum SG <sub>OD</sub>	1.5	2.0	2.4
Maximum AC (%)	20.0	10.0	3.0
Maximum content of material with SSD<2.2 (%)	NA	10.0	10.0
Maximum content of material with SSD<1.8 (%)	10.0	1.0	1.0
Maximum content of material with SSD<1.0 (%)	1.0	0.5	0.5
Maximum content of foreign materials (metals, glass, soft material, bitumen) (%)	5.0	1.0	1.0
Maximum content of metals (%)	1.0	1.0	1.0
Maximum content of organic materials (%)	1.0	0.5	0.5
Maximum content of filler (<63 microns) (%)	3.0	2.0	2.0
Maximum content of sulfate (%)	1.0	1.0	1.0

#### 2.4.5 Germany

Standard DIN 4226-100 contains the specification for RCA use in concrete and mortar. According to this standard, the classification of RCA consists of four types: Type 1 concrete rubble, Type 2 demolition debris, Type 3 masonry rubble, and Type 4 mixed rubble. Whereas Type 1 and 2 are allowed to be used in structural concrete applications (not allowed in prestressed concrete), Type 3 and 4 can only be used in non-structural concrete elements. Recycled aggregate requirements based on DIN 4226-100 are presented in Table 7.

**Table 7 Summary of RCA criteria for different types per DIN 4226-100**

RCA class	Minimum SG	Maximum AC (%)	Maximum chloride content (%)	Maximum sulfate content (%)	Maximum amount of contaminants (%)*
Type 1	2.0	10.0	0.04	0.8	1.0
Type 2	2.0	15.0	0.04	0.8	1.0
Type 3	1.8	20.0	0.04	0.8	1.0
Type 4	1.5	NA	0.15	NA	NA

\*Asphalt is not included

#### 2.4.6 Other countries

Table 8 presents the criteria of RCA in specifications for other countries. Brazilian specification ABNT NBR 15.116 allows the use of both coarse and fine fractions of RCA. This specification classifies two types of RCA: RCA (>90% of concrete and natural resources) and mixed aggregate (MA) (<90% of concrete and natural resources). The standard does not permit RCA use in structural concrete applications. Australian specification AS1141.6.2 divided RCA

into two classes: Class 1A, well-graded RCA with no more than 0.5% brick content, and Class 1B, Class 1A RCA blended with no more than 30% of crushed brick. Spain (EHE 2008) and Korea (KS F 2573) appear to have relatively strict requirements for absorption with a lower allowable maximum absorption.

**Table 8 Summary of RCA criteria for different types/classes**

Specification	RCA type	Minimum Specific gravity	Maximum absorption (%)	Maximum chloride content (%)	Maximum sulfate content (%)
Spain	-	No limit	5.0	0.05 (mass concrete and RC); 0.03 (prestressed concrete)	0.8 (water soluble); 1.0 (total)
Korea	Coarse	2.5	3.0	NA	NA
	Fine	2.2	5.0	NA	NA
Australia	Class 1A	2.1	6.0	NA	NA
	Class 1B	1.8	8.0	NA	NA
Brazil	RCA	NA	7.0	1.00 (water soluble)	1.0 (water soluble)
	MA	NA	12.0	1.00 (water soluble)	1.0 (water soluble)
Hong Kong	NA	2.0	10.0	0.05	1.0

## 2.5 Recycled aggregate concrete mix design methodologies

One of the biggest hurdles to the increased use of RCA in concrete applications is a lack of guidance on how to proportion RAC utilizing obtained characteristics of RCA. There is a strong need for a mixture design methodology that consistently provides desired fresh, mechanical, and durability properties. Commonly used RAC mix design procedures found in literature can be divided into several categories:

1. Direct replacement methods
2. Methods that consider RCA as a two-phase material
  - a. Equivalent mortar replacement method
  - b. Equivalent coarse aggregate mass method
3. Particle packing methods
4. Empirical (experimental) methods

### 2.5.1 Direct replacement methods

In direct replacement methods, RCA is considered a one-phase material, and no RCA characterization such as RMC is taken into account. There are two widely used direct replacement

methods: direct weight replacement (DWR) and direct volume replacement (DVR). Both methods allow the full (100%) replacement of NA by RCA. In the DWR method, the total weight of coarse aggregate in the mixture, i.e., the combined weight of NA and RCA, the effective amount of water, and cement content, are all kept constant for any replacement ratio. When RCA replacement occurs, due to the lower specific gravity of RCA compared to NA, the volume of coarse aggregate in the mixture can slightly increase. Therefore, the amount of fine aggregate has to be reduced to obtain the same volumetric yield. Because of the slight increase of coarse aggregate volume, workability is generally compromised with the increased replacement ratio. However, according to Knaack and Kurama (2013), in spite of reduced workability, the concrete is still adequately workable to be cast. In the DVR method, the total volume of coarse aggregate, no matter the replacement ratio, is held constant. This method allows the volumes of the remaining concrete ingredients remain exactly the same, which consequently leads to a minimal/negligible workability loss. However, both strength and elastic modulus reductions were reported in DWR and DVR methods (Knaack and Kurama 2013).

### **2.5.2 Methods that consider RCA as a two-phase material**

Unlike the direct replacement methods, in the equivalent mortar replacement (EMR) method, RCA is considered a two-phase material made of original NA and a residual mortar attached to them. In this method, the total mortar volume (fresh mortar and residual mortar from RCA) is kept constant, i.e., with the increased residual mortar (either from increased replacement ratio or RCA quality), the amounts of fine aggregate, cement, water are proportionally decreased (Fathifazul et al. 2009). This method allows to decrease or eliminate loss of mechanical properties (compressive strength and elastic modulus) in RAC. However, due to decreased fresh mortar amount, this method results in a significant workability loss, which limits the replacement ratio to about 20% (Knaack and Kurama 2013).

Gupta et al. (2015) proposed a new method called equivalent coarse aggregate mass (ECAM) replacement. In this method, RCA is also considered a two-phase material. In this method, NA is replaced by RCA, with the mass of NA being replaced set equal to the mass of natural aggregate within RCA. Unlike the EMR method, this method states that the residual mortar cannot be considered as a part of the total volume due to the fact that cement in the residual mortar has lost its binding ability and can only act as inert material. Therefore, in the ECAM method, the residual mortar is considered as a part of the total fine aggregate amount. With the increased



replacement ratio, the amount of fine aggregate reduces, while the amounts of cement and water are held constant. Considering residual mortar as a part of the fine aggregates has an advantage over direct replacement methods as it does not negatively influence mechanical properties. In addition, the ECAM method recommends a maximum 50% replacement ratio.

### **2.5.3 Particle packing methods**

Another way of proportioning RAC without compromising mechanical properties is to incorporate particle packing theory to enhance the granular skeleton of the mix. Although several particle packing methods of mixture proportioning have been suggested, the Compressive Packing Model (CPM) seems to be the most commonly used one (Pradhan et al. 2017, Amario et al. 2017). However, the extent to which different researchers used the CPM differs. The CPM developed by De Larrard (1999) is capable of not only obtaining the packing degrees but also proportioning concrete mixtures to achieve desired fresh and mechanical properties. Pradhan et al. (2017) used the excess paste theory, which states that to provide sufficient workability, in addition to the paste that fills the voids among aggregates, an excess paste is required. They used a CPM approach just to obtain packing degrees of different aggregate blends and used an excess paste amount of 16% to proportion RAC based on trial tests. Amario et al. (2017) used a special software developed based on CPM to proportion RAC. However, only a few constants related to aggregate strength were empirically obtained in the concrete strength prediction equation. Moreover, while Amario et al. (2017) used the CPM to obtain the optimum replacement ratio, Pradhan et al. (2017) used a 100% replacement ratio of RCA and used the CPM to obtain the optimum blend of different RCA size fractions. While one study (Amario et al. 2017) resulted in reasonable workability and mechanical properties (due to a low replacement ratio), another study (Pradhan et al. 2017) resulted in compromised workability and reduced strength.

### **2.5.4 Empirical (experimental) methods**

Another way to develop a mixture design procedure is to rely completely on experimental data and design an empirical model. Hu et al. (2013) developed a nomograph-based mix design procedure for concrete with recycled aggregate from deconstructed lead-contaminated masonry materials. The authors used Abram's law, Lyse's law, and Molinari's law along with the data from 48 RAC mixtures, to develop a mix proportioning procedure to achieve desired fresh and strength properties.

## CHAPTER 3. EXPERIMENTAL PROGRAM

### 3.1 Aggregates Collection

A variety of different RCAs in terms of RMC, crushing value, and air-entrainment of parent concrete, were collected from multiple states (Nebraska, North Carolina, Iowa, and Texas). A limestone aggregate from Nebraska and a granite aggregate from Nevada were used as NA for comparison. For most tests, aggregates were tested for each sieve size individual for better accuracy. Fraction size is defined as the sieve size aggregate retained after passing the larger followed sieve size. For example, 1/2" size aggregate refers to the aggregate passed 3/4" sieve and retained on 1/2" sieve. Figure 4 illustrates the aggregate identification scheme.

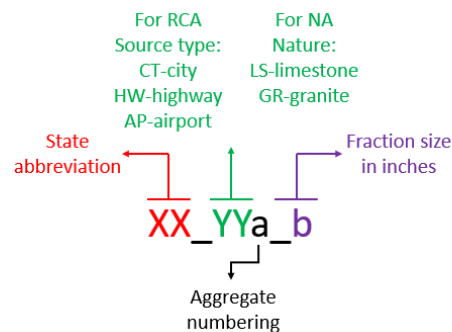


**Figure 4 Aggregate identification**

Table 9 and Figure 5 presented the twelve aggregates (2 NA and 10 RCA) collected for this study. Images presented were taken before sieving aggregates into different sizes.

**Table 9 Sources and information of collected RCA specimens**

Aggregate ID	State	Source	Crushing method
NE_LS	Nebraska	-	-
NV_GR	Nevada	-	-
NE_HW1	Nebraska	Highway 30	-
NE_HW2	Nebraska	Highway 75	-
NE_CT1	Nebraska	Heims city	Both jaw and impact crusher
NE_CT2	Nebraska	Fucinaro	Primary: jaw crusher (to 8" and smaller) Secondary: impact crusher (to 1.5" and smaller)
NC_CT1	North Carolina	DH Griffin	Primary: jaw crusher (to 5" and smaller) Secondary: cone crusher (to 3" and smaller)
NC_CT2	North Carolina	Coastal aggregate	Impact crusher
NC_AP1	North Carolina	Charlotte Airport	Primary: jaw crusher; Secondary: impact crusher
NC_HW1	North Carolina	Highway I-40	-
IA_CT1	Iowa	City pavement	-
TX_CT1	Texas	-	-

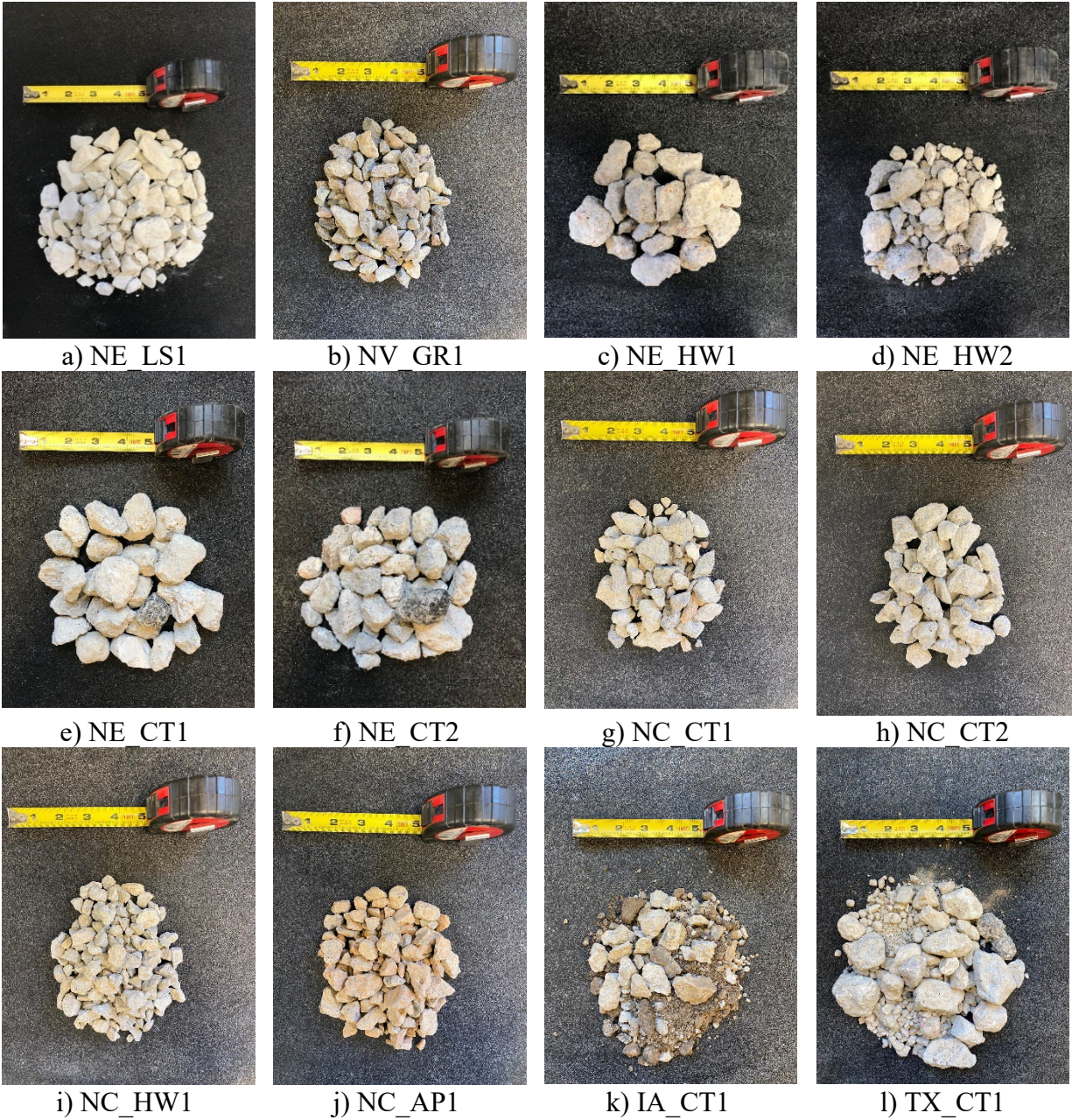


**Figure 5 Images of collected RCA specimens**

### **3.2 Test methods for aggregates**

Based on the efficiency and effectiveness of test methods for different RCA characteristics (as described in Chapter 2), several test methods, as specified in Table 10, were selected for inclusion in the experimental program.

**Table 10 Proposed tests for RCA characteristics**

Test Methods	Standards	Equipment
Specific gravity, absorption, and absorption speed	ASTM C127 and C128	Specific gravity test set
Void content (Coarse)	ASTM C29	Aggregate unit weight measures
Shape and texture	-	AIMS2
Crushing value	Modified BS 812-110	Crushing value test set, compressive machine, vibrating table
Residual mortar content	-	Furnace, jar mill
FT resistance	CSA 23.2-24A	Freezer
Chemical composition	-	PHXRF

### 3.2.1 Specific gravity and absorption

The specific gravity and absorption properties of NA and RCA were obtained in accordance with ASTM C127 and ASTM C128, respectively. In order to better correlate specific gravity and absorption to other properties such as RMC and crushing value, the tests were performed for each sieve size (1", 3/4", 1/2", 3/8", and No. 4) separately for more. During concrete mixture design, a weighted average was taken based on the gradation of the specific RCA.

In addition, in order to obtain information on the speed of water absorption, the absorption rate of RCA was evaluated. In this test, the oven-dried aggregate sample was placed in a pycnometer, and water was subsequently added to the top of the lid (Figure 6). As the RCA began to absorb water, the water level drop became noticeable. By adding water to the original level, the water absorption rate in real-time can be assessed. The same procedure was used by Tam et al. (2008). The readings were taken at 2, 5, 15, 30, 60 mins, and 2, 6, 12, 24, 48, 72 hours. The absorption ratio ranges from 0 to 1, where 0 is an oven-dry condition, and 1 is a fully saturated condition. It can be calculated as follows:

$$Absorption\ ratio = \frac{\frac{M_t - M_0}{M_{OD}} * 100\ (\%)}{\frac{M_f - M_0}{M_{OD}} * 100\ (\%)} \quad (Eq. 10)$$

Where,  $M_0$  is the initial mass ( $t=0$ ) of the setup (pycnometer, RCA sample, and water),  $M_t$  is the mass of the setup at a given time,  $M_f$  is the final mass ( $t=72$  hours) of the setup, and  $M_{OD}$  is the mass of an oven-dried sample. Once the seven data points were obtained, a graph of absorption ratio versus time was plotted to describe the absorption speed.





**Figure 6 Aggregate absorption rate test setup**

### **3.2.2 Void content**

Bulk density and void content properties were determined according to ASTM C29. In addition to the uncompacted procedure that is usually used for RCA, a vibration plus pressure method was used due to a better correlation with the Modified Toufar scientific model (Mamirov et al. 2021).

### **3.2.3 Shape and texture**

RCA shape and texture parameters were obtained using the AIMS2 machine (Figure 7). The test was performed for each size fraction of RCA (1", 3/4", 1/2", 3/8", and No. 4) separately. The main parameters obtained from the AIMS2 machine are angularity, sphericity, texture, flat and elongated particle distribution. Prior to testing, each aggregate sample was carefully prepared by removing any contaminants such as asphalt, brick, wood, and metal. For comparison purposes, this test was also performed for NA.

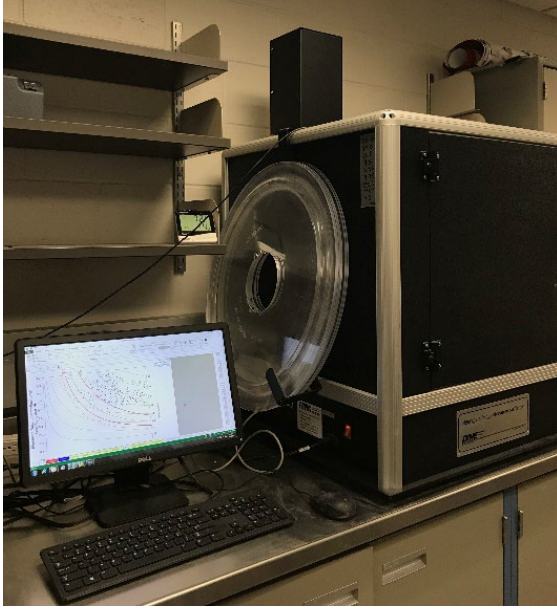


**Figure 7 Aggregate Image Measurement System setup**

### *Angularity*

Gradient angularity is evaluated by determining the quantity of changes along a particle boundary and is related to the sharpness of the corners of particles' 2D images. A higher gradient value indicates a more angular shape.

$$Angularity = \frac{1}{\frac{n}{3}-1} \sum_{i=1}^{n-3} |\theta_i - \theta_{i+3}| \quad (\text{Eq. 11})$$

Where  $\theta$  is an angle of orientation of the edge points, and  $n$  is the total number of points. Figure 8 demonstrates different angularity rankings.

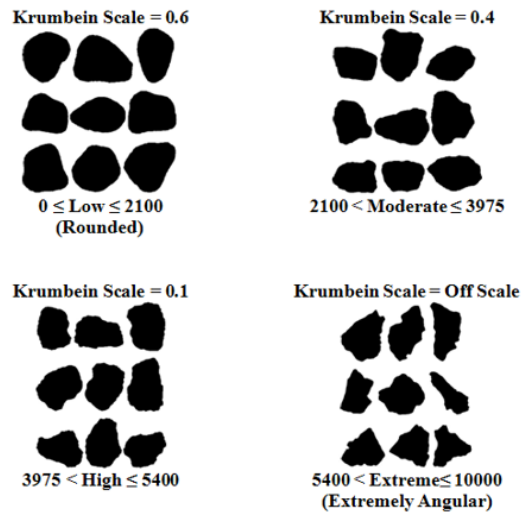


**Figure 8 Aggregate angularity rankings (adapted from the AIMS2 Manual)**

### *Sphericity*

Sphericity is the parameter describing the overall 3D shape of a particle. Sphericity has a relative measurement, ranging from 0 to 1, where 1 indicates a particle with equal dimensions.

$$Sphericity = \sqrt[3]{\frac{d_S d_I}{d_L^2}} \quad (\text{Eq. 12})$$

Where,  $d_S$ ,  $d_I$ , and  $d_L$  are the particle's shortest, intermediate, and longest dimensions, respectively.

### *Texture*

Texture is the parameter representing the relative smoothness or roughness of particles. It has a relative scale from 0 to 1000, where the higher value indicates a rougher surface. The AIMS2 texture analysis utilizes the wavelet method to quantify texture (Gates et al. 2011). The texture value is the arithmetic mean of the squared values of the wavelet coefficients for horizontal, vertical, and diagonal directions. Figure 9 shows different texture rankings.

$$Texture = \frac{1}{3N} \sum_{i=1}^3 \sum_{j=1}^N (D_{i,j}(x, y))^2 \quad (\text{Eq. 13})$$

Where  $D$  is decomposition function,  $n$  is decomposition level,  $N$  is the total number of coefficients in an image,  $j$  is wavelet index,  $x, y$  is the location of the coefficients in the transformed domain.

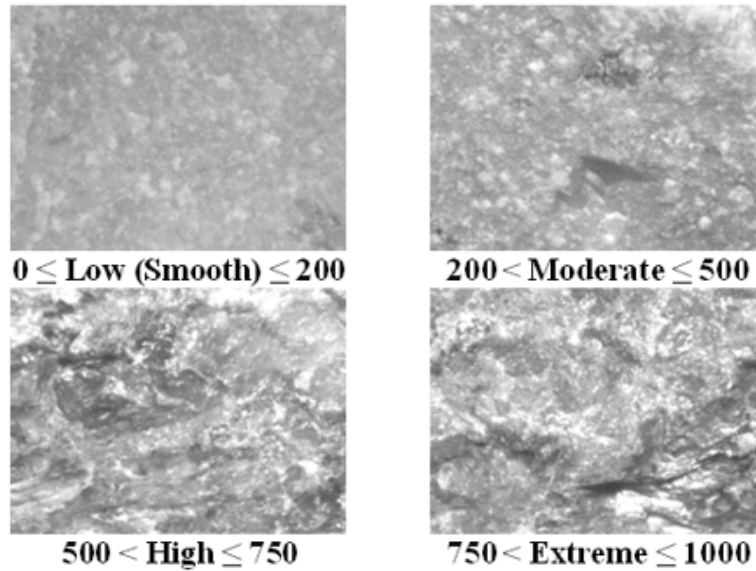


**Figure 9 Aggregate texture rankings (adopted from AIMS2 Manual)**

#### *Flat and/or elongated distribution*

Flatness ratio and elongation ratios can be described as follows:

$$Flatness = \frac{d_s}{d_I} \quad (Eq. 14)$$

$$Elongation = \frac{d_I}{d_L} \quad (Eq. 15)$$

Where,  $d_s$ ,  $d_I$ , and  $d_L$  are the particle's shortest, intermediate, and longest dimensions, respectively. AIMS2 can provide a distribution of either "flat and elongated" or "flat or elongated particles".

### **3.2.4 Aggregate crushing value**

#### *Background*

The residual mortar fraction of RCA is softer than the aggregates, causing RCA to exhibit a lower stiffness than most NA. Therefore, aggregate crushing value tests designed for NA cannot be used. The maximum applied load mentioned in the standard method for determination of ACV (BS 812-110) load at 90 kips is too high for RCA, which results in RCA test specimens being smashed into a compacted disc that is difficult to remove after the test. Butler (2012) used a mallet to strike out the crushed RCA disc from the steel ring after the test. However, this approach could introduce a human factor into the test since this mechanical action can cause an additional and uncertain crushing of RCA. Additionally, due to the varying nature of RCA with different sizes even within the same source, it is believed that the crushing value test for RCA should be performed for all size fractions, not only for the 3/8" size as the standard specifies. Therefore, it is important to modify the procedure of the crushing value test so it can be implemented for RCA.

#### *Procedure selection*

The testing matrix included varying two factors, i.e., the maximum applied load (90 kips, 45 kips, and 30 kips) and the height of the sample in the steel ring (4 in., and 2 in.). The initial study was conducted on a 3/4" size RCA. The test was performed by placing RCA inside the steel ring up to a given height and compacting the RCA specimen with rodding. A load was then applied at a rate of  $0.35 \pm 0.05$  in./min until the maximum load was reached. The steel ring with the crushed RCA was placed on a vibrating table until the crushed RCA was loosened. If vibration was ineffective within 2 minutes, the crushed RCA was removed by means of rodding. Then, the



crushed RCA was sieved using a No. 8 sieve to obtain the crushing value, which is the percentage (by weight) of crushed material (passing No. 8 sieve).

Table 11 demonstrates the comparison of the six procedures used, and Figure 10 illustrates the displacement of RCA samples during the test. As expected, the lower the total displacement, the easier it was to remove the crushed RCA from the steel ring. When 90 kips and 45 kips load were used, the use of the vibrating table did not successfully separate the crushed RCA from the ring, and rodding action was necessary to loosen the crushed RCA. Applying a load up to 30 kips to a 2 in. tall specimen (Procedure 6) seemed to be a reasonable option due to the effective crushing of RCA and the relative ease of removing the crushed RCA from the steel ring without requiring a manual effort that could introduce human factor variability into the method.

**Table 11 Summary of the procedure comparison for crushing value test**

Procedure	Sample height (in.)	Applied load (lb)	Vibrating time required to remove RCA from the ring (sec)	Difficulty to remove RCA
1	4	90,000	-	Very difficult
2	2	90,000	-	Very difficult
3	4	45,000	-	Difficult
4	2	45,000	-	Difficult
5	4	30,000	120	Medium
6	2	30,000	30	Easy

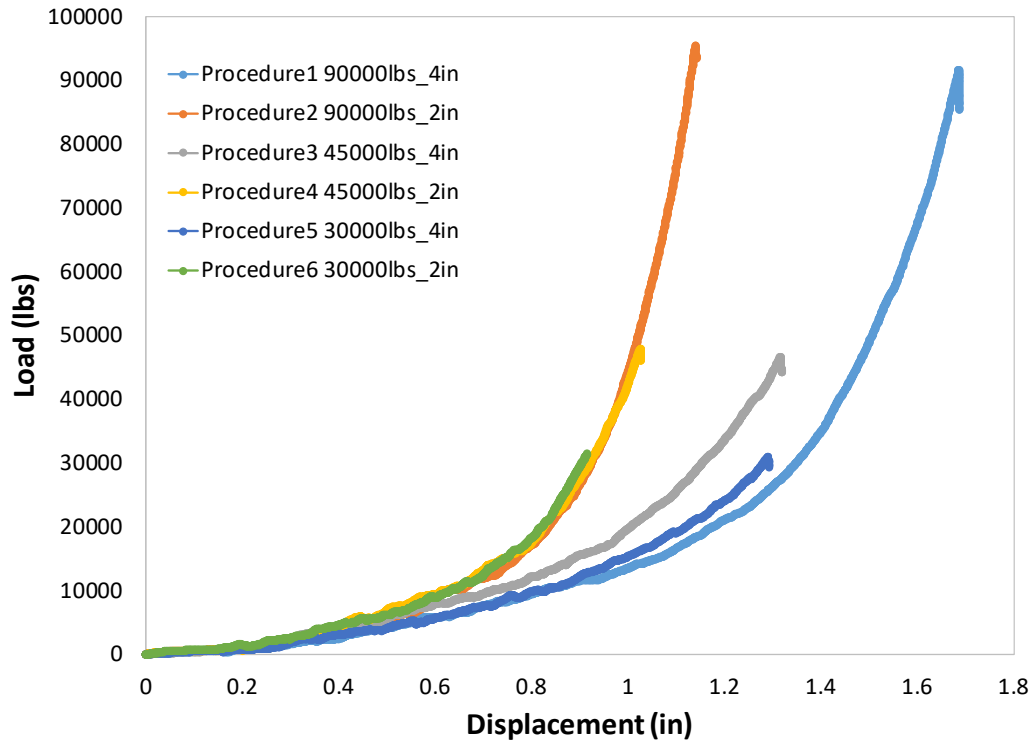


**Figure 10 Displacement of RCA samples at different procedures**

Once the optimal procedure approach was identified, it was used to evaluate other sizes of RCA (1", 1/2", 3/8", and No. 4 in addition to already tested 3/4") to demonstrate its feasibility for use in testing of RCA of different size fractions. As shown in Table 12, 30-40 seconds of vibrating appears to be sufficient to remove each size of the RCA from the steel ring. Figure 11 shows the difference in displacement for different RCA sizes. As expected, the smaller the size of the RCA, the lower the total displacement due to the higher packing degree.

**Table 12 Vibration time requirement for separating crushed RCA samples.**

RCA size	Vibrating time required (sec)
1"	30
3/4"	30
1/2"	40
3/8"	40
#4	40

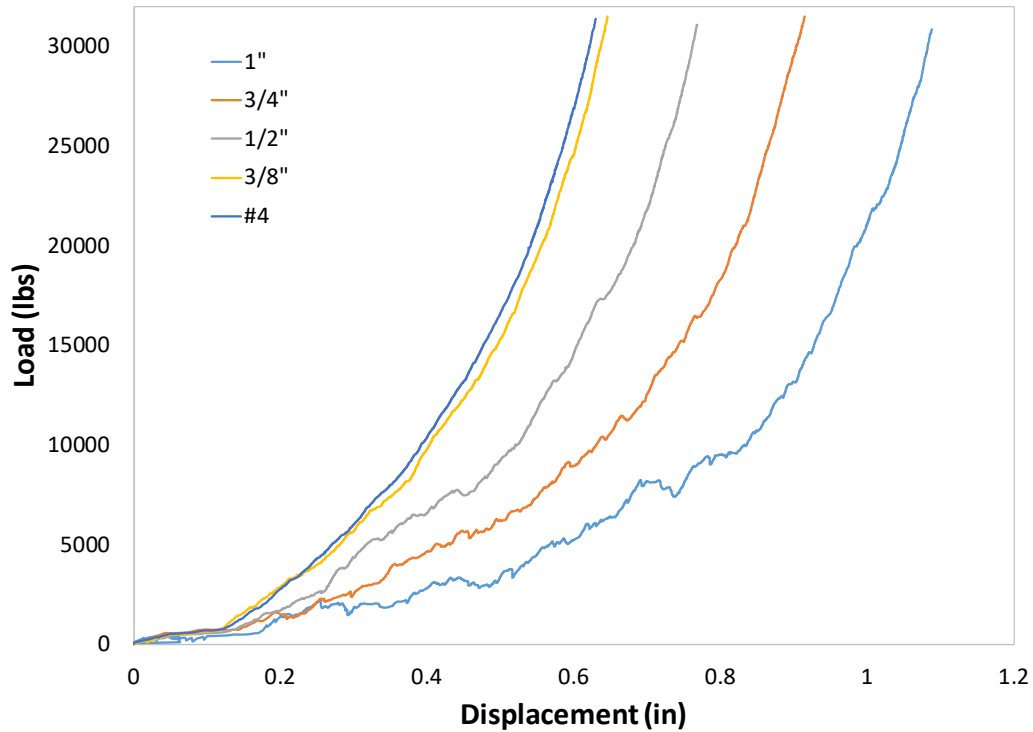


**Figure 11 Displacement comparison for different RCA sizes during crushing value test**

*Finalized test procedure*

Based on the findings of the analysis performed, the following procedure for an RCA crushing test is recommended:

1. Place single-sized RCA sample inside the steel ring up to 2 in. height and rod them 25 times to compact (Figure 12a).
2. Apply load at  $0.35 \pm 0.05$  in/min until the load of 30 kips is reached, followed by an immediate load release (Figure 12b).
3. Place the steel ring with the crushed RCA on a vibrating table for 30-40s (Figure 12d).
4. Sieve the crushed RCA using a No. 8 sieve (Figure 12e).
5. Calculate the ACV as a weight percentage of particles that passed the No. 8 sieve.
6. Repeat the procedure for all coarse sizes of the same RCA source (1", 3/4", 1/2", 3/8", and No. 4)
7. Take the weighted average based on the gradation to obtain the final ACV.



a) Placing sample in a steel ring



b) Applying load



c) Sample appearance after crushing process



d) Vibrating a sample



e) Sieving a sample



f) Crushed amount

**Figure 12 Aggregate crushing value test setup**

### 3.2.5 Residual mortar content

The RMC is one of the most important RCA properties affecting other properties such as absorption, specific gravity, resistance to crushing, and abrasion. As mentioned in the previous chapter, current RMC measurement methods include chemical dissolution of residual mortar (sodium sulfate, hydrochloric acid, sulfuric acid, etc.), residual mortar disintegration through thermal methods (thermal shock, freeze/thaw), and image analysis techniques (optical microscope, computed tomography, image analysis software). Based on the efficiency in terms of time, equipment, and relative simplicity, the thermal shock method was selected for determining the RMC for RCA in this study.

#### *Procedure selection*

The thermal shock method was used by de Juan et al. (2008), Butler et al. (2011), and Pepe et al. (2014). However, there is a lack of a detailed description of the procedure, including important parameters such as the sample size, amount and temperature of water RCA are soaked

in, and time of soaking RCA after heating. Moreover, in this procedure, the step of manually removing residual mortar after thermal shock is performed utilizing a rubber hammer to scratch the surface. Besides being labor-intensive, this approach introduces a source of human error. The authors listed above also did not provide a method of determining that mortar was completely removed other than the use of visual inspection. Therefore, the research team determined it is necessary to develop a detailed procedure to support the RMC measurement by the thermal shock method. The main parameter in this test is the temperature of heating, and efforts were made to determine an optimal temperature for the recommended method.

Cement paste exposed to high temperatures experiences dehydration that leads to a decrease in strength and increased pore pressure. In addition to this, when a sudden temperature drop is introduced, thermal shock occurs, and cement paste becomes extremely brittle and detached from the aggregate. As an example, Figure 13 shows one RCA particle subjected to thermal shock and separation of residual mortar from original NA by means of crushing. It can be seen that one original RCA particle (on the left) can be effectively broken down into six smaller coarse particles and residual mortar (on the right).



**Figure 13 Example of RCA mortar disintegration after temperature shock**

It is important to carefully select the right temperature at which the cement paste will fully dehydrate, while the original NA remains intact. According to Zhang et al. (2012), the dehydration of C-S-H and C-H occurs at 105-1000°C and 400-550°C, respectively. Alonso et al. (2004) stated that C-S-H gel is completely disintegrated at 750°C. According to Xing et al. (2011), most of the NA does not crack under heating until 750°C. Therefore, it was decided to explore the effectiveness

of different temperatures starting from 500°C as suggested by de Juan et al. (2009) and then gradually increase the temperature by 50°C intervals until 750°C or until the complete residual mortar removal, whichever occurred first.

Regardless of the temperature used, the procedure starts with the preparation of a 500g representative sample of coarse (retained on No. 4 sieve size and above) RCA with any contaminants such as asphalt, brick, wood, and metals removed prior to the test. Then, the RCA sample is soaked in 23±2°C water for two hours to provide additional vapor pressure during heating. After soaking, the RCA sample was placed in a muffle furnace for 2 hours, which was preheated to the desired temperature in advance (Figure 14a). Once 2 hours of the heating process is completed, the RCA sample is submerged in 1350g of 23±2°C water for 0.5 hours to generate thermal shock (Figure 14b). Then the RCA sample is placed in an oven to dry at 110±5°C for 24±4 hours. The removal of residual mortar, which becomes very brittle after a thermal shock, is performed using a jar mill to eliminate the human factor. The RCA sample is ground in the jar mill with 575g of 13/16" × 13/16" cylindrical alumina grinding media at 70 rpm speed and is regularly checked for progress. Once the residual mortar is removed, the RCA sample is sieved using a No. 4 sieve (Figure 14d) to separate natural coarse aggregate (Figure 14e) and removed residual mortar (Figure 14f). The RMC is then calculated as follows:

$$RMC (\%) = \frac{\text{Mass of material passed \#4 sieve}}{\text{Total mass}} \times 100\% \quad (\text{Eq. 16})$$





a) Heating process



b) Submerging in water



c) Removing mortar by grinding



d) Sieving process



e) Original NA in RCA










f) Removed residual mortar

**Figure 14. RMC measurement by thermal shock method**

#### *Heating temperature and grinding time selection*

Four RCA samples from the same source were tested to determine the RMC using the procedure above with varying heating temperatures. Removal of the residual mortar was monitored by stopping the grinding process and sieving out the removed mortar every 2, 5, 10, 20, 40, 100, 160, 220 minutes unless no significant change in RMC between two adjacent readings was observed before that. It can be seen from Table 13 that when 500°C and 550°C heating temperatures were used, there were some mortar particles that were not broken down and separated. At the 600°C temperature, no mortar particles could be observed, and only NA with a minimum amount of mortar on the surface was observed. At 650°C, however, a complete residual mortar removal occurred.

**Table 13 Residual mortar removal at different heating temperatures**

	500°C	550°C	600°C	650°C
Time of grinding	220 min	160 min	160 min	160 min
Original NA after residual mortar removal				
Aggregates/mortar particles failed to be cleaned/broken down				None

According to the mortar removal monitoring results presented in Figure 15, 100 minutes of grinding appears to be sufficient, since there was no significant change observed after that. It is also can be noticed that the procedure using a 650°C heating temperature resulted in the highest level of mortar removal, as mentioned previously.

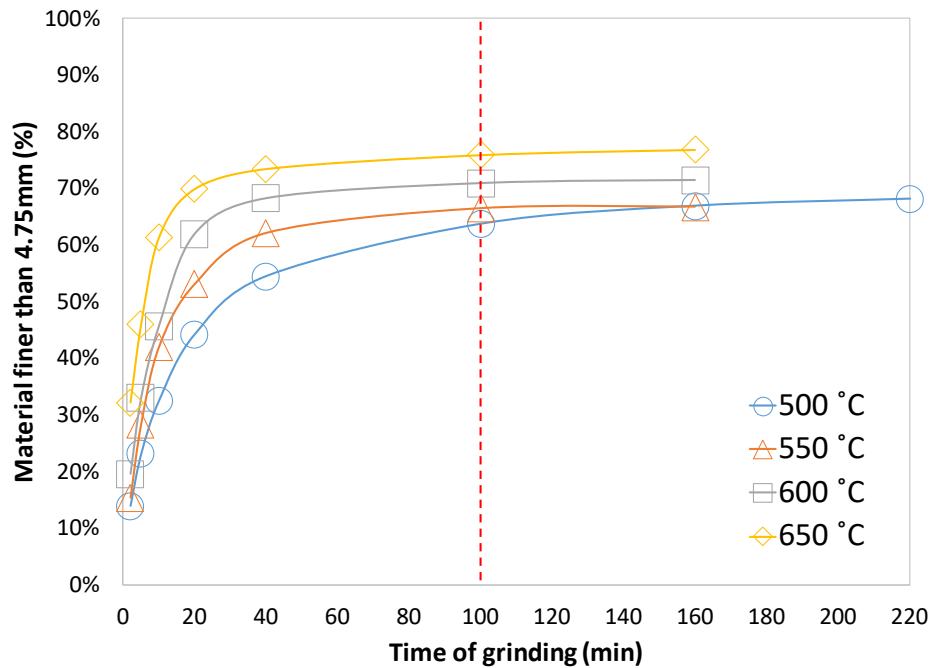


**Figure 15 Residual mortar removal over grinding time**



To justify the 100 minutes grinding time requirement, a sample of RCA was evaluated using the selected 650°C heating temperature. Since the residual mortar is rougher in texture compared to most NA (Butler 2012), the residual mortar removal rate can be justified by monitoring the change in the surface texture of RCA. Aggregate Image Measurement System 2 (AIMS2) was used to quantify the surface texture

The test was run before the grinding and after 20, 80, 100, and 140 minutes of grinding. The test was performed for particles of each sieve size individually; therefore, at the abovementioned time intervals, RCA was sieved into 1", 3/4", 1/2", 3/8", No. 4 sieve sizes. By determining the mass of passing No.4 sieve size particles, the residual mortar removal rate (by mass) could also be determined. Results shown in Figure 16 demonstrated that initially, the surface texture index ranged from 230 to 300 with an average of approximately 250. After 20 minutes of grinding, there were no more 1" particles left, since they were broken down into smaller pieces. This is likely the reason that an increase in the texture of 1/2" particles was observed. As expected, particles of other sizes had reduced surface texture. The surface texture of all particles continued to decrease until the 100 minutes grinding threshold, after which no significant change was observed, i.e., the residual mortar was completely removed. As an example, Figure 17 illustrates the visual change in the texture of two particles over the grinding period. The findings of visual observations while monitoring the residual mortar removal were consistent with the fact that no mass change was observed after 100 minutes of grinding. Thus, it can be concluded that with the configuration of the jar mill and the RCA used in this study, 100 minutes of grinding is the optimum time to remove the residual mortar of RCA after thermal shock at the temperature of 650°C.

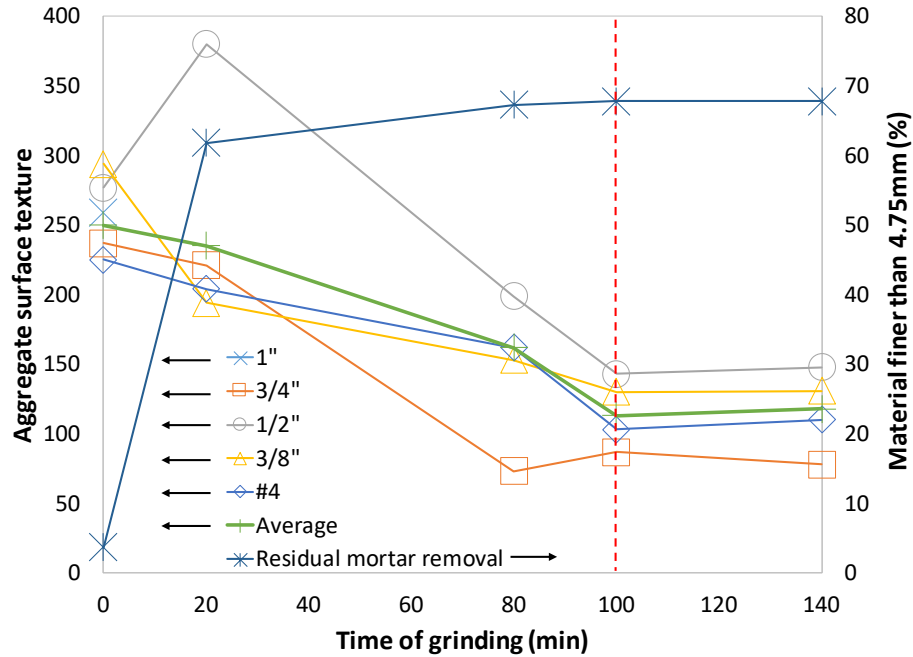


**Figure 16 Aggregate surface texture change over grinding time**

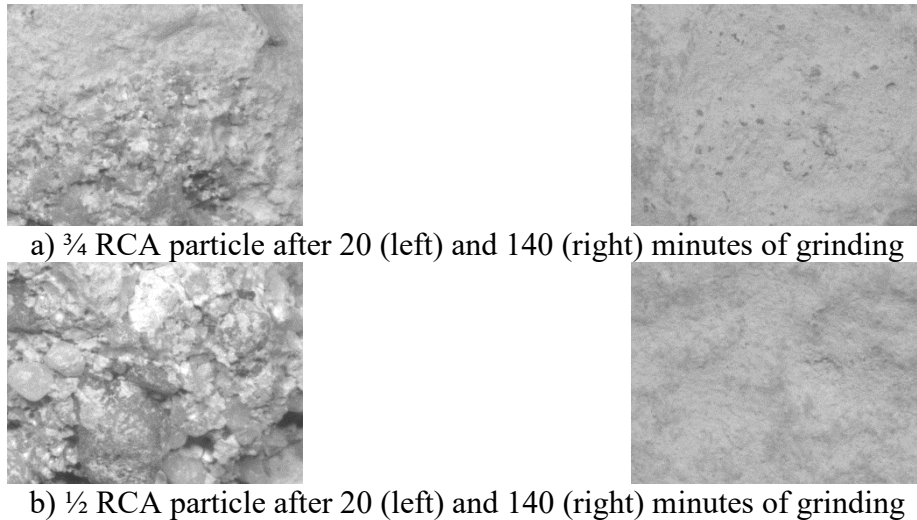


**Figure 17 Effect of grinding on RCA texture**

#### *Justification of jar mill configuration*

In order to ensure that the proposed procedure is reasonable, it was decided to examine if the specified thermal shock and following grinding in a jar mill will result in a significant mass loss of original NA that can potentially interfere with the measurements of RMC. Nebraska limestone, Nebraska granite, and Nevada granite with the maximum sizes of 1", 1", and 3/4" respectively were used in this study. The same amount of these aggregates were subjected to the same environment as RCA, and material loss was evaluated at 2, 5, 10, 20, 40, 100, and 160

minutes. As shown in Figure 18, the highest material loss was experienced by Nebraska limestone (1.42%), followed by Nevada granite (0.88%) and Nebraska granite (0.31%). It can be concluded that the impact of the material loss of original NA is negligible, at least for those included in this study. RCA containing soft or highly abrasive NA could potentially have an additional loss.

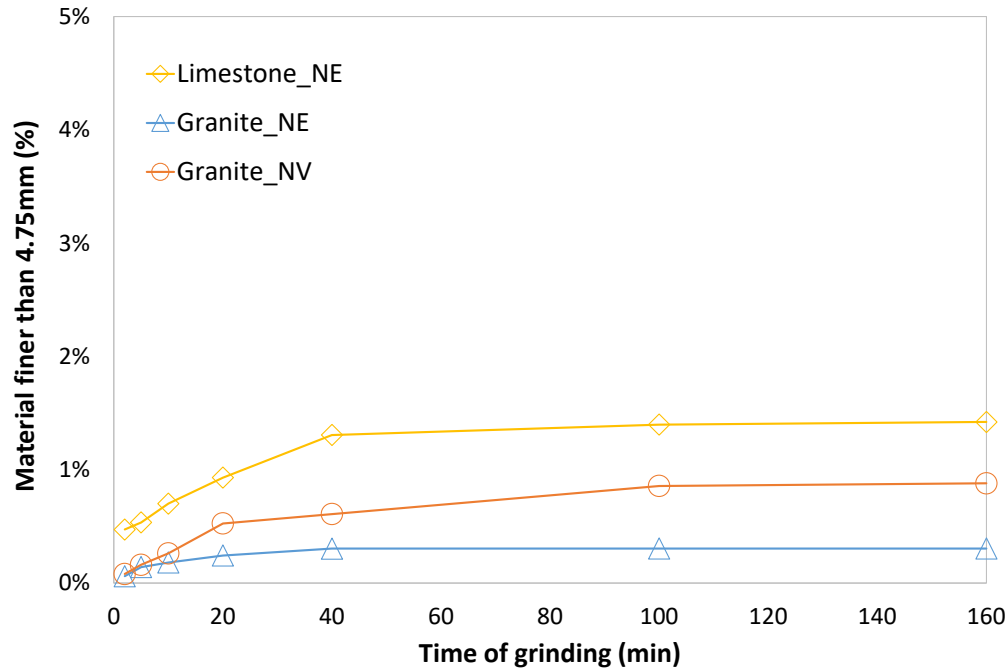


**Figure 18 Effect of thermal shock and grinding on the material loss of NA**

#### *Justification of used amount of water*

Once the procedure for the RMC measurement was established, it was decided to evaluate the effect of the amount of water used for soaking the heated RCA on the residual mortar removal and the potential decrease in required grinding time. Instead of 1350g, 5000g of water was used to soak the RCA. As expected, the residual mortar was completely removed in both cases. Figure 19 shows that the time required to remove the residual mortar has not decreased with the higher amount of water used, and remained to be 100 minutes, meaning that increasing the amount of water used for the soaking step does not have a positive impact on the test procedure. Oppositely, it had a negative effect on the test, because it was observed that some of the original NA particles within RCA became too brittle and were broken into pieces, experiencing too large of a thermal shock (Figure 20).

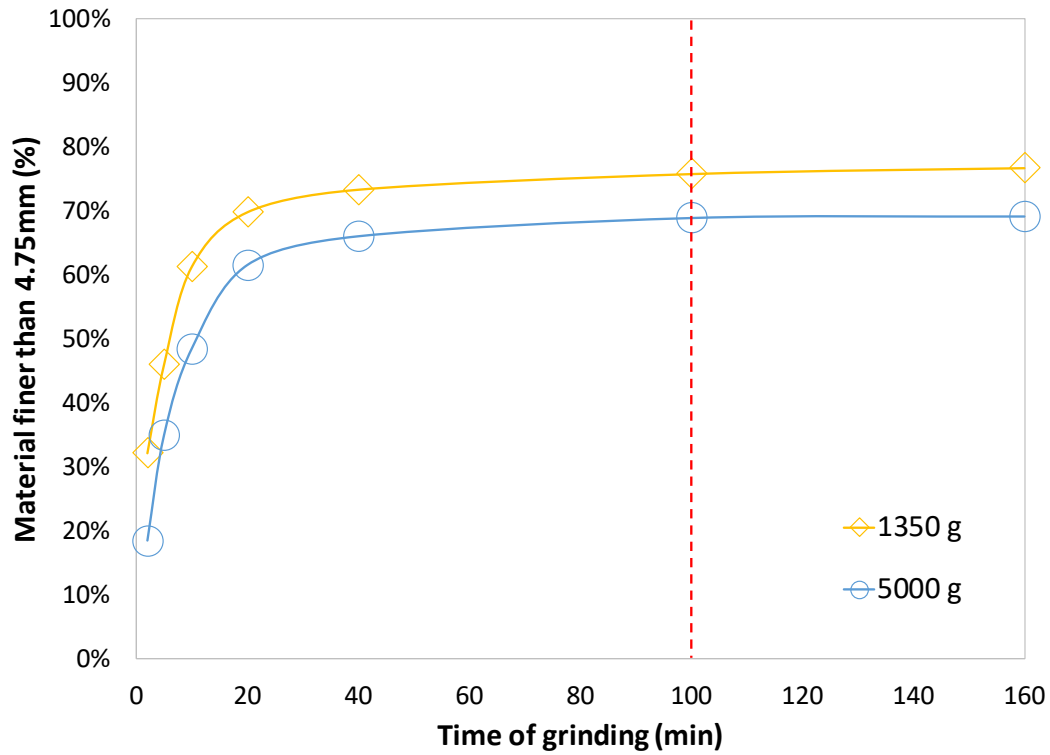


**Figure 19 Impact of soaking water amount on the residual mortar removal rate**



**Figure 20 Example of natural aggregate becoming too brittle**

*Recommended test procedure*

The recommended test procedure of the thermal shock method to determine the RMC is as follows:

1. Carefully prepare  $500 \pm 25$  g of a single-sized coarse RCA (1", 3/4", 1/2", 3/8", No. 4 for this study) by removing any contaminants such as asphalt, brick, wood, and metal. For aggregate sizes larger than 1", it is recommended to increase the sample size to have a more representative specimen.
2. Soak RCA in  $23 \pm 2^\circ\text{C}$  water for 2 hours.

3. Preheat a furnace to 650°C.
4. Remove RCA from water and place it in the preheated furnace, and allow the RCA to heat at 650°C for 2 hours.
5. Submerge the heated RCA instantaneously upon removal from the furnace in 23°C water for 0.5 hours with water-to-RCA ratio of 2.70 (by mass).
6. Drain the RCA sample, and allow it to oven-dry at 110±5 °C for 24±4 hours.
7. Place RCA in a jar mill with 3/16” by 13/16” cylindrical alumina grinding media and grind it at 70 rpm speed for 100 minutes (approximately 1/1 sample-to-grinding medium ratio).
8. Sieve the RCA sample using a No. 4 sieve to separate residual mortar from the original NA
9. Calculate the RMC using the following equation:

$$RMC (\%) = \frac{\text{Mass of material passed \#4 sieve}}{\text{Total mass}} \times 100 \quad (\text{Eq. 17})$$

### 3.2.6 Freeze-thaw resistance

The Freeze-thaw resistance test was performed based on CSA A23.2-24A. Since the purpose of performing this test is to determine whether the parent concrete of RCA was air-entrained, only one size of RCA particles (1/2” was used for each RCA source. The procedure can be summarized as follows:

1. Carefully prepare the oven-dried RCA sample (2.75lb) by removing any contaminants such as asphalt, brick, wood, and metal.
2. Place the oven-dried RCA sample in appropriately sized (0.25 gallon in this case) containers.
3. Fill the containers with the prepared 3% sodium chloride solution to completely immerse all aggregate particles. Containers should then be sealed and kept at room temperature for 24 hours (Figure 21b).
4. Drain the solution by inverting a container over a screen smaller than 0.2 in. mesh (Figure 21c).
5. Seal the container and place it in a freezer at -18°C for 16 hours (Figure 21d).
6. Remove the container from the freezer and allow the contents to thaw at room temperature for 8 hours (Figure 21e).
7. After five cycles of freezing-thawing, the RCA sample should be washed by filling the container with tap water, and draining the container by inverting it over a 0.2 in. mesh for

5 seconds. This step is repeated five times to ensure the RCA particles are thoroughly washed.

8. Oven-dry the sample at 110°C.
9. Sieve the oven-dried RCA sample using an appropriate sieve (1/2" in this case), and mass loss is recorded (Figure 21f).

$$FT \text{ mass loss (\%)} = \frac{\text{Mass of the material passed 12.5 mm}}{\text{Initial mass of the sample}} \times 100 \quad (\text{Eq. 18})$$



a) RCA sample preparation



b) Soaking RCA in NaCl solution



c) Draining solution using a screen mesh



d) Freezing RCA



d) Thawing RCA



d) Sieving RCA

**Figure 21 FT resistance of aggregates test setup**



### **3.2.7 Handheld XRF for chemical characterization**

#### *Approach and Data Analysis*

PXHRF data was used to develop models to estimate the mortar content and chemical composition of each RCA sample. Model predictions were compared to reference values obtained via laboratory testing. The reference values for the composition of each RCA sample, including mortar (alone), coarse aggregate (alone), and fine aggregate (alone) were determined using the results of the thermal shock method (to determine mortar content) and chemical composition by weight percent (whole rock analysis). By comparing PHXRF results to values determined by outside laboratories using more extensive, time-consuming techniques, the accuracy and repeatability of the results obtained from the PHXRF could be evaluated, and selected sample preparation and analysis techniques refined into a recommended testing protocol. This approach is shown in Figure 22. An additional “reference sample” was considered to be the test results from the PHXRF testing of the mortar (alone) and aggregate (alone) removed from each RCA sample. Although this approach does not provide an indication of the accuracy of the device, it should provide insight into the repeatability of results of testing fractionated sizes of RCA.

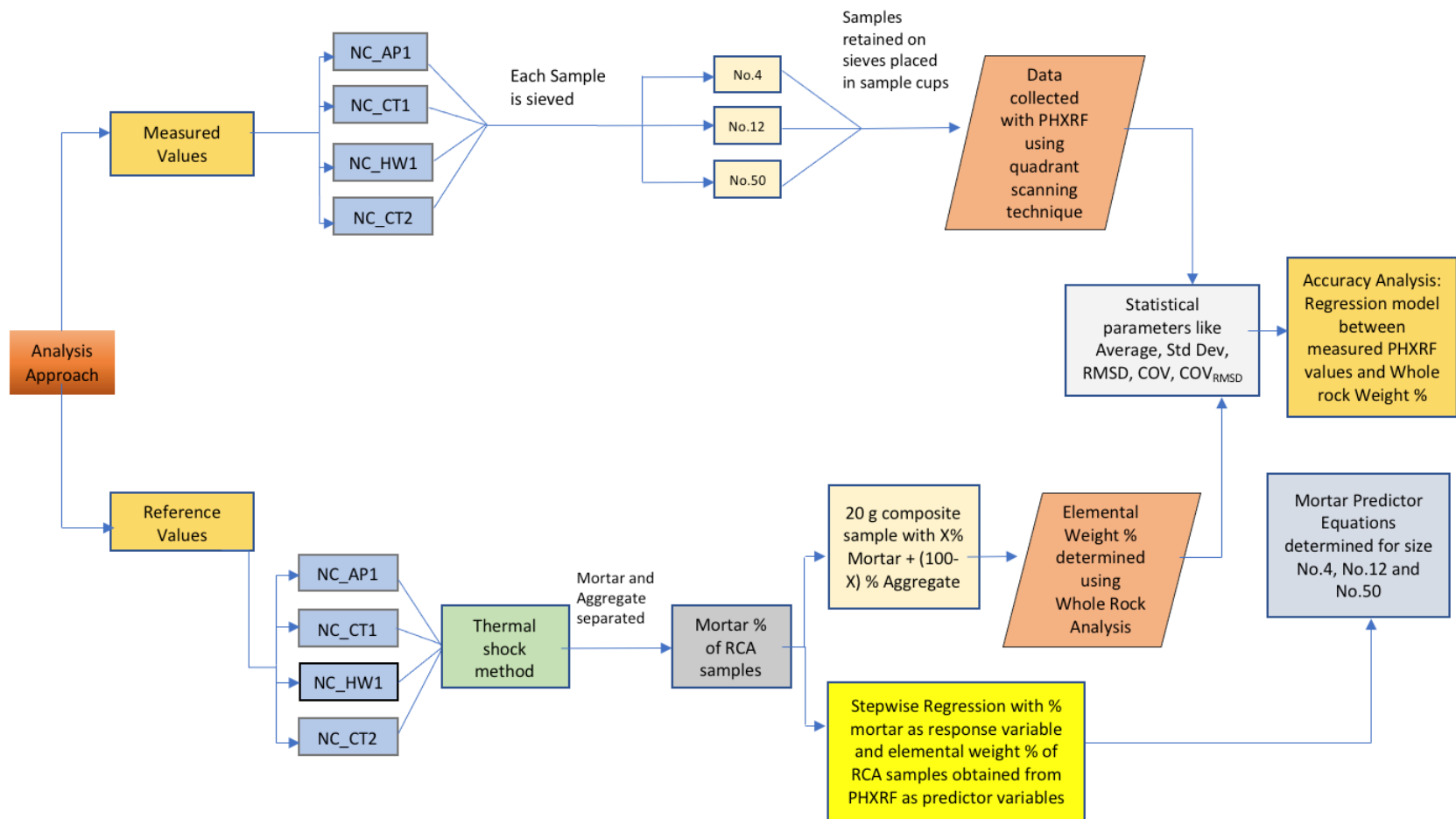


**Figure 22 Approach utilized to evaluate accuracy and precision of PHXRF for chemical characterization of RCA**



As shown in Figure 22, the approach of the analysis was to obtain values from PHXRF for the RCA samples and then compare the results against reference values. To obtain measured values, the samples were sieved through sieve sizes 1½", 1", ¾", ½", ⅜", No. 4, No. 12, and No. 50. The samples retained on sieve sizes No. 4, No. 12, and No. 50 were then bagged for analysis. The elemental weight percentages of the elements present in the samples were determined by PHXRF analysis. For the reference samples, the thermal shock method was first used to separate the mortar and aggregate from RCA samples to determine the percent mortar (by weight) and percent aggregate (by weight). Using the mortar percent, a 20 g composite sample was prepared, which comprised of X% of 20g + (100-X)% of 20 g, where X = mortar content and 100-X is the aggregate content. This process was repeated for each of the RCA samples and then was sent for "whole rock analysis" to determine its chemical composition in weight percent.

After data collection, models were constructed to predict the mortar content using stepwise regression from the PHXRF results and the mortar % computed from the thermal shock method. For determining the chemical composition of RCA samples, a simple linear regression was performed to predict the relationship between the PHXRF elemental weight % and the weight % of elements obtained from laboratory testing (whole rock analysis). Based on the  $R^2$  values observed from this regression analysis, the most suitable particle size was recommended for the PHXRF analysis. The procedure for the PHXRF analysis will be described in the subsequent sections.

Statistical analysis tools utilized for this work included root-mean-squared deviations (RMSD), regression analysis with coefficients of determination ( $r^2$ ), 95% confidence and prediction intervals, and between the PHXRF and reference laboratory measurements and calculated quantities (Cerato et al. 2017). The standard deviation indicates how dispersed the data is around its mean. Data clustered around its mean is indicated by a low standard deviation value (closer to 0), and data spread out around the mean is represented by a high value (National Library of Medicine 2019). Another statistical term  $COV_{STDEV}$  is the ratio of the standard deviation of a data set to its mean. This parameter determines the measure of the variability of a random variable from its mean (Koopmans et al. 1964). The repeatability or precision of the PHXRF can be determined using this parameter. A low value of  $COV_{STDEV}$  (closer to 0) indicates more repeatability. The RMSD is defined as the standard deviation of the residuals. The purpose of

RMSD is to indicate how spread out the data points is from the regression lines. Values closer to 0 suggest higher accuracy (Glen 2020). Lastly,  $COV_{RMSD}$  is used in a model setting and is represented as the ratio of RMSD to the mean of the dependent variable. This parameter indicates the variability of measurements relative to true deviation. Once these statistical parameters were calculated, a regression analysis was used to compare the accuracy of the measured values vs. reference values.

#### *Test configuration and procedure*

For conducting this research study, a Bruker Tracer III-SD series handheld XRF analyzer was used (Figure 23). This device is based on energy dispersive X-ray fluorescence technology and uses a rhodium target (X-ray source) and a Silicon Drift Detector system for x-ray detection. The PHXRF analyzer can be operated as either a handheld device or in a bench-top setup. Based on the testing requirements, the bench-top test setup was deemed the most suitable configuration. In this testing setup, the instrument is mounted on a desktop stand, and a sample table is fixed to the nose of the instrument to provide a flat working surface. The sample cup is then placed on the sample table in an inverted fashion such that the open end of the sample cup secured with mylar film rests on the nose of the device. The sample cup is then enclosed in a sample shield to prevent radiation exposure to the user. Once the instrument is physically configured, the instrument is connected to a PC notebook with a USB cable. This connection enables the user to control the instrument and analyze the spectrum generated from the analysis of the sample via the S1PXRF software. The elements detected by the instrument are quantified using the relevant calibration file which comes with the software.



**Figure 23 Bruker Tracer III-SD PHXRF**

*List of influencing factors considered*

Scan Duration: A scan duration of 180 seconds and 60 seconds was selected for major (Na to Fe) and trace (Fe to U) elements, respectively, for the analysis of samples. A 180-second scan duration was utilized to excite light elements (Na to Fe), and the 60-second scan duration was utilized to excite heavier elements (Fe to U). Despite the observation made by Cerato et al. (2017) that “*longer scan durations do not yield appreciable benefits in terms of precision or accuracy and are, therefore, unnecessary,*” the scan duration was selected based on the ‘Mudrock/Ceramic’ calibration file suggested for use by the PHXRF manufacturer (Bruker). For the ‘Mudrock/Ceramic’ calibration file to quantify results accurately, the instrument was used under the same settings under which it was calibrated. A detailed description of the Mudrock/Ceramic calibration and the corresponding instrument settings is discussed in a subsequent section. Hence, the testing was done with a scan duration of 180 and 60 seconds for light and heavy elements, respectively.

Sample Type and Preparation: Loose aggregate samples were used in this analysis. This sample type was selected due to its relatively easy preparation. Alternative sample preparations suggested in the literature, such as a pressed pellet sample, require a substantial amount of time to prepare and may not be feasible to prepare in the field or in some laboratories. The loose aggregate sample retained on sieve No. 4, No. 12, and No. 50 were tested, one size fraction per sample cup. Each

sample was placed into a cylindrical sample cup with an internal diameter of 1.5 in. and an internal height of 0.6 in. and was secured using a 6  $\mu\text{m}$  thick mylar film over the opening of the sample cup (Figure 24).



**Figure 24 PHXRF sample preparation**

Apart from samples prepared from the fractionated sizes of the four types of RCA, other samples were also prepared for validation. These additional samples included mortar (alone) and aggregate (alone) obtained from each RCA. The mortar and aggregate samples were separated using the thermal shock method. Once the mortar and aggregate were separated, they were placed in different sample cups and secured using mylar film. In addition to these samples, other samples like Type I/II cement, class F fly ash, and a mixture of cement and fly ash was also prepared to assist in evaluating the PHXRF measurements of the RCA samples. The cement sample was prepared by making a cement paste with a w/c of 0.45, whereas the cement/fly ash mixture was prepared in a manner similar to the cement paste, but by substituting Class F fly ash for cement at a 20% replacement by weight. A water-to-cementitious materials ratio (w/cm) of 0.45 was used to prepare this sample. Both of these samples were prepared in a manner similar to that used by Taylor et al. (2012).

Scan Technique: For the analysis, a quartering technique was used similar to the approach developed by Cerato et al. (2017). Each sample cup was divided into four quadrants, and each quadrant was scanned three times at three different locations for a total of 12 scans per sample cup. The average value of the 12 scans was computed for both major and trace elements. Major and

trace elements, respectively, listed in order of atomic weight, are listed in Table 14. As shown in Figure 25 below, the sample cup was divided into four quadrants and was placed on the nose of the instrument in an inverted position.

**Table 14 Major elements and trace elements quantified by the PHXRF for this study**

Major elements	Trace elements
Na	Co
Al	Ni
Si	Cu
P	Zn
S	As
K	Rb
Ca	Sr
Ti	Y
V	Zr
Cr	Nb
Mn	Mo
Fe	Sn
	Sb
	Ba
	Th
	U

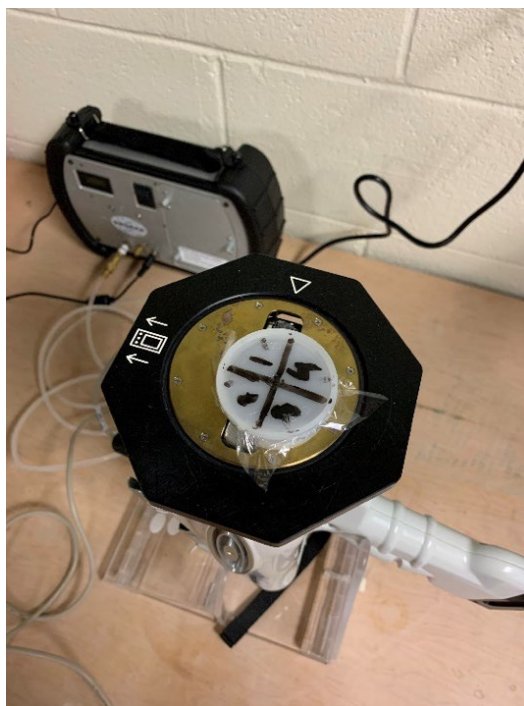


**Figure 25 Quadrant scanning technique**

Surface Thickness: Another important influencing factor, surface thickness, was also taken into consideration. As previously described in the literature review, the minimum thickness of each element is correlated to its characteristic x-ray energy (Padilla et al. 2019). Each sample must meet the minimum thickness criteria, which describes the minimum depth of the sample required to absorb the primary x-ray emitted from the PHXRF followed by the emission of characteristic x-ray from the sample. There are two essential terms associated with this concept. ‘Penetration Depth,’ which refers to how deep into the sample the primary x-ray penetrates, and the second term, ‘Escape Depth’, which refers to the depth from which the secondary radiation can be detected from. It is normally assumed that escape depth is exceeded upon exceeding the penetration depth (Bruker 2020). Therefore, it was important to evaluate the surface thickness of a sample because it will be different for every material. Denser samples tend to require less thickness. In one experiment conducted to differentiate an obsidian source using PHXRF, the minimum depth required for precise and accurate results for obsidian was determined to be 3mm (Forster and Grave 2012). In the experiment conducted by Imanishi et al. (2010) to quantify the presence of harmful elements in soil using XRF, the minimum soil thickness was determined to be 6mm, and for the sake of analyzing all elements from light to heavy, a fixed thickness of 10 mm was adopted for the experiment. Since the manufacturer-prepared Mudrock/Ceramic calibration file is being used for this work, the manufacturer has provided a list of minimum thicknesses for various elements at different characteristic energies. The list is shown in Table 15

**Table 15 Mudrock/Ceramic analysis depth (from Bruker)**

Element	Photon emitted energy (keV)	Analysis depth in ceramic (cm)
O	0.53	0.000001
Na	1.04	0.0007
Mg	1.2	0.00096
Al	1.47	0.0017
Si	1.74	0.0027
P	2.01	0.0013
Ca	3.69	0.0064
Cr	5.41	0.0192
Fe	6.4	0.03
Cu	8.01	0.058
Zn	8.64	0.077
Pb	10.55	0.113
Zr	15.78	0.384

It should be noted that the above observations related to the minimum depth, the sample cup was chosen for this analysis had a depth of 0.59 in. to mitigate the inaccuracies caused due to the infinite thickness phenomenon. A cross-section of the sample cup used for the purpose of experimentation is shown in Figure 26.

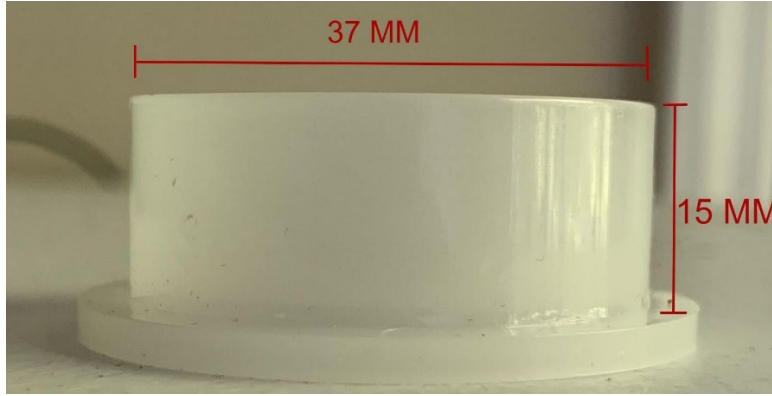


**Figure 26 Sample cup dimension**

Particle size: As described in the literature review, particle size has been shown to play the most significant role in the accuracy of the results obtained from the handheld XRF. The RCA samples were sieved through the sieve sizes 1½", 1", 3/4", 1/2", 3/8", No. 4, No. 12, and No. 50. The objective was to achieve highly accurate results by selecting the appropriate particle size for analysis. After sieving, the sample portions retained on sieve sizes No. 4, No. 12, and No. 50 were collected and bagged for XRF analysis. The main goal was to identify the lowest value of RMSD at the largest particle, as shown in Table 16. Beyond this value, the effects of particle size on RMSD would level off (Cerato et al. 2017). This is also shown in Table 16.

**Table 16 Effects of particle size on XRF STDEV,  $COV_{stddev}$ , RMSD,  $COV_{RMSD}$** 

RCA Type	Particle Size	n Scans	Std Deviation	$COV_{STD\ Dev}$	RMSD	$COV_{RMSD}$
RCA A ↓	½"					
	#4					
	#40					
	#100					
	#200					
RCA B ↓						

Needs to be statistically significant

Look for lowest value at largest particle size

Calibration and Instrument Settings: As per the PHXRF manufacturer's recommendation, the 'Mudrock/Ceramic' calibration file was used for quantifying the elements obtained from PHXRF analysis. The results are reported as the weight percentage of the elements that are measured. Some elements like carbon, oxygen, and hydrogen cannot be measured by the device as these elements are not detected by the detector of the instrument. Due to this reason, the total weight % will not add up to 100% (Bruker 2013).

The Mudrock calibration has two parts; the first part is to quantify major (lighter) elements, i.e., Na to Fe, and the second part is the quantification of trace elements, i.e., Fe to U. The instrument requires different settings for the quantification of major and trace elements and are listed in Table 17.

**Table 17 Instrument settings**

	Major Element Settings	Trace Element Settings
Voltage	15 kV	40 kV
Current	35 $\mu$ A	10 $\mu$ A
Scan duration	180 seconds	60 seconds
Filter	None	Yellow
Vacuum	Pump attached	No Vacuum



The Major Element settings require the use of a vacuum pump provided with the device (Figure 27). The use of this vacuum pump aids in obtaining highly accurate measurements of light elements by removing the surrounding air present between the detector and the sample, which allows a maximum number of X-rays to reach the detector. This pump was connected to the PHXRF with a hose that had a slide valve with an open/close mechanism. Once connected, the instrument was ready for measurement when the display of the pump read less than 10 Torr.



**Figure 27 PHXRF connected to a vacuum pump**

Another important setting for trace element analysis included a filter. The primary function of the filter is to optimize the excitation conditions for a group of elements (heavy elements) when used with a certain voltage setting (Bruker 2010). The combination of the filter and the tube voltage made the device more sensitive to certain elements. Hence, a yellow filter (Figure 28), composed of Ti and Al was used for trace element analysis which allowed x-rays from 12 to 40 KeV to reach the sample (Speakman 2015).



**Figure 28 Yellow filter for trace element analysis**

### **3.3 Test methods for concrete**

#### **3.3.1 Fresh concrete properties**

##### *Slump test*

Slump of the concrete mixtures was measured according to ASTM C143 to measure the consistency (Figure 29). The test was performed immediately after the concrete mixing was completed.



**Figure 29 Slump test setup**

#### *Air content test*

Air content of the mixtures was measured according to ASTM C231 using a type B meter (Figure 30).



**Figure 30 Type B air meter (pressure meter)**

#### *Box Test*

For the Box Test, fresh concrete was loosely placed into a temporarily fixed wooden box with an open top and bottom and a dimension of 1ft×1ft×1ft (Figure 31), as described by Cook et al. (2013). A portable electrical vibrator was then used to consolidate the concrete for 6 seconds. A vibrator was inserted vertically at the center of the specimen to full depth for 3 seconds, and then raised for 3 seconds. The wooden box was then removed sideways, and the surface was visually examined for surface voids, and a straight edge was used to examine edge slumping. The procedure was modified by Mamirov et al. (2021) with the utilization of image analysis to evaluate the surface quality. The new ranking range using the image analysis method was designed as follows: 0-3% classified as ranking 1, 3-5% as 2, 5-15% as 3, and over 15% as 4. The edge quality ranking was modified as follows and is based on the greatest defect along edges: 1-good (<1/16 in), 2-average (1/16-1/8 in), 3-poor (1/8-1/4 in), 4-failed (>1/4 in). Finally, a dual index was used to describe Box Test performance, with “E” standing for edge quality and “S” for surface quality. For example, “E2-S1” stands for a mixture with an average edge quality and ranking 1 in terms of

surface voids. More details of the test method and the determination of the index can be found at Mamirov et al. (2021).



**Figure 31 Box Test setup**

### **3.3.2 Specimen casting and curing**

Upon the completion of mixing, specimens were prepared according to ASTM C192. All specimens were stored in a 73°F room prior to demolding at 24 hours. After being removed from molds, specimens were stored in a curing room maintained at 100% R.H. and 73°F until testing.

### **3.3.3 Hardened concrete properties**

#### *Compressive strength test*

Three 4" by 8" cylinders per mixture were used to determine the compressive strength based on ASTM C39 at 7 and 28 days of age. A Forney compressive machine with a capacity of 400 kips (1,779 kN) was used (see Figure 32).



**Figure 32 Compressive strength test setup**



#### *Static modulus of elasticity test*

A test to determine the modulus of elasticity was performed at 28 days of age according to ASTM C469. A frame with two dial gauges to monitor both axial and radial deformations was used (see Figure 33). Each test was recorded and later used to build a graph of the load-deformation relationship, from which the modulus of elasticity and Poisson's Ratio were determined.



**Figure 33 Static modulus of elasticity test setup**

#### **3.3.4 Durability tests**

##### *Surface and bulk resistivity*

One cylinder specimen was randomly selected from each mixture to be tested for the surface (Figure 34a) and bulk resistivity (Figure 34b) using a Proceq Resipod testing device at 28-day based on AASHTO TP95. The device works based on the Wenner probe principles and measures the electrical resistivity of concrete. The specimen was tested in a fully saturated condition. To perform this test, an electric current is applied through the outer probes, while the inner probes measure the voltage.



a) Surface resistivity



b) Bulk resistivity

**Figure 34 Resistivity test setup**

### *Free shrinkage*

Three shrinkage prisms 3" by 3" by 11.25" per mixture were casted to determine the free shrinkage test according to ASTM C157. The initial reading was taken after demolding the specimens and soaking them in lime-saturated water for 30 minutes. Afterward, specimens were cured in water until 28 days, and then stored in an environmental chamber maintained at 73°F, and 50% R.H. The first reading after curing was taken right after the specimens were moved from the curing room to the environmental chamber using the length comparator (see Figure 35). The average values from three specimens were recorded. The following readings were taken at 1, 3, 7, 14, 28, and 90 days after the initial reading.



**Figure 35 Length comparator used for shrinkage measurement**

## **CHAPTER 4. RCA CHARACTERISTICS**

This chapter presents the results of RCA characterizations, including RMC, physical and mechanical properties, and chemical compositions. As mentioned earlier, all tests, except the freeze-thaw resistance test, were performed for each coarse size separately to provide a basis for comparison, and to support the evaluation of the variation of different properties for different size fractions of RCA.

### **4.1 Residual Mortar Content**

Results showed that for the RCA specimens included in this study, the RMC varied from 14.14% to 86.64%. It should be noted that the Nebraska RCA exhibited most of the high RMC values. Different from most other states, Nebraska Department of Transportation specifications include provisions that result in unique mixture designs for concrete, where the major proportion of aggregate is a combination of sand and gravel (70%, by mass) that is mostly fine aggregate yet includes a small fraction with a typical coarse aggregate size range; a relatively small amount (30%, by mass) of limestone is used as coarse aggregate. This type of design results in concrete with high mortar content, which is why RCA derived from Nebraska concrete consequently has a higher RMC.

As shown in Figure 36, most of the RCA sources followed a similar trend that exhibited specific gravity, absorption, and ACV test results, where No. 4 (4.75 mm) sized aggregates have a higher RMC than the larger sizes. This is expected since all these properties are, to some extent, interrelated. The potential reason why No. 4 sized aggregates have a higher RMC is due to the fact that No. 4 size is the smallest size that is considered as coarse aggregate. Thus, there is much less chance of No. 4 RCA particles consisting of No. 4 NA, i.e., No. 4 RCA particles consist mostly of NA smaller than No. 4, which are considered as natural fine aggregate and a part of residual mortar. There is no clear trend among the other sizes of RCA.

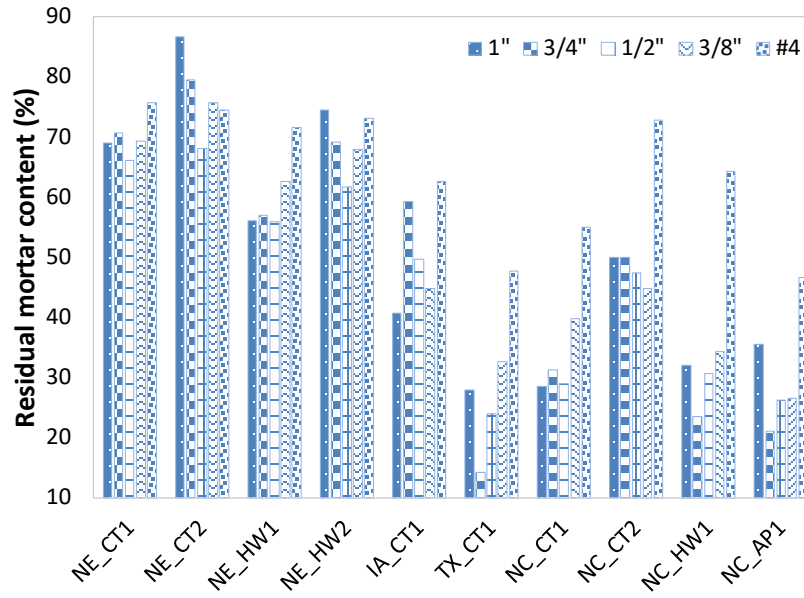


**Figure 36 Variation of RMC with source**

Linear regression analysis for RMC and other properties was performed with the data collected, and the results are summarized in Table 18. Unexpectedly, there is no good correlation between absorption and RMC, and the effect of absorption on RMC was not determined to be statistically significant. The correlation between specific gravity and RMC is also relatively poor, as is the correlation between a combination of absorption and specific gravity and RMC. It implies that the current practice of characterizing RCA based on absorption and specific gravity only is insufficient, as it cannot effectively predict the RMC. This lack of correlation might be due to the fact that the relationship is also influenced by other critical factors, such as w/c of the residual mortar and the absorption of virgin aggregates. The ACV, however, has a stronger correlation to RMC and can be used to predict the RMC. When all three parameters are combined, a stronger correlation can be established, with an adjusted  $R^2$  value of 0.644.

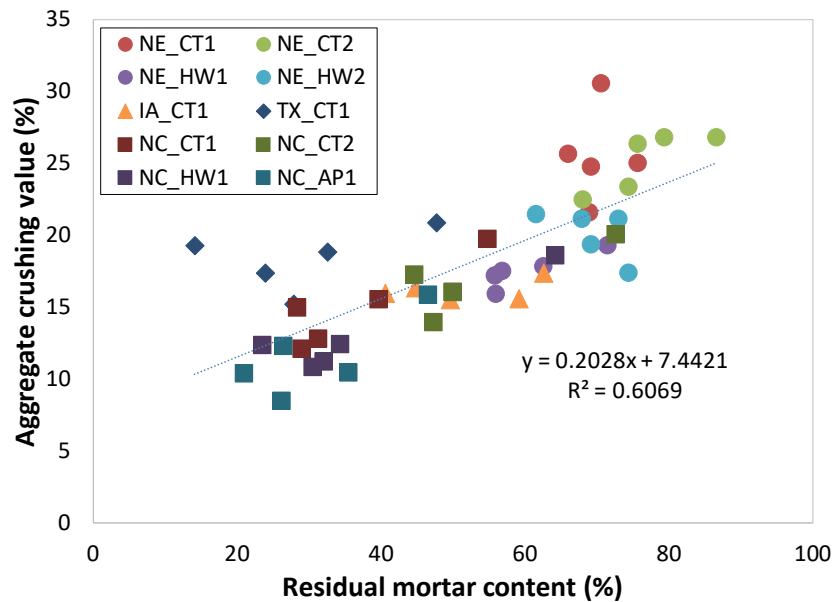
**Table 18 Linear regression analysis summary for RMC prediction**

Variables	Adjusted R-square	Standard error	F significance	Statistically significant
SG	0.223	16.668	3.1E-04	Yes
AC	0.007	18.846	2.5E-01	No
ACV	0.599	11.982	2.7E-11	Yes
SG&AC	0.321	15.588	4.3E-05	Yes
AC&ACV	0.623	11.610	4.1E-11	Yes
ACV&SG	0.590	12.106	2.9E-10	Yes
SG&AC&ACV	0.644	11.278	5.0E-11	Yes

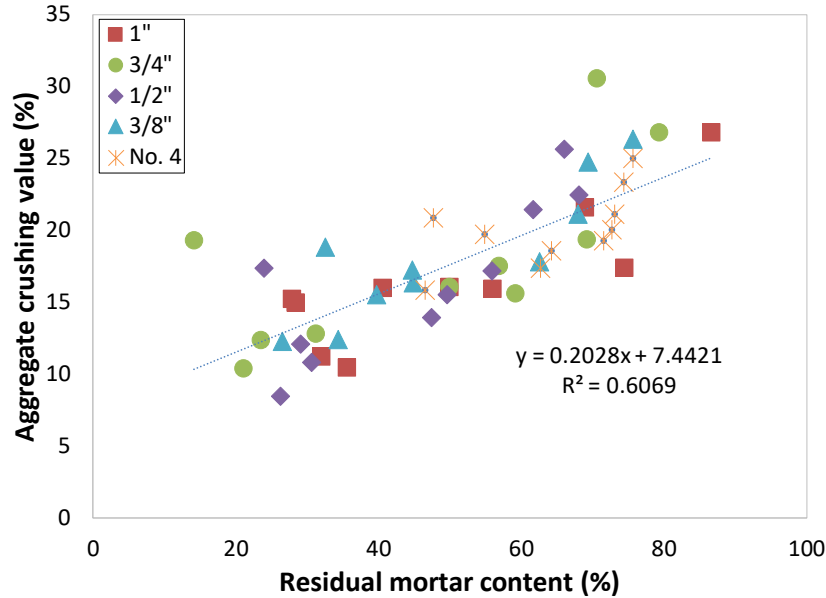


Note: SG-specific gravity, AC-absorption capacity, ACV-aggregate crushing value

As shown in Table 18, the ACV and RMC have a relatively strong linear relationship. Further analysis was performed to evaluate the variation of these parameters with the source and the size. As can be observed from Figure 37, most Nebraska RCAs included in this project have noticeably higher RMC than other RCAs. In terms of mechanical properties, Nebraska RCAs also have higher crushing indices than others, except for the Texas RCA, which despite having low RMC, has a comparable ACV to some of the Nebraska RCAs. This might be due to the different qualities of parent concrete. Figure 37b shows that all the sizes other than No. 4 are spread uniformly along the best trend line, whereas No. 4 size RCAs tend to have a higher ACV and RMC.



a) Variation of ACV and residual mortar content with different RCA sources



b) Variation of ACV and residual mortar content with different RCA sizes

**Figure 37 Relationship between ACV and residual mortar content**

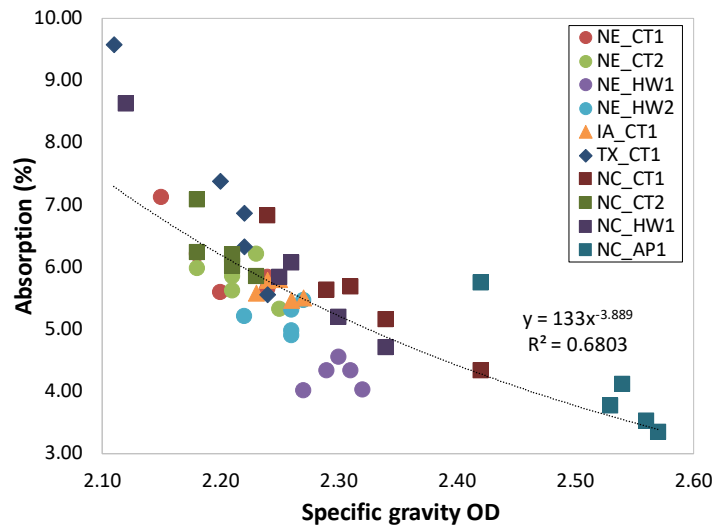
## 4.2 Physical and Mechanical Properties

### 4.2.1 Specific gravity and absorption

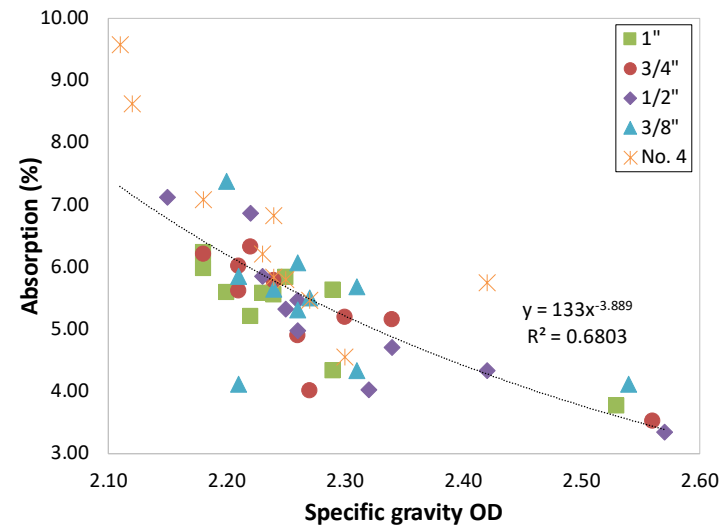
Specific gravity values for RCA included in this study ranged from 2.11 to 2.57, where higher values correspond to RCA crushed from a higher-quality concrete, such as highway or airport pavement. It is worth noting that one of the high-quality RCA (NC\_API1) resulted in a specific gravity even higher than one of the NA (Nevada granite). Other than that, as expected, the specific gravity values of RCA are lower than NA, which is attributed to the porous structure of residual mortar in RCA. In general, there is an anticipated clear correlation between absorption capacity and specific gravity (Figure 38) following the power relationship.

The aggregates with a higher absorption (more porous) exhibited a lower specific gravity, which could be expected. In terms of absorption, due to the same reason mentioned earlier, RCA has significantly higher absorption capacities, ranging in 3.35-9.58%, compared to NA absorption of 0.91-2.81%. The values obtained for both specific gravity and absorption are consistent with the values found in the literature (De Juan et al. 2008, Silva et al. 2014). As can be observed in Figure 38b, No. 4 size aggregates have noticeably higher absorption and thus lower specific gravity compared to larger sizes, including 1" 3/4", 1/2", and 3/8" aggregates. However, the absorptions of aggregates of these four sizes do not follow any clear trend. Thus, a statement is often appearing in the literature (De Juan et al. 2008), claiming that with the decrease of size, the absorption

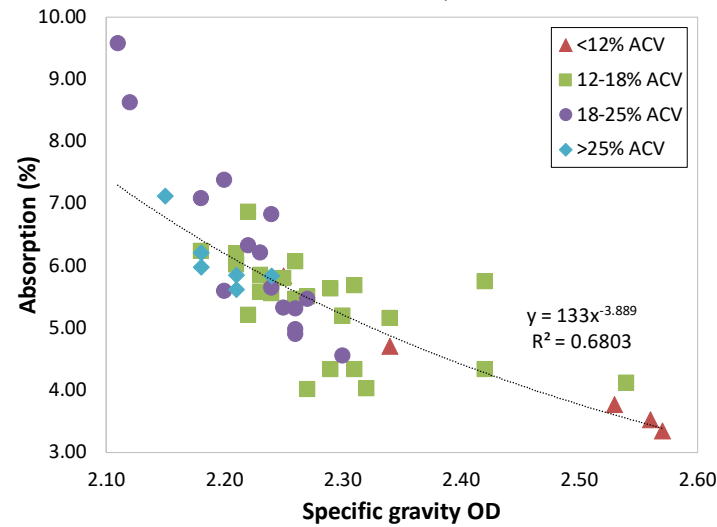
increases, was not confirmed with the current study. Figure 38c shows the variation of specific gravity and absorption with different ACV categories. In general, there is a clear trend of RCAs with lower crushing indices (stronger) having higher specific gravity and lower absorption, except for one RCA source (NE\_CT1) that differs significantly from the trend. From Figure 38d, it can be noticed that there is a relatively clear relationship between RMC and specific gravity, but not as clear as the trend observed in absorption.



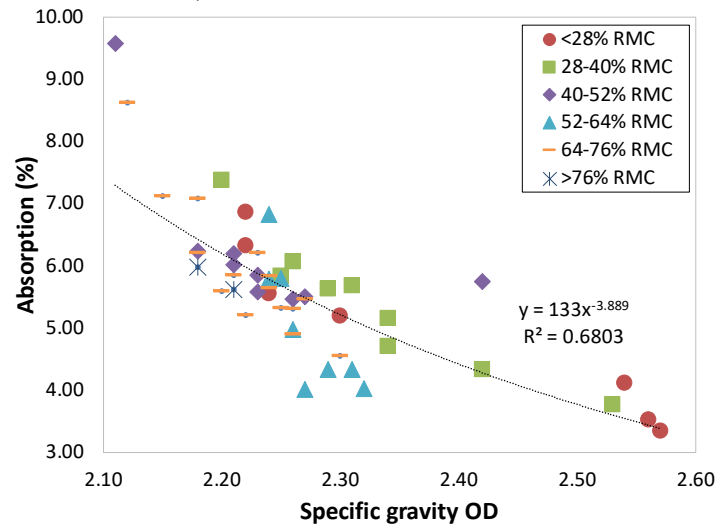
a) Per source



b) Per size



c) Per crushing value categories



d) Per residual mortar content categories

**Figure 38 Correlation between absorption and specific gravity, and other RCA characteristics**

#### 4.2.2 Aggregate crushing value

As expected, RCA has a lower crushing resistance (higher ACV) due to the residual mortar being more susceptible to crushing because of its weaker nature compared to virgin aggregates (Figure 39). The ACV for RCA ranged from 8.48% to 30.51%, while NA had an ACV ranging from 4.73 to 10.09%. RCA sourced from higher-quality pavement concrete (such as NE\_HW1, NC\_HW1, NC\_AP1) exhibited the lowest ACV, indicating the highest crushing resistance. Similar to the absorption and specific gravity results, it was noticed that No. 4 size aggregates have a higher ACV than larger size aggregates, while there is no clear trend between the other sizes.

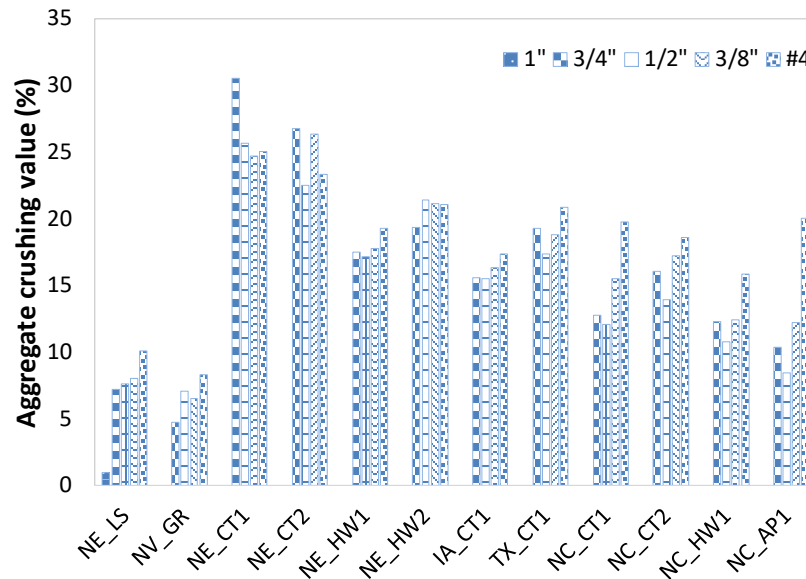


**Figure 39 Variation of ACV with source**

When aggregate samples with multiple size particles are included in the ACV test, particles of certain sizes could be crushed first, and thus the ACV might not be able to accurately represent the whole sample. As a result, many standard procedures require the use of a single-sized aggregate sample, namely 3/8". The method proposed by the authors recommends performing the ACV test for different sizes separately, then subsequently computing a weighted average based on the gradation of the RCA. It is believed that this approach will provide a more representative and useful measure.

Linear regression analysis was also performed to obtain the relationships between the ACV and other parameters. Table 19 presents a summary of the linear regression analysis. It can be noticed that the correlation between the ACV and specific gravity is low, which demonstrates that specific gravity can not be used solely to characterize RCA's mechanical performance. On the

other hand, there is a relatively good correlation between the ACV and RMC. This is likely due to the fact that during the crushing process, residual mortar in RCA is subjected to crushing first because of a weaker nature compared to NA. Even though the effect of absorption on the ACV is statistically significant, the correlation is very low. Multiple regression analysis demonstrated that there is a clear improvement in correlations and standard errors. The most promising prediction model for the ACV would include all three parameters, i.e., specific gravity, absorption, and RMC.

**Table 19 Linear regression analysis summary for ACV prediction**

Variables	Adjusted R-square	Standard error	F significance	Statistically significant
SG	0.397	3.824	5.7E-07	Yes
AC	0.159	4.516	2.4E-03	Yes
RMC	0.599	3.120	2.7E-11	Yes
SG&AC	0.398	3.822	2.5E-06	Yes
AC&RMC	0.681	2.782	8.3E-13	Yes
RMC&SG	0.682	2.777	7.7E-13	Yes
SG&AC&RMC	0.685	2.765	3.2E-12	Yes

Note: SG-specific gravity, AC-absorption capacity, RMC-residual mortar content

#### 4.2.3 Freeze-thaw resistance

Nebraska Department of Transportation (DOT) requires 6.5-9.0% of air content for pavement concrete and 6.0-8.5% for bridge deck and rapid patching concrete. North Carolina DOT requires 4.5-7.5% of air content for pavement concrete. Iowa DOT states that the requirement is 6.0-10.0% of entrained air when measured on the grade just prior to consolidation, while for non-slip-forming pavement concrete, the requirement is 5.5-8.5%. Texas DOT requires the air content to be at least 3.0%. Based on this information, collected RCAs were divided into three categories based on the air content requirements:

- Low air-entrainment level (Texas)
- Medium air-entrainment level (North Carolina)
- High air-entrainment level (Iowa and Nebraska)

As shown in Figure 40, there is no clear trend in F/T total mass loss with different levels of air entrainment. This result is expected due to the significant differences in RMC in RCAs. It can be noticed that the total mass loss from F/T cycles for NA is extremely low. Therefore, it is reasonable to assume that during F/T cycles, RCA will lose their residual mortar (RM) first, and only afterward the original NA will be dislodged and lost. Therefore, it was decided to compare the percentages of RM loss instead of the total mass. Figure 41 demonstrates a more expected trend,

with Texas RCA losing all of its RM and some portion of virgin aggregates, and Nebraska HW RCA having the highest freeze-thaw resistance. Additionally, Figure 41 illustrates the difference in crushing indices not only related to the level of air entrainment, but also aggregates' (tensile) strength as it is directly related to residual mortar loss. Results showed that Iowa and Nebraska RCAs have higher crushing indices (weaker), which could partially contribute to the higher % of RM loss. In order to take the RCA ACV into account, an RM loss-to-ACV was determined. Figure 42 demonstrates the RM loss-to-ACV ratio comparison, and there is a clear differentiation notable between different air-entrainment levels. The performed test seems to be able to differentiate levels of air entrainment, and can be used as an additional guide in a mixture design of RAC that is expected to be exposed to freeze-thaw cycles.

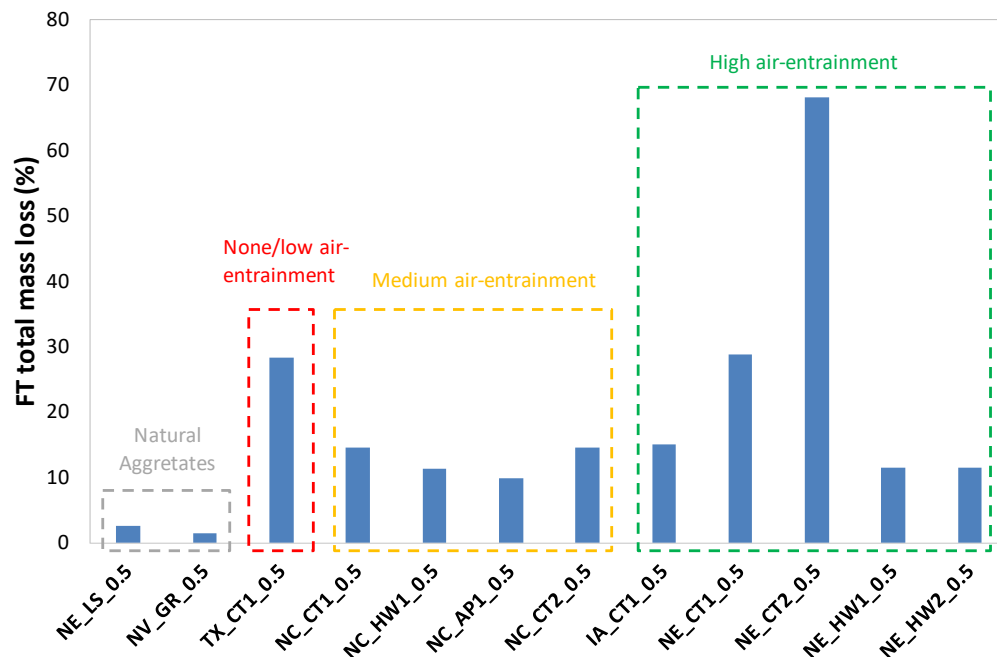


**Figure 40 Total freeze-thaw mass loss comparison**

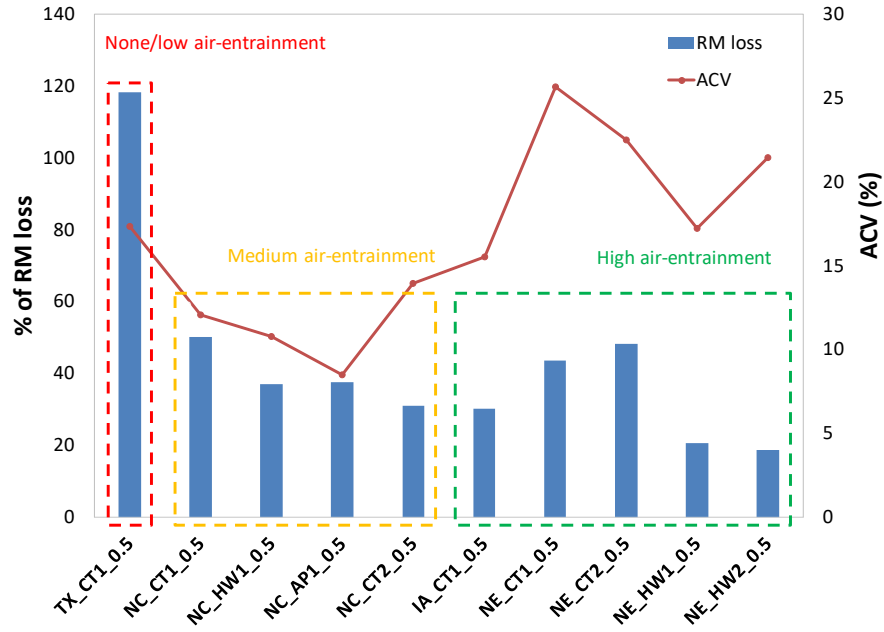


**Figure 41 Percentages of residual mortar loss comparison**

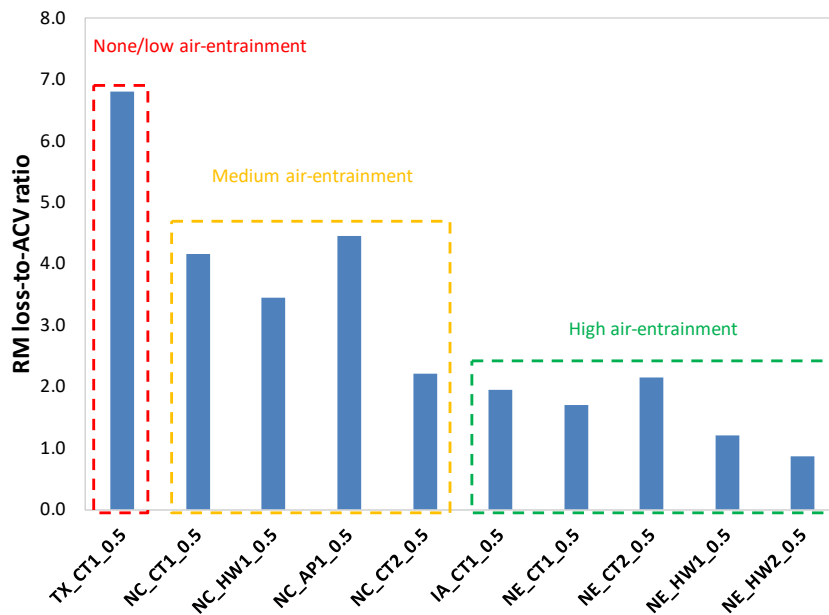


**Figure 42 RM loss-to-ACV ratio comparison**

#### 4.2.4 Shape and surface texture

Results from AIMS2 analysis show that RCA angularity ranges from 2750 to 3640, while NA has slightly lower angularity ranging from 2350 to 3170. However, all of them lie in the category of moderate angularity. The difference in angularity is attributed to the residual mortar



of RCA. In regards to the variation of angularity with a size, Figure 43 demonstrates that no clear trend can be observed.

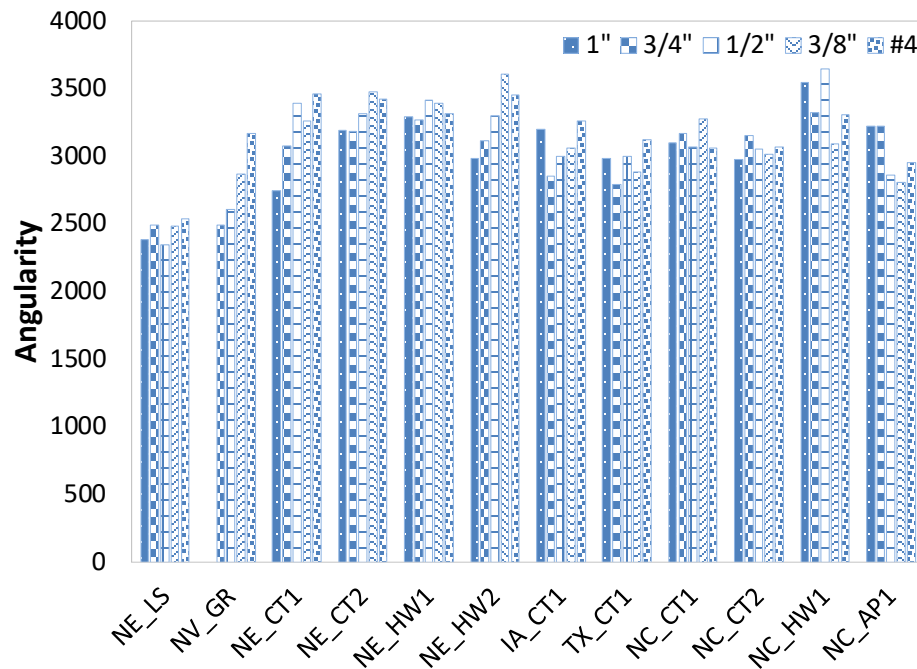


**Figure 43 Variation of angularity with source**

The surface texture index of RCA was found to range from 193 to 410, and no clear trend was observed when compared to NA. RCA has a significantly higher texture compared to NE limestone aggregate (ranges from 143 to 190), and yet the texture is comparable to the texture of NV gravel (ranges from 304 to 375). It seems that the texture is attributed to the nature of aggregates, and whether an aggregate is recycled or natural is not the primary factor driving the variation in texture. Figure 44 illustrates that there is a general trend of texture decrease for smaller sizes of RCA.

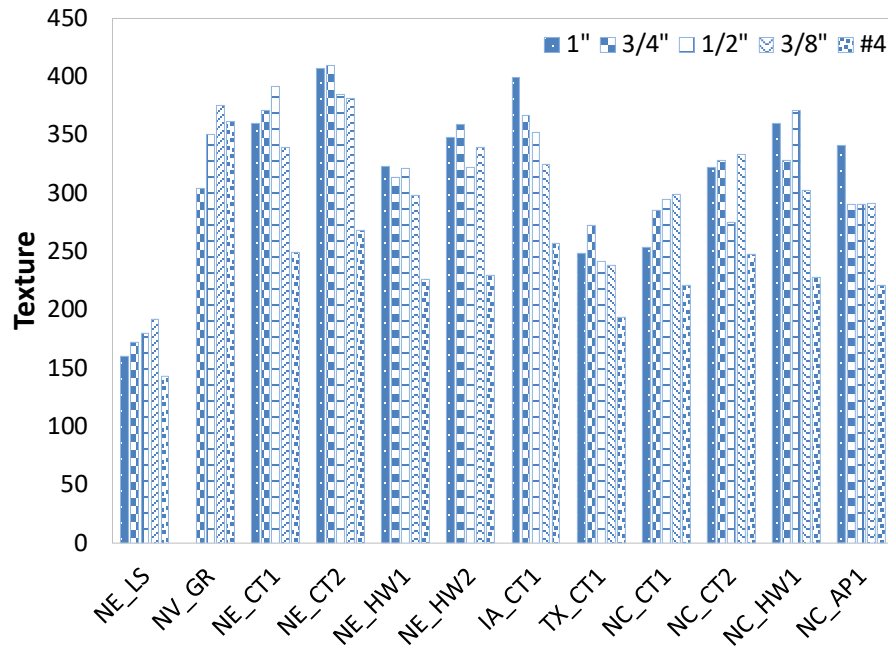
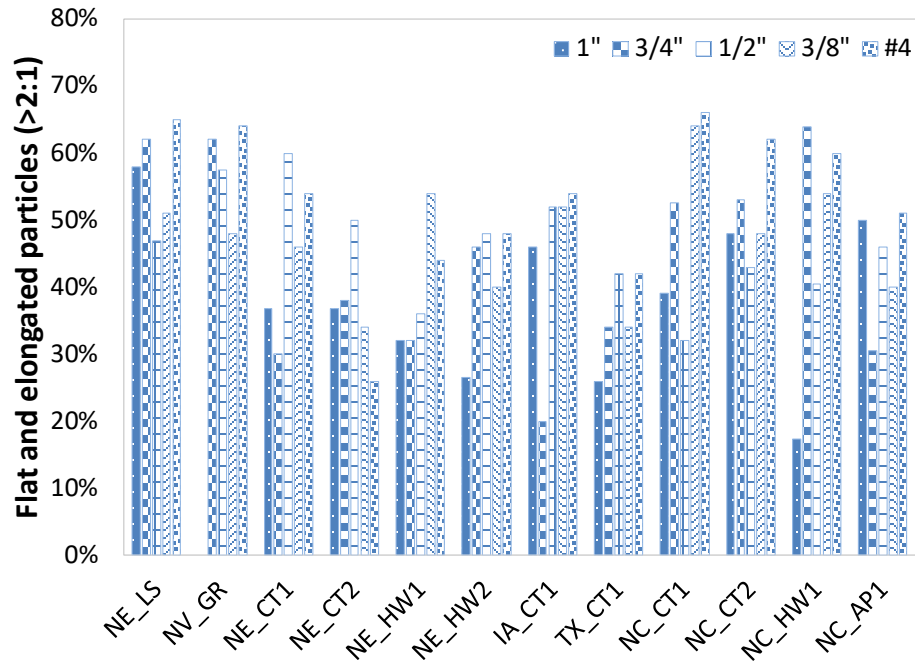
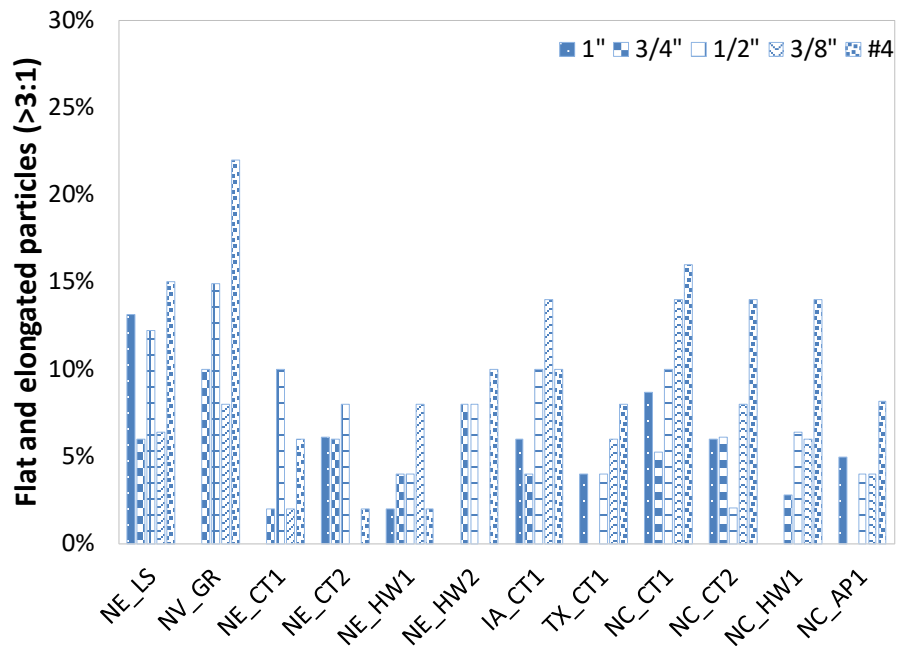


**Figure 44 Variation of surface texture with source**

Another important parameter to consider is the distribution of flat and elongated particles, as they affect the packing degree of the aggregate blend. For concrete applications, it is preferable to minimize the amount of flat and elongated particles. Figure 45 demonstrates the percentages of flat and elongated particles for different sources. There is no clear trend observed neither in terms of source nor the size. The difference in this parameter is likely due to the different crusher types used during the RCA production.



a) Percentage of flat and elongated particles (>2:1)

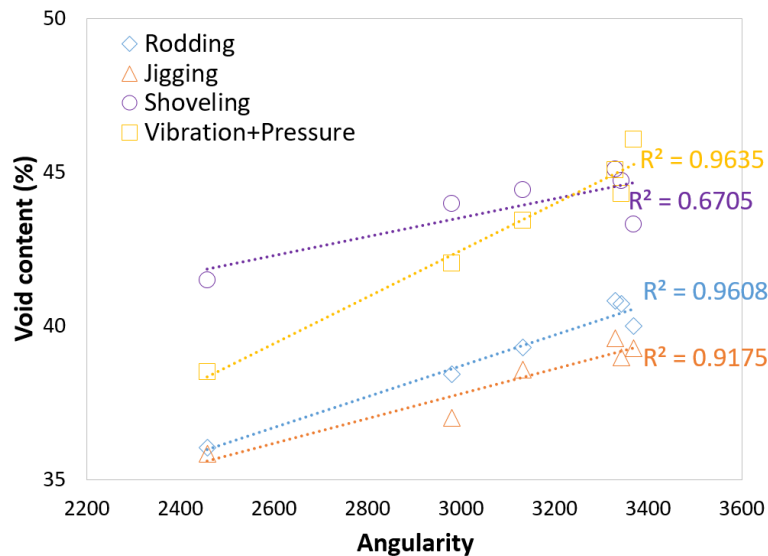


b) Percentage of flat and elongated particles (>3:1)

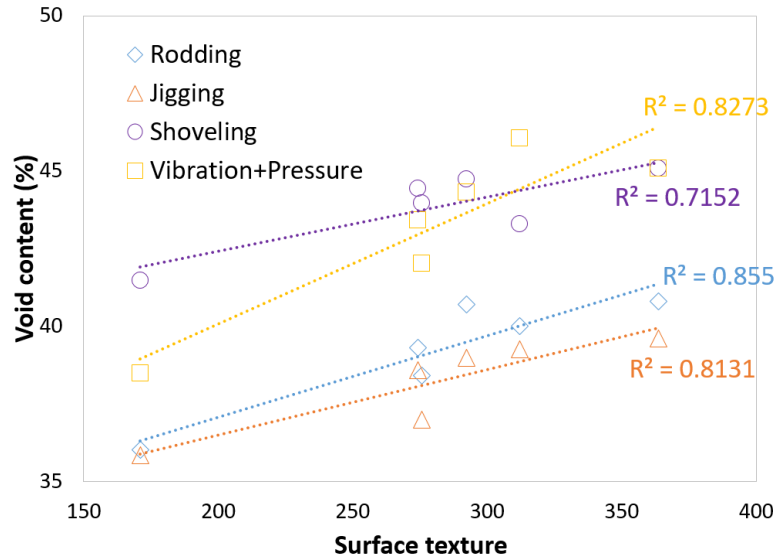
**Figure 45 Variation of flat and elongated particles with source**

#### 4.2.5 Void content

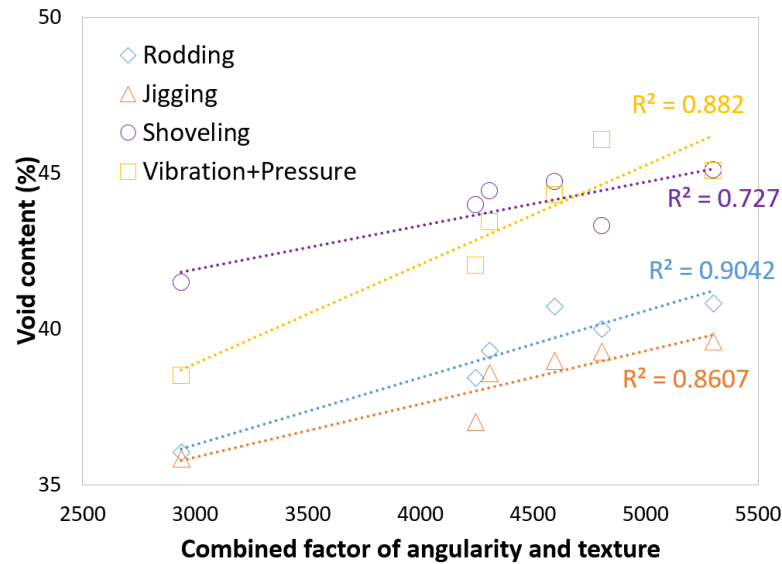
Besides the particle size distribution, particle angularity and surface texture are the main parameters driving the variation in particle packing. Figure 46 demonstrates the effect of angularity, texture, and the combined factor of the two on the void content of selected RCAs (NE\_LS, NE\_CT2, NE\_HW1, NC\_CT1, NC\_HW1, NC\_AP1), which were reblended to the same gradation (No. 57) to eliminate the influence of gradation on the analysis. As expected, void content increases with the increase of angularity and texture following a linear relationship. Use of the prescribed jigging procedure results in the highest compaction, followed by use of the rodding procedure, use of vibration plus pressure, and use of the shoveling procedure, which is consistent with findings from Mamirov et al. (2021).



a) Effect of angularity on void content



b) Effect of surface texture on void content



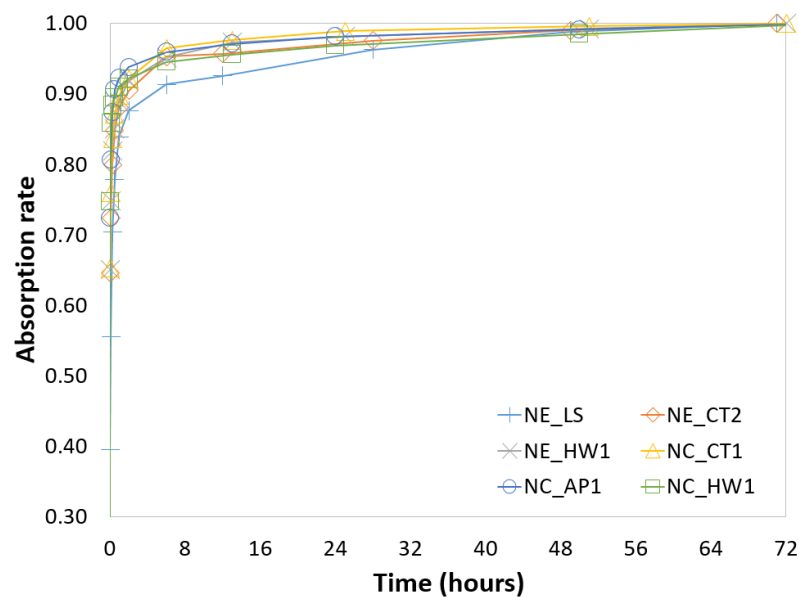
c) Effect of the combined factor on void content

**Figure 46 Effect of shape and texture parameters on particle packing**

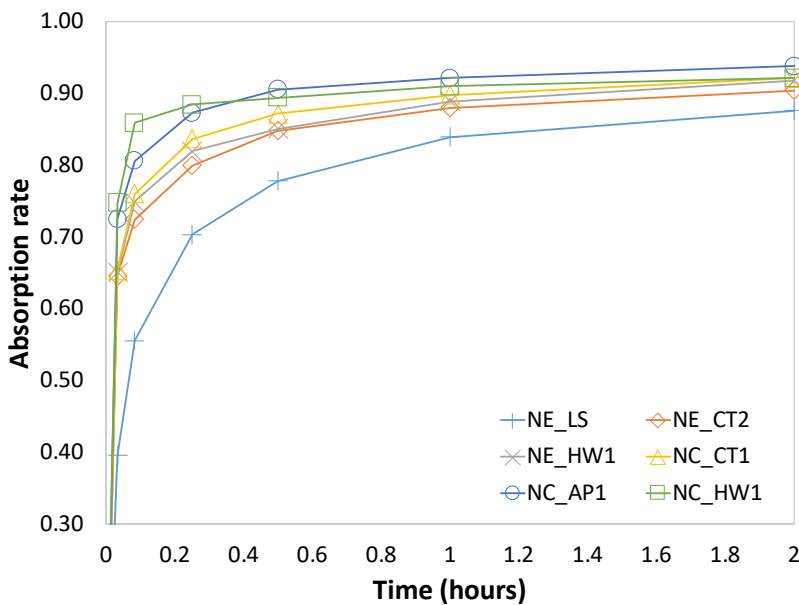
#### 4.2.6 Absorption rate

Selected RCAs (NE\_CT2, NE\_HW1, NC\_CT1, NC\_HW1, NC\_AP1) along with one NA (NE\_LS), which were blended to a similar gradation, were tested for the absorption rate property. As expected, RCA resulted in a higher absorption rate due to a significantly higher porosity (as compared to NA). As shown in Figure 47 and Figure 48, in general, the absorption rates of NA and RCA reached approximately 40% and 65-75% of their absorption capacity, respectively, after 2 minutes of being submerged in water. At 2 hours, the absorption ratio reaches 88% for NA and

90-94% for RCA. Considering that the absorption rate of RCA mixed into concrete could be lower than its absorption submerged in water, aggregates will not reach their full absorption capacity within the casting time (1 to 2 hours). Therefore, from the workability standpoint, it might not be necessary to account for the full absorption during the moisture adjustment stage in the mixture design process.



a) Relative absorption rate over 72 hours



b) Relative absorption rate over 2 hours

**Figure 47 Relative absorption rate over time**

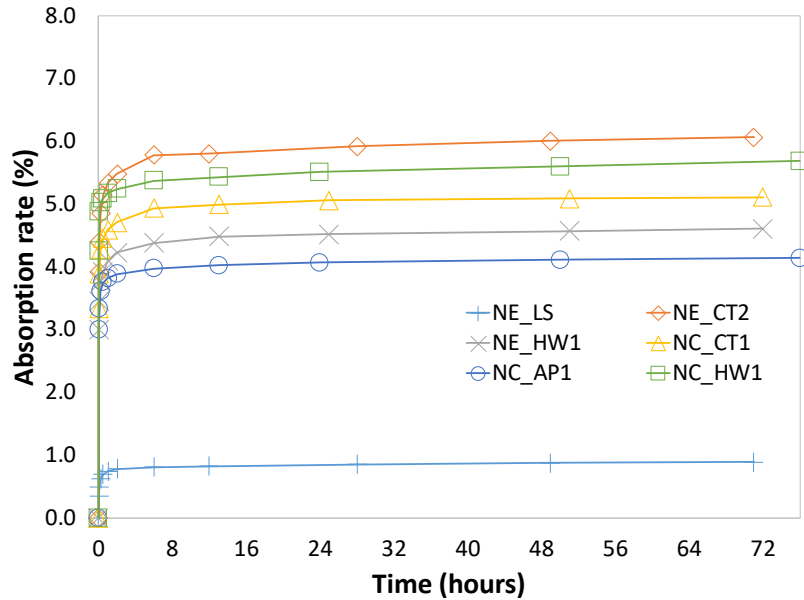


**Figure 48 Absolute absorption rate over time**

### 4.3 Chemical compositions

This section provides information about the statistical procedure and parameters used to analyze the data collected by the evaluation of the chemical compositions of the RCA samples. After the physical characterization of the RCA samples, the samples were tested according to the procedure described earlier in section 3.2.7 to obtain the PHXRF test results.

#### 4.3.1 Control Sample

To evaluate the results obtained from the PHXRF testing of RCA samples, control samples for each of the four NC RCA samples were prepared and then sent to an external laboratory for whole rock analysis to determine the chemical composition. Results of the whole rock analysis are provided in Table 20. It is noted that the whole rock analysis results are from a heated, fused sample, ground into powder, and tested using inductively coupled plasma (ICP) analysis and X-ray fluorescence (XRF) analysis.

**Table 20 Element weight % obtained via whole rock analysis**

Element	Element Weight %			
	NC CT1	NC CT2	NC HW1	NC AP1
Si	29.822700	10.050000	29.448700	27.251800
Al	5.451300	0.555700	6.298100	6.960000
Fe	3.175400	0.615400	1.972400	6.294900
Ca	7.897400	30.446200	7.504400	7.575800
Mg	1.260500	0.494500	0.373900	2.508900
Na	1.372400	0.089000	2.270100	1.617300
K	1.021100	0.157700	2.781000	0.448300
Cr	0.004800	0.008900	0.003400	0.006200
Ti	0.311700	0.054000	0.115900	0.767400
Mn	0.054200	0.031000	0.038700	0.100700
P	0.061100	0.144000	0.048000	0.130900
Sr	0.042300	0.042300	0.033800	0.067600
Ba	0.035800	0.009000	0.080600	0.044800
C	0.660000	8.280000	0.830000	0.350000
S	0.170000	0.210000	0.140000	0.160000
Ba	0.033300	0.005740	0.078300	0.044100
Ce	0.004690	0.000960	0.007710	0.003720
Cr	0.004000	0.008000	0.003000	0.006000
Cs	0.000080	0.000029	0.000255	0.000056
Dy	0.000238	0.000097	0.000523	0.000314
Er	0.000138	0.000050	0.000305	0.000163
Eu	0.000082	0.000021	0.000116	0.000155
Ga	0.001510	0.000160	0.001920	0.001600
Gd	0.000300	0.000088	0.000516	0.000329
Ge	<0.0005	<0.0005	<0.0005	<0.0005
Hf	0.000460	0.000240	0.000600	0.000280
Ho	0.000049	0.000016	0.000099	0.000059
La	0.002330	0.000560	0.003850	0.001640
Lu	0.000022	0.000007	0.000042	0.000022
Nb	0.000650	0.000200	0.001030	0.000680
Nd	0.002020	0.000540	0.003410	0.002170
Pr	0.000520	0.000134	0.000901	0.000482

Element	Element Weight %			
	NC CT1	NC CT2	NC HW1	NC AP1
Rb	0.003970	0.000640	0.011100	0.001260
Sm	0.000391	0.000106	0.000639	0.000388
Sn	0.000200	<0.0001	0.000200	0.000100
Sr	0.044100	0.036000	0.033000	0.074600
Ta	0.000050	0.000010	0.000080	0.000040
Tb	0.000043	0.000014	0.000079	0.000051
Th	0.000737	0.000149	0.001620	0.000206
Tm	0.000018	0.000007	0.000040	0.000024
U	0.000240	0.000283	0.000436	0.000073
V	0.010500	0.002100	0.004200	0.021500
W	0.000100	0.000200	0.000100	0.000100
Y	0.001360	0.000480	0.002660	0.001590
Yb	0.000146	0.000055	0.000286	0.000153
Zr	0.018900	0.010600	0.021800	0.011500
As	0.000440	0.000320	0.000300	0.000170
Bi	0.000009	0.000004	0.000006	0.000004
In	0.000002	0.000001	0.000002	0.000002
Hg	<0.0000005	0.000010	<0.0000005	<0.0000005
Re	0.000000	0.000000	0.000000	0.000000
Sb	0.000048	0.000028	0.000022	0.000019
Se	0.000060	0.000030	0.000020	0.000040
Te	0.000001	0.000003	0.000001	0.000002
Tl	0.000016	0.000003	0.000017	0.000010
Ag	0.000005	0.000002	0.000003	0.000003
Cd	0.000015	0.000038	0.000007	0.000010
Co	0.001385	0.000345	0.000359	0.002810
Cu	0.004080	0.000562	0.001290	0.006520
Li	0.001670	0.000460	0.002960	0.001070
Mo	0.000488	0.000110	0.000127	0.000106
Ni	0.002090	0.001530	0.001025	0.006420
Pb	0.001385	0.000482	0.001950	0.000600
Sc	0.001220	0.000117	0.000510	0.002320
Zn	0.007170	0.004340	0.006320	0.007200

To prepare the control samples, the thermal shock method as described in section 3.2.5 was used to separate the aggregate and mortar. Using this method, the mean RMC was calculated for No. 67 graded aggregate size, which was selected as the representative size for analysis. Once the RMC was determined for each sample, a 20g composite sample (mixture of mortar and aggregate) was prepared according to the laboratory-measured RMC percent shown in Table 21. The 20-g of composite mixture is comprised of X% of 20g + (100-X)% of 20g, where X = RMC%, and 100-X = Aggregate wt%. Table 23 shows the RMC percent and weight distribution of each RCA sample.



**Table 21 Control sample Composition**

RCA Sample	Laboratory-measured Mean RMC%	X% of 20 grams	(100-X)% of 20 grams	Total Weight (grams)
NC AP1	33.67	6.73	13.26	20
NC CT1	41.93	8.38	11.61	20
NC HW1	43.93	8.78	11.21	20
NC CT2	55.76	11.15	8.84	20

Table 22 provides the average weight % of each element from the four RCA samples tested using the PHXRF. Note that for each RCA sample, the PHXRF results are provided for the three particle sizes of interest, No. 4, No. 12, and No. 50. As a reminder, these averages represent the mean computed from 12 measurements (three measurements taken randomly from each of the four quadrants of the sample). The raw data for all PHXRF measurements are provided in Dey (2020).

**Table 22 Average element concentrations in weight % from PHXRF**

Elements	NC AP1			NC CT1			NC HW1			NC CT2		
	No. 4	No. 12	No. 50	No. 4	No. 12	No. 50	No. 4	No. 12	No. 50	No. 4	No. 12	No. 50
Na	0.0809	0.0000	0.0516	0.0008	0.0112	0.0000	0.0000	0.0329	0.0000	0.2808	0.2490	0.1556
Mg	0.0000	0.0000	0.0000	0.0000	0.0000	0.0000	0.0000	0.0000	0.0000	0.0000	0.0000	0.0000
Al	1.1005	1.1205	1.4142	0.3400	0.4525	0.4540	0.5891	0.8335	0.9614	0.0000	0.0042	0.0084
Si	4.2152	4.3376	5.1253	3.8349	4.2804	6.7317	4.5482	4.1852	4.8632	2.3525	2.2261	3.0400
P	0.0190	0.0040	0.0109	0.0069	0.0147	0.0012	0.0117	0.0014	0.0005	0.0188	0.0091	0.0000
S	0.5025	0.4984	0.5051	0.5628	0.5662	0.5866	0.5608	0.5012	0.5017	0.2613	0.2855	0.3591
K	0.2779	0.2708	0.2967	0.2366	0.3005	0.2588	0.5808	0.6666	0.9526	0.1108	0.1468	0.1474
Ca	4.1318	4.4303	4.0024	6.3559	7.3314	5.8792	4.4733	4.7039	5.1282	13.3876	14.0301	13.0233
Ba	0.3778	0.6236	0.8227	0.2238	0.0098	0.0966	0.0480	0.0769	0.0027	0.0000	0.0287	0.0103
Ti	0.2132	0.0970	0.0812	0.0246	0.1109	0.0701	0.0519	0.0645	0.0883	0.0192	0.0198	0.0325
V	0.0000	0.0000	0.0000	0.0013	0.0019	0.0055	0.0033	0.0042	0.0063	0.0049	0.0038	0.0054
Cr	0.0047	0.0063	0.0066	0.0045	0.0039	0.0060	0.0043	0.0054	0.0052	0.0023	0.0025	0.0034
Mn	0.0284	0.0275	0.0282	0.0223	0.0243	0.0281	0.0248	0.0239	0.0240	0.0215	0.0226	0.0224
Fe	2.0522	1.0289	0.9035	0.3143	1.5305	0.8296	0.9243	0.9277	1.3025	0.2938	0.3408	0.4266
Co	0.0345	0.0061	0.0012	0.0027	0.0043	0.0065	0.0057	0.0008	0.0075	0.0022	0.0029	0.0028
Ni	0.0017	0.0036	0.0031	0.0026	0.0024	0.0012	0.0012	0.0022	0.0012	0.0021	0.0026	0.0018
Cu	0.0019	0.0072	0.0083	0.0042	0.0083	0.0032	0.0006	0.0043	0.0023	0.0038	0.0049	0.0011
Zn	0.0027	0.0056	0.0061	0.0053	0.0097	0.0025	0.0027	0.0062	0.0026	0.0031	0.0006	0.0025
As	0.0002	0.0004	0.0004	0.0004	0.0006	0.0002	0.0003	0.0005	0.0005	0.0003	0.0002	0.0002
Pb	0.0012	0.0012	0.0009	0.0010	0.0011	0.0011	0.0014	0.0012	0.0015	0.0010	0.0010	0.0011
Th	0.0003	0.0004	0.0004	0.0004	0.0004	0.0003	0.0006	0.0010	0.0008	0.0003	0.0003	0.0003
Rb	0.0010	0.0010	0.0015	0.0019	0.0022	0.0007	0.0040	0.0102	0.0060	0.0005	0.0004	0.0005
U	0.0044	0.0004	0.0005	0.0006	0.0007	0.0003	0.0002	0.0005	0.0004	0.0005	0.0004	0.0005
Sr	0.0374	0.0818	0.0554	0.0357	0.0354	0.0108	0.0156	0.0392	0.0240	0.0404	0.0358	0.0290
Y	0.0008	0.0025	0.0026	0.0023	0.0025	0.0018	0.0037	0.0023	0.0010	0.0019	0.0020	0.0017
Zr	0.0089	0.0103	0.0115	0.0092	0.0132	0.0072	0.0176	0.0188	0.0112	0.0097	0.0136	0.0093
Nb	0.0008	0.0007	0.0007	0.0006	0.0007	0.0005	0.0010	0.0012	0.0010	0.0004	0.0005	0.0005
Mo	0.0079	0.0003	0.0005	0.0018	0.0008	0.0082	0.0063	0.0005	0.0069	0.0013	0.0022	0.0031
Rh	0.0000	0.0000	0.0000	0.0000	0.0000	0.0000	0.0000	0.0000	0.0000	0.0000	0.0000	0.0000
Sn	0.0002	0.0002	0.0002	0.0001	0.0001	0.0002	0.0002	0.0002	0.0002	0.0002	0.0002	0.0002
Sb	0.0001	0.0001	0.0002	0.0001	0.0001	0.0005	0.0001	0.0001	0.0004	0.0002	0.0000	0.0003

#### **4.3.2 Statistical analysis to determine optimal particle size for PHXRF characterization of RCA**

As there is a large number of different major/trace elements detected from the PHXRF analysis, a statistical analysis is necessary to identify the elements that can be used to determine the RMC%. Statistical analysis of the data obtained using the PHXRF began with a one-way analysis of variance that was performed on the data sets to prove a statistically significant difference between the test results obtained for different size fractions of RCA (of the same type), and RCA obtained from different sources (using the same size fraction). The ANOVA test is used on more than two data sets to determine if the population means are equal with some statistical certainty. This test helps identify if there is a significant difference between the data sets by using either the F-test or Welch's F-test, depending on whether the variances of each data set are equal. The ANOVA tests the following hypotheses:

Null Hypothesis:

$$H_0 = \mu_1 = \mu_2 = \dots = \mu_n \quad (\text{Eq. 19})$$

Alternate Hypothesis:

$$H_1 = \text{The mean of at least one population is unequal} \quad (\text{Eq. 20})$$

The fundamental concept behind the ANOVA test is that the total variation is divided into two parts in the dependent variable, whereas one part is the variation within the samples, which is attributed to chance, and the second part is the variation between samples, which is attributed to specific causes (Molugaram and Rao 2017).

The ANOVA test was performed on data sets to prove a statistically significant difference between the test results for different sizes (No. 4, No. 12, and No. 50) within each RCA sample and, for each fractionated size, across each of the four RCA samples. To conduct this test, Minitab, a general-purpose statistical analysis software, was used. Before conducting the ANOVA test, Levene's test, a test for testing the equality of variances, was performed on the data sets, to determine which ANOVA test is used. If the variances are equal, then the standard F-test is used, whereas, in the case of unequal variances, Welch's F-test is used to test the hypotheses. Based on the equality of variances, the post-hoc test also changes. For equal variances, Tukey's test is used, and for unequal variances, the Games-Howell test is used to show a pairwise comparison that indicates which data sets are statistically different and which are not.

These tests were performed at a significance level of 5% ( $\alpha=0.05$ ). Therefore, tests that returned a p-value of less than or equal to 0.05 were considered statistically significant (highlighted in green). The Summary tables of ANOVA test are shown in Table 23 and Table 24. The null and alternate hypothesis for Table 23 would be  $H_0$ , in which the sample size has no effect on the elemental concentrations, and  $H_1$  in which the sample size affects the elemental concentrations of at least one size group. For Table 24,  $H_0$  is that the sample source has no effect on the elemental concentrations of the samples, and  $H_1$  is that the sample source affects the elemental concentrations of at least one sample group. In this table, “Yes” means the p-value for the given element is less than 0.05 and is statistically significant, and “No” means the p-value for the given element is greater than 0.05 and is statistically insignificant.

**Table 23 ANOVA test for RCA samples- No.4, No.12, No.50**

Major/ Trace Elements	P-value				Statistically significant			
	NC_ AP1	NC_ CT1	NC_ HW1	NC_ CT2	NC_ AP1	NC_ CT1	NC_ HW1	NC_ CT2
Al	0.000	0.182	0.005	--	Yes	No	Yes	--
Si	0.001	0.000	0.189	0.000	Yes	Yes	No	Yes
P	0.169	0.007	0.023	--	No	Yes	Yes	--
S	0.928	0.471	0.226	0.000	No	No	No	Yes
K	0.236	0.171	0.000	0.090	No	No	Yes	No
Ca	0.233	0.008	0.311	0.535	No	Yes	No	No
Ba	0.212	0.005	0.276	--	No	Yes	No	--
Ti	0.010	0.000	0.007	0.032	Yes	Yes	Yes	Yes
V	--	0.058	0.075	0.064	--	No	No	No
Cr	0.007	0.012	0.020	0.001	Yes	Yes	Yes	Yes
Mn	0.864	0.013	0.562	0.092	No	Yes	No	No
Fe	0.034	0.000	0.054	0.333	Yes	Yes	No	No
Co	0.002	0.023	0.379	0.300	Yes	Yes	No	No
Ni	0.007	0.000	0.002	0.078	Yes	Yes	Yes	No
Cu	0.000	0.000	0.000	0.073	Yes	Yes	Yes	No
Zn	0.000	0.000	0.000	0.023	Yes	Yes	Yes	Yes
As	0.000	0.000	0.381	0.036	Yes	Yes	No	Yes
Pb	0.020	0.788	0.248	0.830	Yes	No	No	No
Th	0.074	0.013	0.000	0.001	No	Yes	Yes	Yes
Rb	0.058	0.003	0.000	0.834	No	Yes	Yes	No
U	0.018	0.082	0.630	0.940	Yes	No	No	No
Sr	0.000	0.000	0.000	0.007	Yes	Yes	Yes	Yes
Y	0.000	0.011	0.000	0.162	Yes	Yes	Yes	No
Zr	0.058	0.000	0.001	0.042	No	Yes	Yes	Yes
Nb	0.066	0.002	0.003	0.009	No	Yes	Yes	Yes
Mo	0.000	0.001	0.000	0.184	Yes	Yes	Yes	No
Sn	0.000	0.000	0.001	0.016	Yes	Yes	Yes	Yes
Sb	0.342	0.042	0.016	0.125	No	Yes	Yes	No

**Table 24 ANOVA test for NC\_API/NC\_CT1/NC\_CT2/NC\_HW1 RCA sample- No.4, No.12 & No.50**

Major/Trace Elements	P-value			Statistically significant		
	NC_API, NC_CT1, NC_HW1, NC_CT2					
	No.4	No.12	No.50	No.4	No.12	No.50
Al	--	0	0	--	Yes	Yes
Si	0	0	0	Yes	Yes	Yes
P	0.381	0.025	0.008	No	Yes	Yes
S	0	0	0	Yes	Yes	Yes
K	0	0	0	Yes	Yes	Yes
Ca	0	0	0	Yes	Yes	Yes
Ba	--	0.027	0.002	--	Yes	Yes
Ti	0	0	0	Yes	Yes	Yes
V	--	--	--	--	--	--
Cr	0	0	0	Yes	Yes	Yes
Mn	0.004	0.001	0	Yes	Yes	Yes
Fe	0	0	0	Yes	Yes	Yes
Co	0	0	0	Yes	Yes	Yes
Ni	0	0	0	Yes	Yes	Yes
Cu	0.055	0.001	0	No	Yes	Yes
Zn	0.018	0	0	Yes	Yes	Yes
As	0.029	0	0.25	Yes	Yes	No
Pb	0.063	0.683	0.001	No	No	Yes
Th	0	0	0	Yes	Yes	Yes
Rb	0	0	0	Yes	Yes	Yes
U	0.01	0.394	0.815	Yes	No	No
Sr	0	0	0	Yes	Yes	Yes
Y	0	0.004	0	Yes	Yes	Yes
Zr	0.021	0	0.001	Yes	Yes	Yes
Nb	0	0	0	Yes	Yes	Yes
Mo	0	0.012	0.012	Yes	Yes	Yes
Sn	0	0	0.038	Yes	Yes	Yes
Sb	0.487	0.793	0.053	No	No	No

Based on the ANOVA test results and the interpretation of p-value, it was observed that for particle size within each sample, the majority of the elements are statistically significant (Table 23). This implies that the PHXRF results were affected by particle sizes for major and trace elements, although there were few elements that were insignificant and indicated that the results were not affected by particle size, at least for the samples used in this analysis.

Similarly, another set of ANOVA tests was performed across samples of the same particle size (Table 24). It was observed that the majority of the elements were statistically significant, indicating that the results were indeed affected by the source concrete of the samples obtained.

However, a few elements, including P (No. 4), Cu (No. 4), As (No. 50), Pb (No. 4 and No. 12), U (No. 12 and No. 50), and Sb (No. 4, No. 12, and No. 50) were statistically insignificant which could be attributed to the fact that they were present in very low concentrations. The test results (output) obtained from Minitab software are presented in Dey (2020).

Once the ANOVA tests were completed, a series of statistical parameters, including the mean, standard deviation, RMSD, and COV were determined to analyze the accuracy of the PHXRF analysis. As discussed in Chapter 2, to understand the effects of particle size on PHXRF results, RMSD values were computed for each element present in the sample. The RMSD was calculated by determining the sample standard deviation of the difference between the laboratory measurements and PHXRF measurements (Cerato et al. 2017). The RMSD values were observed for each particle size to make conclusions about the effects of particle size on the elemental concentration. As mentioned previously, the raw data for the PHXRF measurements are provided in Dey (2020).

The statistical parameter values discussed above are presented in Table 48 through Table 58 in Appendix B, with one table for each RCA source and particle size.

- Table 48 to Table 49 show analysis results for NC\_AP1, sizes No. 4, No. 12, and No. 50, respectively
- Table 50 to Table 52 show analysis results for NC\_CT1, sizes No. 4, No. 12, and No. 50, respectively
- Table 53 to Table 55 show the analysis results for NC\_HW1, sizes No. 4, No. 12, and No. 50, respectively
- Table 56 to Table 58 show the analysis results for NC\_HW2, sizes No. 4, No. 12, and No. 50, respectively

In these tables, the RMSD column showing high, medium, and low values are highlighted in red, yellow, and green, respectively. As a reminder, a high RMSD (red) indicates low accuracy, while a low RMSD (green) indicates high accuracy. The symbol double hyphen (--) indicates that the RMSD and  $COV_{RMSD}$  values could not be computed as the element weight % was zero.

Figure 49 shows the relationship between the particle size and the RMSD values. Similar to the findings of Cerato et al. (2017), significant drops were observed in the RMSD and  $COV_{RMSD}$

values with decreasing particle size. However, contrary to the observations made by Cerato et al. (2017), with the exceptions of elements K, Cr, Ba, Co, Zn, and Zr, the RMSD and  $COV_{RMSD}$  values for all the other elements did not decrease with the decrease in particle size. Results indicate that the decrease in particle size did not bring about any significant benefits in terms of accuracy. Rather, in some cases, the change in RMSD values was either insignificant or the values did not follow the decreasing pattern from No.4 to No.50.

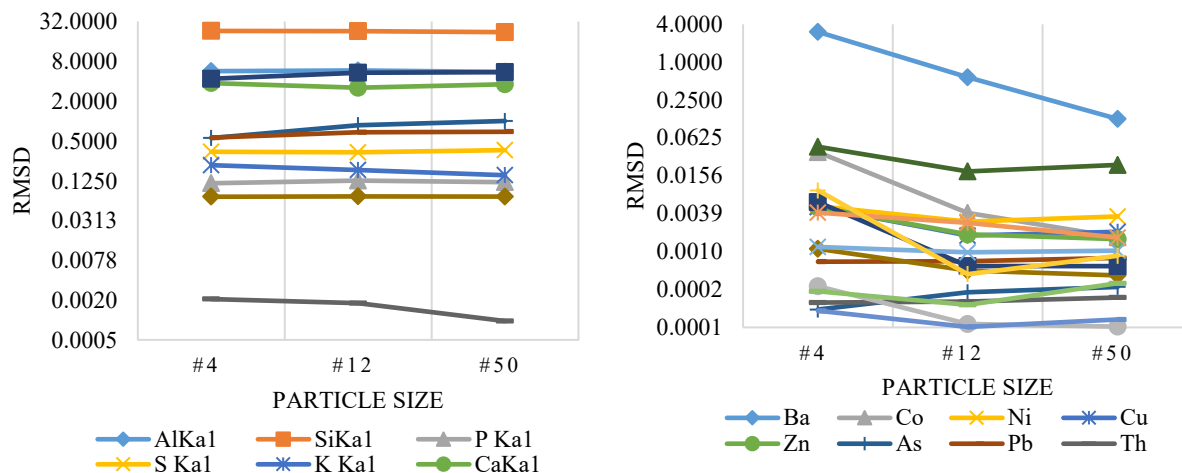


**Figure 49 Sieve size vs. RMSD (NC\_API RCA sample-major and trace elements)**

As shown in Figure 50, similar to the observations made for NC\_API, for sample NC\_CT1, only a handful of elements, including Al, Si, V, and Mn, showed improved accuracy when the particle decreased. The rest of the elements did not show any decrease in RMSD or  $COV_{RMSD}$  values with the decrease in particle size.

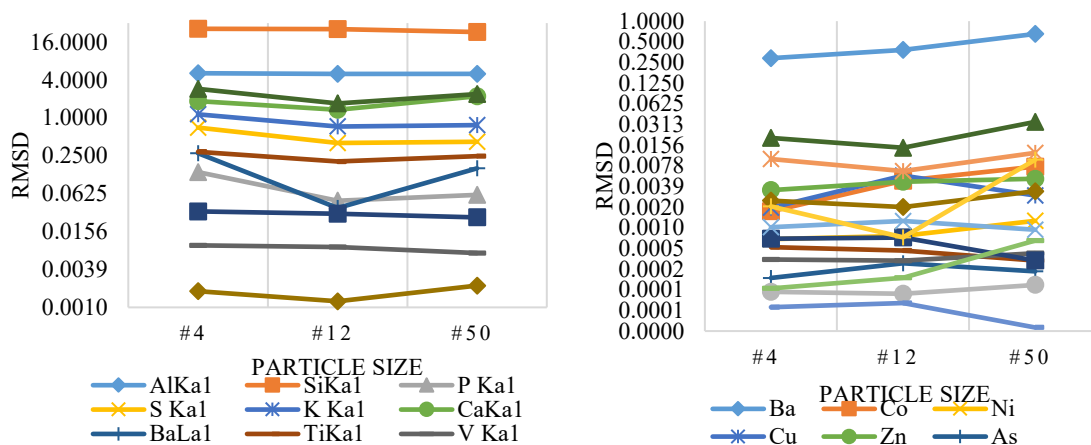


**Figure 50 Sieve size vs. RMSD (NC\_CT1 RCA sample-major and trace elements)**

As can be seen in Figure 51, with the exception of the elements Al, S, K, Ca, Ti, Fe, Ni, and Th, no significant benefits were observed for the rest of the elements in terms of improvement in accuracy with a reduction in particle size for sample NC\_HW1.

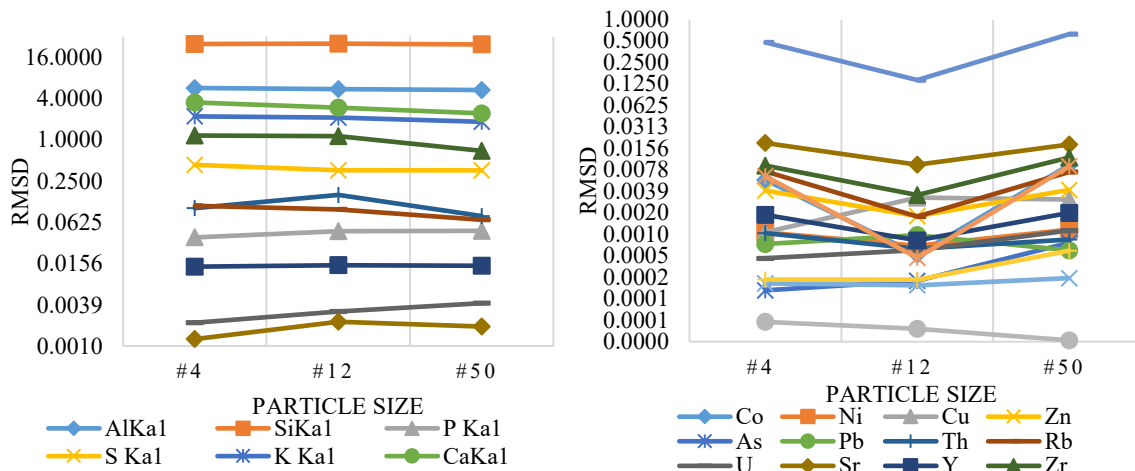


**Figure 51 Sieve size vs. RMSD (NC\_HW1 RCA sample-major and trace elements)**

The RMSD values plotted for NC\_CT2 are shown in Figure 52. Similar to the other RCA samples discussed previously, only elements K, Cr, Mn and Fe showed a decreasing trend in RMSD values with decrease in sample size indicating there was improved accuracy in the above-mentioned elements with decrease in particle size.

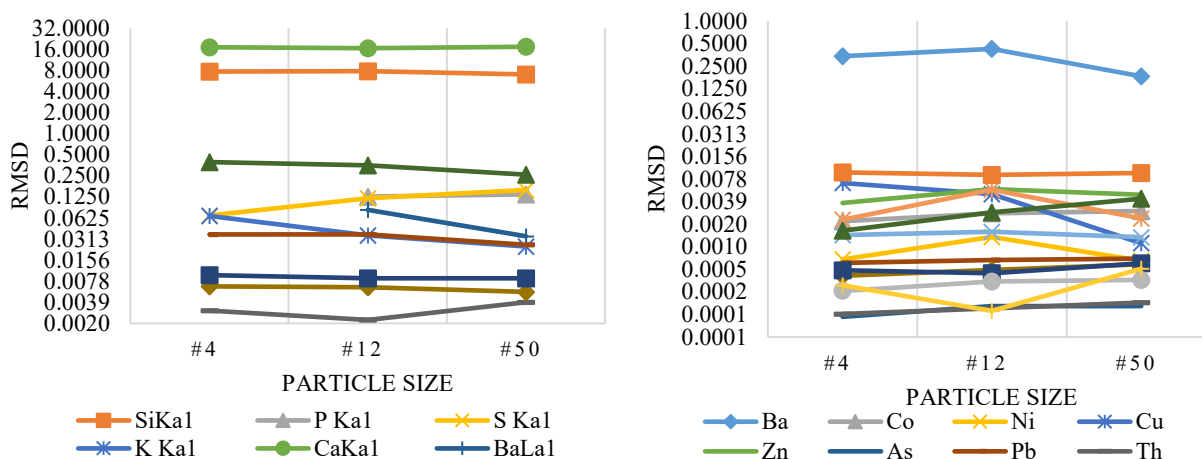


**Figure 52 Sieve size vs. RMSD (NC\_CT2 RCA sample-major and trace elements)**

Based on the RMSD values computed by taking the standard deviation of the difference between the whole rock values (shown in Table 23) and PHXRF results, it was observed that

barring a handful of elements, there was no specific trend that the RMSD values followed when going from a larger to smaller particle size for the sample. The values appeared to vary from element to element across the different samples without any readily discernable pattern.

The RMSD values for Si (NC\_AP1, NC\_CT1& NC\_HW1) and the Ca value (NC\_CT2) were high and in the unacceptable range, whereas the rest of the elements were reasonable, with most of the trace elements showing RMSD values under one indicating that the trace elements are close to the whole rock values and that the data is concentrated around the line of best fit. Contrary to what was observed in a similar analysis of soils (Cerato et al. 2017), the RMSD values for RCA samples did not decrease with a decrease in particle size. This could be attributed to RCA's heterogeneous composition due to the presence of adhered mortar and other contaminants, whereas the sample under consideration in the literature review was soil that had a more homogenous composition.

Therefore, based on the RMSD values, it can be concluded that the particle size should not have a significant impact on the elemental concentrations of the majority of the elements for the samples tested in this research study using PHXRF.

#### **4.3.3 Development of models to predict mortar content using PHXRF**

PHXRF data was used to develop models to predict the mortar content of the RCA. Models were developed using the stepwise regression method. The stepwise regression method falls under the multiple linear regression category in which the relationship between the response and predictor variables is determined (Minitab 2019). This method uses a combination of the forward selection and backward elimination methods to build a best-fitted combination of the independent and dependent variables (Chen et al. 2013). During each step, the least significant variables are removed, and the most significant ones are added to the model. To perform this analysis, Minitab software was used to build a regression model equation with the best predictor variables for the mortar content. During each step of the process, variables are added and deleted from the model based on the selected alpha to enter and alpha to remove values. Minitab systematically adds and removes the variables based on the p-values of the variables at each step.

Based on the p-value, Minitab tests the null hypothesis for each regression coefficient to check if it is zero. Thus, predictors with lower p-values make a meaningful contribution to the model. The process stops adding or deleting variables into the model when the p-values of all the



predictors present outside of the model are greater than the alpha-to-enter value and when the p-values of the predictors in the model are less than or equal to the alpha-to-remove value (Minitab 2019).

To predict the mortar content, the mortar contents computed for the RCA samples from the four different sources were chosen as the response variable and the PHXRF results obtained from the separated mortar comprising of both major and trace elements were taken as the predictors. The data was entered into the Minitab software, and stepwise regression was performed with an alpha-to-enter value and alpha-to-remove value of 0.15 (Penn State Eberly College of Science 2020). A regression model was developed for the RCA particle sizes No. 4, No. 12, and No. 50. The models developed are shown in Table 25. Supporting information and output from Minitab are provided in Dey (2020).

**Table 25 Regression equations for No. 4, No. 12, No. 50**

Particle Size	Model to predict mortar content	R <sup>2</sup>
No.4	RCA mortar content (weight %) = $54.52 + 3787 \times V - 16911 \times Pb$	0.999
No.12	RCA mortar content (weight %) = $189.97 - 524.0 \times P - 124820 \times Pb$	0.998
No.50	RCA mortar content (weight %) = $78.66 - 6588 \times Cr$	0.958

The actual mortar content was compared to the predicted mortar content determined using regression equations, and it was observed that the models were fairly strong predictors of the mortar content (Table 26, Table 27, and Table 28). Although the predicted values for the three different sizes were fairly close to the actual mortar content, based on the difference of the mortar content between the actual and predicted values, it can be concluded that size No.4 was the best predictor of the mortar content as the predicted values are very close to the laboratory-measured mortar content for the RCA samples. The reason behind greater differences for No. 50 particle sizes compared to No. 4 and No. 12 could be attributed to the proportion of each component (mortar and aggregate) varying by particle size. With the increase in the nominal size of RCA, the adhered mortar fraction tends to decrease (Zheng et al. 2018). Therefore, No.50 Particle size, which is much finer than No.4 and No.12 size, differs in composition as compared to No.4 and No.12 particle size as they have both an aggregate portion as well as the adhered mortar portion.

**Table 26 Percent difference between predicted and actual mortar content for No.4 size**

RCA Sample	Laboratory Measured Mortar Content	Predicted Mortar Content	% Difference
NC AP1	33.70	33.92	-0.01
NC CT1	41.90	41.64	0.01
NC HW1	43.90	43.79	0.00
NC CT2	55.80	55.94	0.00

**Table 27 Percent difference between predicted and actual mortar content for No.12 size**

RCA Sample	Laboratory Measured Mortar Content	Predicted Mortar Content	% Difference
NC AP1	33.70	33.36	1.02
NC CT1	41.90	42.13	-0.55
NC HW1	43.90	44.29	-0.88
NC CT2	55.80	55.51	0.52

**Table 28 Percent difference between predicted and actual mortar content for No.50 size**

RCA sample	Laboratory Measured Mortar Content	Predicted Mortar Content	% Difference
NC AP1	33.7	35.45	-5.18
NC CT1	41.9	39.27	6.27
NC HW1	43.9	44.59	-1.57
NC CT2	55.8	55.98	-0.32

It is notable that the stepwise regression resulted in the selection of trace elements like vanadium (V), phosphorous (P), lead (Pb), and chromium (Cr) as the strongest predictors of mortar content. This could be attributed to the fact that these elements could be present in the paste only (due to their relatively higher presence in cement and fly ash), and they may be present in very low quantities in the aggregate alone. From the PHXRF data obtained for aggregate only (Appendix A), it was observed that these metals were actually present in low concentrations in the aggregates, which made them good predictors. On the other hand, major elements like Ca, Si, Fe, and Al, which were initially thought to be strong potential predictors of mortar content, were not identified as predictor variables, likely due to the fact that they were present in both the aggregate and the cement paste in significant quantities. Test results indicated that the elements Ca, Si, Fe, and Al were present in significant quantities in both the aggregate (alone) and cement/fly-ash (alone) samples, and their relative weight percentages were high in both of these samples.

Although these models were found to be strong predictors of mortar content, one significant limitation associated with these models would be that the predictor elements would differ based on the source RCA. Additional work would be needed to explore the variability introduced in these models by other RCA sources. Another drawback to these models is that several predictor variables are heavy metals, which can be detrimental to human health. Heavy metals can be present within the RCA in the cement, SCMs such as fly ash, or aggregates. One barrier to the use of RCA, particularly in unbound uses, is the potential for heavy metals from the RCA to leach into waters flowing around/over the RCA (Snyder et al. 2018). Although this approach appears to provide a readily implementable method to predict the mortar content of RCA, it may call attention to a negative aspect of RCA, which could also be a detractor to its use. It is noted, however, that many state transportation agencies allow RCA as unbound base, where it is commonly used. In these unbound applications, metals in leachate have not been found to be problematic in most situations (Snyder et al. 2018).

#### 4.3.4 Using PHXRF to Predict Mortar Content – Expanded Dataset

PHXRF data for the No. 4 particle size fraction of the 5 additional RCA sources TX\_CT1, IA\_CT1, NE\_HW1, NE\_HW2, and NE\_CT2 (shown in Table 29) was combined with the No. 4 particle size PHXRF data from the four NC sources (Table 23) to produce a dataset from 9 different RCA sources. Improved models were developed to predict laboratory-measured mortar content of RCA from the PHXRF data using the stepwise regression method described previously. To develop these improved models, PHXRF data for three of the five additional RCA sources (IA\_CT1, NE\_HW2, and NE\_CT2) were added to the data for NC\_CT1, NC\_HW1, NC\_HW2, and NC\_AP1 and used to train the models. PHXRF data for two of the five additional RCA sources shown in Table 29 were not used to train the models and instead were used to evaluate the models (TX\_CT1 and NE\_HW1).

**Table 29 Average element concentrations in weight % from PHXRF**

New samples	TX CT1	IA CT1	NE HW1	NE HW2	NE CT2
	No. 4	No. 4	No. 4	No. 4	No. 4
Na	0.0000	0.0000	0.0000	0.0000	0.0000
Mg	0.0000	0.0000	0.0000	0.0000	0.0000
Al	0.0292	0.0143	0.0825	0.0000	0.2568
Si	2.4394	2.2996	5.3198	2.3845	3.8575
P	0.0002	0.0000	0.0000	0.0000	0.0000

New samples	<b>TX_CT1</b> <b>No. 4</b>	<b>IA_CT1</b> <b>No. 4</b>	<b>NE_HW1</b> <b>No. 4</b>	<b>NE_HW2</b> <b>No. 4</b>	<b>NE_CT2</b> <b>No. 4</b>
S	0.8788	0.5161	0.5397	0.4063	0.5283
K	0.0610	0.0994	0.2807	0.1539	0.4813
Ca	7.8630	6.9057	3.3849	7.2596	3.4007
Ba	2.4785	0.1702	0.1325	0.1710	0.1192
Ti	0.1307	0.4140	0.2416	0.4081	0.2927
V	0.0000	0.0000	0.0000	0.0000	0.0000
Cr	0.0000	0.0000	0.0000	0.0000	0.0000
Mn	0.0185	0.0193	0.0205	0.0187	0.0198
Fe	0.5345	0.6695	0.2352	0.4746	0.4520
Co	0.0345	0.0006	0.0007	0.0004	0.0006
Ni	0.0017	0.0029	0.0021	0.0027	0.0020
Cu	0.0019	0.0035	0.0004	0.0026	0.0013
Zn	0.0027	0.0057	0.0010	0.0013	0.0045
As	0.0002	0.0007	0.0002	0.0002	0.0006
Pb	0.0012	0.0014	0.0011	0.0012	0.0012
Th	0.0003	0.0004	0.0009	0.0005	0.0010
Rb	0.0010	0.0022	0.0089	0.0037	0.0123
U	0.0044	0.0003	0.0009	0.0009	0.0016
Sr	0.0374	0.0321	0.0244	0.0495	0.0235
Y	0.0008	0.0023	0.0021	0.0016	0.0014
Zr	0.0089	0.0062	0.0093	0.0057	0.0100
Nb	0.0008	0.0006	0.0010	0.0006	0.0010
Mo	0.0079	0.0008	0.0021	0.0004	0.0015
Rh	0.0000	0.0000	0.0000	0.0000	0.0000
Sn	0.0002	0.0001	0.0001	0.0002	0.0001
Sb	0.0001	0.0001	0.0001	0.0001	0.0000

Minitab software's stepwise regression tool was used to build the regression model equation with the best predictor variables for the mortar content, with variables added and deleted from the model based on the selected alpha to enter and alpha to remove values of 0.15. The improved model to predict mortar content using PHXRF data from the No. 4 particle size of seven sources is shown in Table 30.

**Table 30 Model to predict mortar content using No. 4 PHXRF data from seven sources**

Particle Size	Model to predict mortar content	R <sup>2</sup>
No.4	RCA mortar content (weight %) = $77.6874 - 12.683 \times \text{Ba} - 5805.13 \times \text{Cr} - 520.77 \times \text{U} + 29.49 \times \text{Sr} - 52606 \times \text{Sn}$	0.999

As shown in Table 25, preliminary models for predicting mortar content using the four NC RCA sources of three different sizes included the elements of vanadium, lead, chromium, and phosphorus. Of note, the improved model using No. 4 PHXRF data from seven sources again included chromium, along with other trace elements, including barium, uranium, strontium, and tin. The  $R^2$  of the preliminary No. 4 model was 0.999, while the improved model  $R^2$  was 0.999. The VIF for each of the five predictor variables was lower than 10, indicating an acceptably low degree of multicollinearity. A review of the stepwise regression outputs indicated that models with four predictor variables (Cr, U, Sn, and Ba) and three predictor variables (Cr, U, and Sn) would also be suitable for use, with  $R^2$  values for these models being 0.995 and 0.973, respectively.

The improved model was evaluated using the No. 4 PHXRF data from TX\_CT1 and NE\_HW1, which were not used in model development. The percent difference between the mortar content predicted by the improved model was compared to the actual mortar content measured in the laboratory. The percent differences are shown in Table 31.

**Table 31 Percent difference between predicted and actual mortar content for No. 4 size using improved model**

RCA Sample	Laboratory Measured Mortar Content	Predicted Mortar Content	% Difference
TX_CT1	34.86	34.54	-0.32
NE_HW1	63.77	70.99	7.23

This additional analysis reaffirmed that the PHXRF could be used to predict the mortar content of RCA, using the elemental concentrations of trace elements, often heavy metals, as predictor variables. This approach could be reasonably transferred to practice, using the recommended test method presented in Section 8. This method may be most useful for a user if a database of PHXRF measurements for reference RCA could be prepared, including also laboratory-obtained mortar contents (obtained via the thermal shock method) and chemical composition (via whole-rock method). It is envisioned that once data for a reference set of RCA can be prepared, models developed using this reference data could be used to reasonably predict the mortar content and chemical composition of other RCA samples.

#### **4.3.4 Prediction of the chemical composition of RCA using PHXRF data**

Because the PHXRF only detects material to a certain depth (just inside the surface), it was not anticipated that the weight percent value reported by the PHXRF would be directly comparable

to the weight % value determined through laboratory testing (whole rock analysis), where the sample is pulverized, and more extensive testing is performed on the full volume of the sample. Therefore, to evaluate the accuracy of the PHXRF results, a simple linear regression analysis was performed to develop models capable of predicting the laboratory-measured chemical composition using the PXHRF data. A particle size-based simple regression model for each element was created to estimate the relationship between the whole rock values and the PHXRF values from the four RCA samples. For each particle size, “true element content” (from the whole rock analysis) on x-axis vs. measured element content on y-axis was plotted for every individual major and trace element. In each plot, a trendline was produced using regression analysis with an  $R^2$  value for each element pertaining to particle size No.4, No.12, and No.50. All regression models are presented in Dey (2020), and a summary is provided in this report.

The goal of this analysis was to observe the  $R^2$  value and comment on how close the PHXRF values were to the regression line, and determine the predicted value of the elemental concentration from the regression equation of the most suitable size. In Table 32, the  $R^2$  value for the particle size No.4, No.12, and No.50 for each element have been color-coded, where values highlighted in green represent good values (stronger models), values highlighted in yellow represent medium values, and those highlighted in red represent low values (weaker models).

**Table 32 R<sup>2</sup> values for major and trace elements**

Element	R <sup>2</sup>		
	No.4	No.12	No.50
Si	0.8846	0.9718	0.7476
Ca	0.9713	0.9222	0.968
Al	0.5756	0.8575	0.7832
Fe	0.7278	0.2678	0.0753
K	0.9083	0.9754	0.9377
Ti	0.8686	0.4613	0.2612
S	0.813	0.6338	0.4722
Mn	0.7296	0.9777	0.6424
V	0.8797	0.9476	0.8271
Cr	0.5417	0.2254	0.2471
Ba	0.4996	0.6139	0.0522
Co	0.7897	0.8194	0.3271
Ni	0.0017	0.9461	0.849
Cu	0.0002	0.6203	0.879
Zn	0.1048	0.7822	0.221
As	0.8279	0.1985	0.4416
Pb	0.3635	0.0244	0.7677
Th	0.9754	0.9299	0.8021
Rb	0.9902	0.9781	0.8741
U	0.7588	0.0433	0.0531
Sr	0.1808	0.9067	0.6351
Y	0.3753	0.244	0.2045
Zr	0.5204	0.5735	0.0197
Nb	0.9293	0.8138	0.7004
Mo	0.3915	0.0289	0.1974
Sb	0.0249	0.2063	0.6832
Sn	0.3227	0.5313	0.1338

Based on the R<sup>2</sup> values, it was observed that particle sizes No. 4 (14 elements out of 27) and No. 12 (13 elements out of 27) show a strong relationship between the Whole Rock Analysis and PHXRF results for major and trace elements. Elements including Si, Ca, K, V, Th, Rb showed exceptional R<sup>2</sup> values implying that they were more predictable compared to the other elements. This improved predictability could be attributed to the fact that the relative quantities of these elements present in the samples were significant.

#### 4.3.5 Recommendation for particle size for PHXRF analysis

Based on the findings of statistical analysis used to predict the laboratory-measured mortar content based on PHXRF measurements and the chemical composition of RCA using the weight

percent of selected elements, it appears that the No. 4 particle size can be recommended as the representative particle size for PHXRF analysis. The No. 4 particle size clearly exhibited the strongest models used to predict the laboratory-measured mortar content. Although results were more variable in the elemental analysis, there was not a significantly different improvement in prediction between the No. 4 and No. 12 particle size, and the No. 50 size had the least strong correlations of the three particle sizes tested. Regression analysis indicated that the PHXRF results show reasonable accuracy for most of the major and trace elements detected and quantified by the PHXRF using the No 4 size.

Therefore, in order to simplify a recommended testing protocol, the No. 4 particle size is suggested for future use of the PHXRF to analyze RCA, since it shows reasonable accuracy for the elements under consideration. It should be noted that the No. 4 particle size provides an advantage over the No. 12 and No. 50 particle size in that it would likely be present in both the coarse RCA and fine RCA produced from a given source.

#### ***4.3.6 Summary, limitations, and recommendations for future work of PHXRF***

##### *Summary*

The purpose of this work was to determine if the PHXRF could be used to quantify elements present in the RCA samples accurately and to develop a model that would predict the mortar content of the samples. ANOVA tests performed on the weight percentages of the quantified elements between the particle sizes of the same sample and across samples of the same size indicated that between the particle size, most of the elements were statistically significant, indicating the elemental weight percent changed with size. Similarly, the ANOVA results for samples of the same size across the different samples were also statistically significant for the majority of the elements, indicating that the concentrations varied across samples.

To test the accuracy of the results, a reference sample was developed for whole-rock analysis. Using the quantified data from the reference sample, a comparison was made with the results obtained from PHXRF analysis. Statistical parameters including standard deviation, COV, RMSD &  $COV_{RMSD}$  were computed. The RMSD values for the particle sizes No. 4, No. 12, and No. 50 for a majority of the elements did not show a decreasing trend as the particle size decreased, contrary to what was described in the literature review for stabilized soil samples (the closest



material to RCA found in the literature). Instead, for this study, the RMSD values for the detected elements did not show a specific trend with a change in particle size.

The ability to predict the mortar content of RCA should allow it to be more readily utilized by practitioners. In this study, the mortar content of the RCA samples was determined in the laboratory using a thermal shock method developed in this study, and models were developed using stepwise regression to enable the PHXRF elemental analysis in weight percent to predict the RMC. The three equations generated by the software for the sizes No. 4, No. 12, and No. 50 included as predictor variables the trace elements lead, phosphorus, vanadium, and chromium. Once the equations were obtained, the values of these predictor variables were substituted in the equation to obtain the predicted values of mortar content. In a comparison of the three equations, it was observed that the regression equation for the No. 4 particle size provided predictions closest to the laboratory-measured value of mortar content for all four of the samples. Based on this observation, it was concluded that it is possible to predict the mortar content of RCA using the PHXRF, and particle size No. 4 provided the best predictions of the mortar content for the RCA samples tested in this research study.

The PHXRF cannot be expected to directly determine the chemical composition of the RCA due to the fact that for each element, the device only measures the material composition to a certain depth. In addition, the device is incapable of detecting elements lighter than Na. Therefore, elements such as H, O, and C likely present in the RCA will not be detected, and the total weight percent will not add to 100%. A regression model was developed for each element weight percent determined by the PHXRF for each particle size (No. 4, No. 12, and No. 50) of the four samples, correlating the measurement to the corresponding whole rock analysis weight percent. The  $R^2$  value obtained from this regression analysis was observed for each particle size for major and trace elements, and it was concluded that particle sizes No.4 and No.12 showed reasonable  $R^2$  values for major and traced elements. However, since the models used to predict mortar content suggested the No. 4 size to be the most appropriate, the No. 4 size is recommended for this test as well, primarily to save time and perform characterization testing on a single particle size.

It should be noted that, the use of the No. 4 particle size should allow testing of both fine and coarse RCA samples, since this particle size is often present in both gradations of aggregate typically used in building construction. Also, several heavy metals were identified as the strongest

predictor variables for mortar content. It is noted that although these elements allowed for strong models to be developed, they are also negatively linked to human health effects, and their use may bring unwanted attention to the RCA as a material containing these substances.

### *Limitations*

One of the most notable limitations of this research would be the limited number of samples obtained for analysis. Due to time and resource constraints, only a limited number of samples could be collected for this research study. Having more samples to evaluate (i.e., samples from other states where the aggregates must have met QA requirements according to different agency specifications) would help in evaluating how the PHXRF fares against diverse samples. Future research studies should focus on incorporating more samples from a variety of concrete sources to reduce bias.

Sample sets from across the U.S would help capture a broader range in composition. The properties of RCA would also vary due to the w/cm ratio of the source concrete and the presence of organic impurities like alkali-silica reaction, high alumina cement, silt, chloride, and sulfate, etc. (Behera et al. 2014). A wide range of properties and characteristics of the RCA are also influenced by the recycling method and type of crushing equipment utilized in the recycling process. Samples from across the U.S would vary based on crushing methods and equipment used for production and could help strengthen the analysis and findings.

The ‘Mudrock’ calibration file used in the study is a factory-installed calibration file that comes with the device, and this calibration is capable of quantifying from parts per million to percent weight levels as the set includes matrices ranging from limestone to near pure silicates. This calibration set is based on elemental diversity as it contains 26 well-defined reference samples obtained from multiple drill cores. Based on the manufacturer’s recommendation, the Mudrock calibration file was used for quantification purposes (Bruker 2014). Further studies should be conducted to recalibrate existing files by adding additional reference samples to the calibration. This would improve this analysis by capturing a broader range of elements from high to low concentrations, especially for critical elements present in RCA.

In this study, the whole rock analysis method was used for the evaluation of the accuracy of the PHXRF device. Due to monetary constraints, only one sample representative of the whole sample was used for developing the reference sample, which likely limited the findings. Developing a reference sample for each size would likely give more accurate results.

### *Recommendations for Future Work*

Based on the observations made in this research study, the PHXRF shows strong potential for use for the chemical characterization of RCA, as well as for estimating the RMC. Fostering the use of this technology could be highly useful in promoting the use of RCA in concrete construction. As a non-destructive, time-saving, and easy-to-use technology, PHXRF has the potential to aid in the QA and QC requirements for qualifying an RCA source for use in concrete. The recommended test method developed as part of the objective of this research could serve as the basis for a technical procedure for contractors and other users interested in this type of characterization of RCA. Additional research would be needed to help develop this into an AASHTO or ASTM standard. Broadening the work presented in this report with additional RCA sources and validating the models using additional RCA sources should allow users to develop more efficient models for use with their own RCA sources and PHXRF equipment.

### **4.4 Summary**

According to the analysis of RCA characteristics, it was confirmed that RCA has lower specific gravity and absorption due to the more porous nature of a residual mortar. Due to the same reason, RCA results in lower crushing resistance. In general, there is a clear trend of RCA derived from highway or airport pavement concrete having higher quality with considerably lower absorption and ACV. RMC is typically contingent upon the common mix design of concrete in a particular region, e.g., Nebraska RCAs have higher RMC values typically. In terms of aggregate shape, there was no difference observed between NA and RCA. There is, however, a difference in surface texture, but it is attributed more to the nature of NA, and not necessarily a factor of being natural or recycled. There was no clear trend observed regarding the characteristics' variation with size. The freeze-thaw resistance test proved to be able to differentiate air-entrainment levels of parent concretes. While the PHXRF cannot directly determine the chemical composition of the RCA, models could be developed based on reference tests (whole rock analysis) to correlate PHXRF results to measured values. The PHXRF equipment can be potentially used to determine the RMC% and qualify an RCA source for use in concrete.

## **CHAPTER 5. CONCRETE MIXTURE DESIGN AND RESULTS**

### **5.1 Mixture design and concrete performance based on RCA geometry and gradation**

The main objectives of this part of the work were to verify if the current mixture design practices, such as DWR and DVR, will properly work for pavement concrete and or if a mixture design procedure that incorporates the particle packing and excess paste theory principles can be more appropriately used to design concrete that includes RCA. Besides the slump and unit weight tests, fresh concrete behavior was evaluated with the Box Test. Mechanical performance of concrete was analyzed by compressive strength, splitting tensile strength, and modulus of elasticity tests. The durability properties of the concrete were evaluated with the surface and bulk resistivity, and drying shrinkage tests.

#### **5.1.1 Testing matrix development**

Two mixtures based on the DWR and DVR approaches as described in Chapter 2 were developed with NE\_CT2 RCA to verify if these mixture design procedures are effective in designing pavement concrete. One natural coarse aggregate (NE\_LS) and five coarse RCAs (NE\_HW1, NE\_CT2, NC\_AP1, NC\_HW1, and NC\_CT1) with optimized aggregate gradation were used to prepare six optimized mixtures that were designed according to the mixture design procedure from Mamirov et al. (2021) based on particle packing and excess paste theory. A standard Nebraska pavement concrete mix (47B) based on a recently completed Nebraska Department of Transportation (NDOT) study (Mamirov et al. 2019) was also included in this study. A natural sand (NE\_RS) was used as fine aggregate for all the mixtures.

A mixture design improvement procedure, as illustrated in the flow chart shown in Figure 53, was used in the mixture design development. The first step includes obtaining experimental packing degrees of coarse and fine aggregates separately using ASTM C29 and the vibration plus pressure method. From the aggregate gradation results obtained per ASTM C136, the characteristic diameter of coarse and fine aggregates is obtained, which can be done by determining the cumulative % retained and interpolating where 36.8% of particles are retained. Once individual packing degrees and characteristic diameters are determined, the Modified Toufar Model can be used to obtain the optimum aggregate proportions and the packing degree of the aggregate blend.

Then, the combined void content test should be performed for the selected aggregate blend, and the void contents from the aggregate skeletons can be obtained. The experimental packing degree obtained should be very close to the theoretical one. Once the desired aggregate blend is selected, and its void content is known, concrete can be designed with a predetermined minimum  $Pe\%/VB\_agg\%$  ratio of 0.120 based on materials used in the present study. Afterward, a trial concrete mix should be prepared in the lab to justify if the developed mixture has acceptable pavement concrete performance in both fresh and hardened states. An appropriate WR dosage can be applied in this step if it is deemed necessary to meet the criteria in the Box test in terms of surface and edge quality. More details about this mixture design approach can be found in Mamirov et al. (2021).

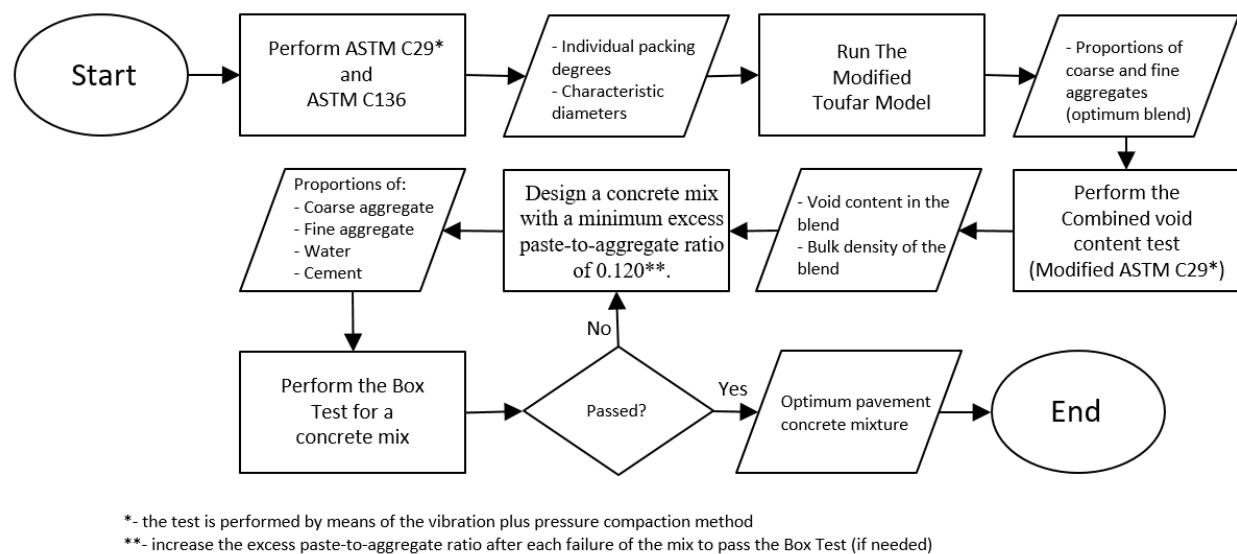


**Figure 53 Proposed mixture design procedure for pavement concrete by Mamirov et al. (2021)**

The optimum blends obtained using the Modified Toufar Model and four different packing methods are shown in Figure 54. According to Mamirov et al. (2021), the vibration plus pressure method provided a better correlation between predicted and actual packing degrees. Moreover, the vibration plus pressure method should be used as it is a more representative method of the actual pavement concrete placement. Results, as shown in Figure 54, demonstrated that, as expected, the NA combination resulted in a better packing with a packing degree at approximately 0.80, which is due to the lower angularity and texture of limestone compared to RCA, with a packing degree at approximately 0.75.

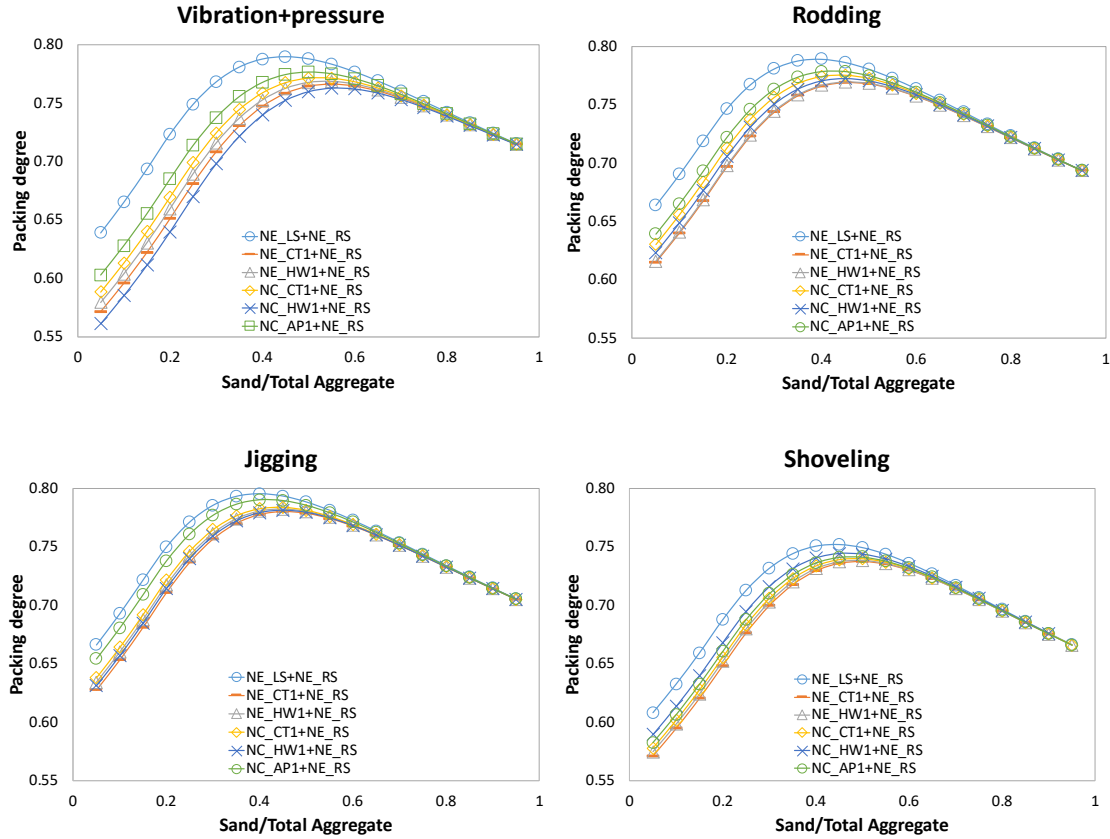


**Figure 54 Theoretical packing degrees from the Modified Toufar Model**

Optimum blends and the resulted theoretical packing degrees, along with the actual packing degree from the combined void content test, are presented in Table 33. While the NA blend has the optimum combination of 55-45 (coarse-to-fine aggregate ratio (by mass)), most of the blends containing recycled RCA have a 45-55 combination that provides the least void content. The difference is likely due to the difference in the surface texture and particle shapes, as the rougher surface and more angular nature of RCA compared to NE\_LS resulted in a need for a higher fine aggregate content to achieve a more optimum gradation. While the error of the model is, on average, about 2.5%, the correlation between theoretical and experimental packing degrees, as shown in Figure 55, is very high.

**Table 33 Summary of theoretical and experimental packing degrees of different aggregate blends**

Aggregate combination	Optimum proportion	Theoretical packing degree	Experimental packing degree	Error (%)
NE LS+NE RS	55-45	0.790	0.802	-1.51
NE CT2+NE RS	45-55	0.766	0.735	4.06
NE HW1+NE RS	45-55	0.769	0.748	2.73
NC AP1+NE RS	45-55	0.777	0.769	2.53
NC HW1+NE RS	45-55	0.763	0.734	3.78
NC CT1+NE RS	50-50	0.771	0.751	1.03

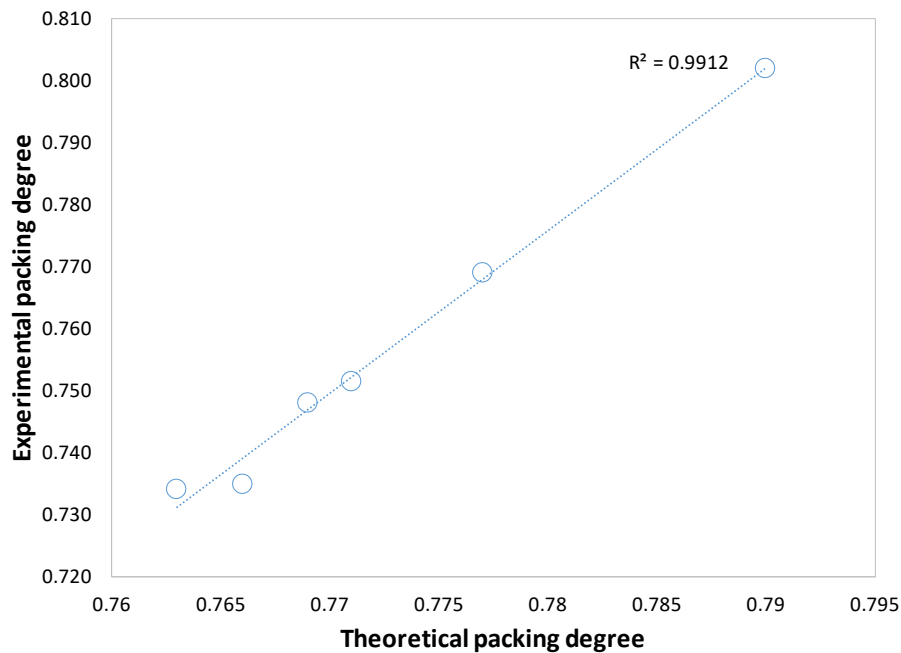


**Figure 55 Correlation between theoretical and experimental packing degrees of optimum blends**

### 5.1.2 Mixture proportions

Once the optimum aggregate blends were obtained, mixture proportions were determined to have a similar excess paste-to-aggregate ratio (0.120) as suggested by Mamirov et al. (2021). Water-to-cement (w/c) ratio was fixed at 0.41, which is a common w/c for pavement concrete mixes. Slump and air content were aimed to be within the ranges of 1 to 3 inches and 5 to 8%, respectively. Figure 56 shows the mixture identification system for the mixtures, and Table 34 summarizes the mixture proportions. Noted that the DVR and DWR mixtures have a compromised gradation, and thus poor matrix skeleton, which leads to the high void content. Because of this,

excess paste in these two mixtures is negative, which physically means that there is not enough paste to fill the voids of the aggregate matrix. The 47B mix has a relatively high excess paste-to-cement ratio (0.190), as it does not use the optimum blend, and thus, cement content is unnecessarily high Mamirov et al. (2021). It is also worth noting that despite all the mixtures designed with the newly proposed mix design method having a similar excess paste-to-aggregates ratio (0.120), the total paste content differs because of the different void contents of the aggregate blends from the different RCA incorporated in these mixtures.

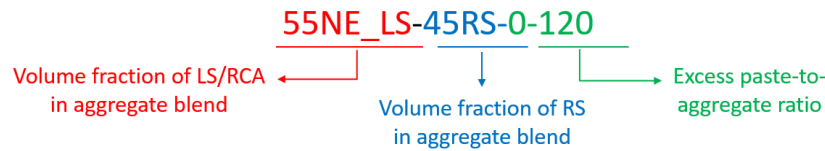


**Figure 56 Mix identification system**

**Table 34 Mixture proportions based on RCA geometry and gradation**

Mix ID	w/c	C*	W	CA	FA	WR	P <sub>t</sub> %	V <sub>O<sub>ble</sub></sub> nd %	P <sub>c</sub> %/ V <sub>B<sub>agg</sub></sub> %
63NE_CT2-37RS--0.111(DWR)	0.41	522	214	1769	1195	18	28.5	37.84	-0.111
55NE_CT2-45RS--0.052 (DVR)	0.41	522	214	1557	1436	18	28.5	33.71	-0.052
47B	0.41	564	231	904	2042**	0	33.0	19.79	0.190
55NE_LS-45RS-0.120 (control)	0.41	522	214	1769	1436	8	28.5	19.81	0.120
45NE_HW1-55RS-0.120	0.41	609	250	1230	1663	8	32.3	25.20	0.120
45NE_CT2-55RS-0.120	0.41	632	259	1190	1639	14	33.3	26.51	0.120
50NC_CT1-50RS-0.120	0.41	605	248	1404	1515	16	32.1	24.85	0.120
45NC_HW1-55RS-0.120	0.41	637	261	1207	1633	16	33.5	26.59	0.120
45NC_API-55RS-0.120	0.41	586	240	1368	1687	8	31.3	23.10	0.120

C-cement content, W-water content, CA-coarse aggregate content, FA-fine aggregate content, WR-water reducer.

All ingredients are in lb/yd<sup>3</sup> except WR, which is in fl oz/cwt

\*Type I/II cement is used for all mixes except 47B, which contains Type IP cement

\*\*47B mix is composed of a combination of sand and gravel instead of plain fine aggregate.

### 5.1.3 Results

#### *Fresh concrete properties*

Table 35 summarizes the fresh properties of the concrete mixtures produced in this study. The first thing worth noting is that target slump, and air content could be achieved with the proposed mixture design procedure and adequate WR adjustments regardless of the use of NA or



RAC. However, for the mixtures designed based on DVR and DWR, due to the lack of paste, slump and air content were extremely low, and the addition of WR was not helpful. In terms of the Box Test, the results showed very poor performance of the DWR and DVR mixes, with the index of E4-S4 for both mixtures (see Figure 57). These results verify that these mixture design approaches are not capable of efficiently designing pavement concrete with RCA without compromising fresh concrete properties. On the contrary, the RAC mixtures designed with the proposed approach with optimum gradation and excess paste content performed similarly or better than concrete made with NA. The results prove the hypothesis that no matter what aggregates are used (NA or RCA), adequate workability for pavement concrete mixture can be obtained, as long as sufficient excess paste is provided. The used excess paste-to-aggregate ratio of 0.120 seems to be reasonable for both coarse NA-fine NA and coarse RCA-fine NA aggregate combinations. Further research is needed to verify the effectiveness of this mixture design procedure for coarse RCA-fine RCA combinations. The Box Test images can be seen in Figure 57.

**Table 35 Fresh concrete properties**

Mix ID	Slump (in.)	Unit weight (pcf)	Air content (%)	Box Test Ranking	Surface voids (%)
47B	3.00	139.2	7.0	E1-S2	3.6
DWR	0.00	140.5	3.5	E4-S4	18.1
DVR	0.00	140.9	3.9	E4-S4	15.4
55NE LS-45RS-0.120 (control)	2.00	142.1	7.8	E1-S1	1.8
45NE HW1-55RS-0.120	1.25	138.9	6.0	E1-S1	1.4
45NE CT2-55RS-0.120	2.75	137.1	6.2	E1-S1	1.9
45NC AP1-55RS-0.120	2.25	142.3	6.4	E1-S1	2.4
45NC HW1-55RS-0.120	3.00	135.1	7.6	E1-S1	2.4
50NC CT1-50RS-0.120	2.25	141.2	5.2	E1-S1	1.9



DWR mix



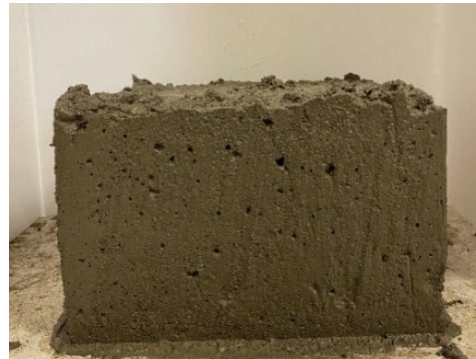
DVR mix



47B



55NE\_LS-45RS-0.120 (control)



45NE\_HW1-55RS-0.120



45NE\_CT2-55RS-0.120



45NC\_AP1-55RS-0.120



45NC\_HW1-55RS-0.120



50NC\_CT1-50RS-0.120

**Figure 57 Box test results**

### *Mechanical properties*

Figure 58 demonstrates the compressive strength test results. Mixtures designed with conventional DWR and DVR procedures exhibited slightly lower strength in comparison to the control optimized mix and comparable strength to the standard 47B mix. The possible reason for this is the low air content in the paste, which in this case almost compensates for the poor concrete matrix due to the compromised combined gradation. It can be seen that RAC mixtures designed with the proposed mixture design procedure resulted in comparable or better performance than the reference concrete mixtures with NA and those designed by DWR and DVR. At 28 days, all RAC mixtures designed with this proposed method had higher compressive strength than the control mixture and the 47B mixture.

It is worth noting that cement content varied in this study as it was targeted to keep excess paste constant. Due to the difference in aggregate void content, in order to keep the excess paste constant, the total paste content (thus, cement content) varied too. Table 36 presents the cement content, aggregate strength, air content, and the resulting 28-day strength of the different mixtures. The fact that RAC has similar or higher compressive strength while having significantly weaker (higher ACV) aggregates implies that cement paste strength (cement content and air content) might be a more significant factor driving the change in compressive strength of concrete. There could be a certain threshold value of ACV, where aggregate with strength above that threshold will not negatively impact the concrete strength. Another potential reason for RAC having higher strength is the rougher surface texture of RCA, which could lead to a stronger ITZ.

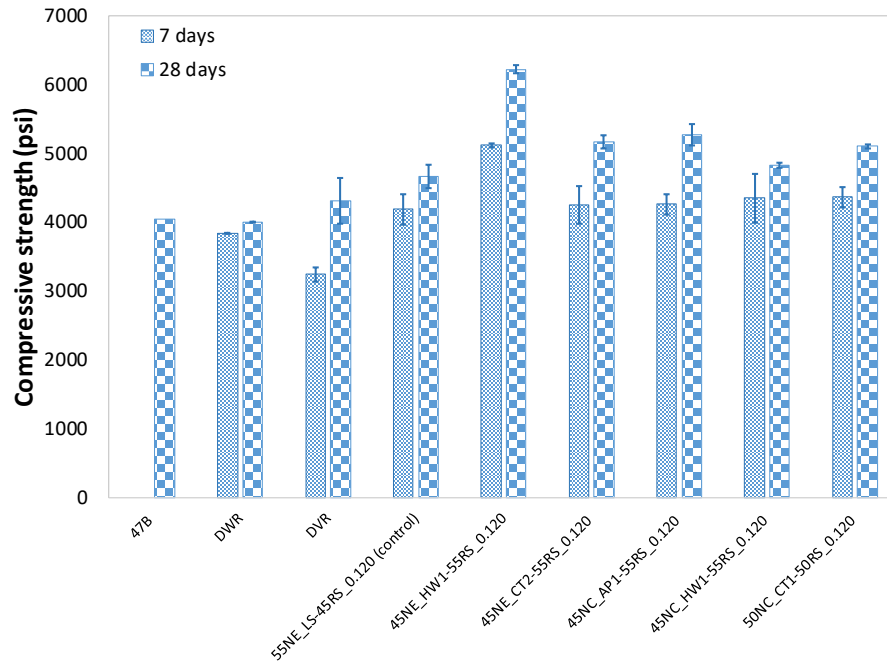


**Figure 58 Compressive strength results**

**Table 36 Summary of factors affecting concrete compressive strength**

Mix ID	Cement content (pcy)	Air content (%)	ACV (%)	$f_{c, 28d}$ (psi)
47B	564	7.6	8.17	4043
DWR	522	3.5	24.71	4006
DVR	522	3.9	24.71	4311
55NE_LS-45RS-0.120 (control)	522	7.8	8.17	4665
45NE_HW1-55RS-0.120	609	6.0	17.85	6222
45NE_CT2-55RS-0.120	632	6.2	24.71	5171
45NC_AP1-55RS-0.120	586	6.4	11.50	5274
45NC_HW1-55RS-0.120	637	7.6	13.38	4832
50NC_CT1-50RS-0.120	605	5.2	14.81	5106

As shown in Figure 59, unlike the compressive strength results, compared to the control mixture with NA, RAC mixtures designed with both the new and conventional mixture design procedures resulted in lower splitting tensile strength. It seems that under tensile stresses, where cement paste is significantly weaker than under compression, the variation in aggregate strength becomes more critical and the incorporation of RCA negatively impacts the splitting tensile strength of the concrete. It is worth noting that even with the reduction of the splitting tensile

strength, all mixtures included in this study still exhibit a reasonable splitting tensile strength with a reduction of between 13% and 25% compared to the reference mixture.

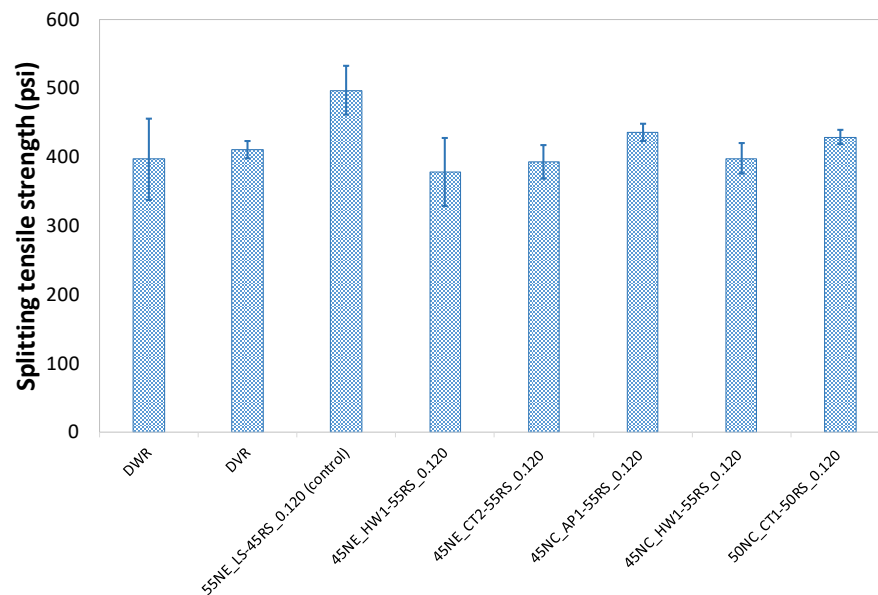


**Figure 59 Splitting tensile strength results**

Besides measuring the maximum strength, the cross-sections of failure of each specimen were analyzed, and the percentage of fractured aggregates was visually estimated (Table 37). An example of the visual inspection of the fracture surface is shown in Figure 60. Note that a fracture surface through RCA particles generally indicates that the surrounding cement paste is stronger than RCA. It can be seen from Figure 61 that there is a strong linear relationship between the percentage of fractured aggregates and ACV up to a certain value of ACV. By drawing the lines along with the curve fits, it can be seen that the threshold ACV value is approximately 15%. With the ACV below this threshold value, aggregates are too weak to carry the load, and the particles are likely to fracture along the cross-section of failure.

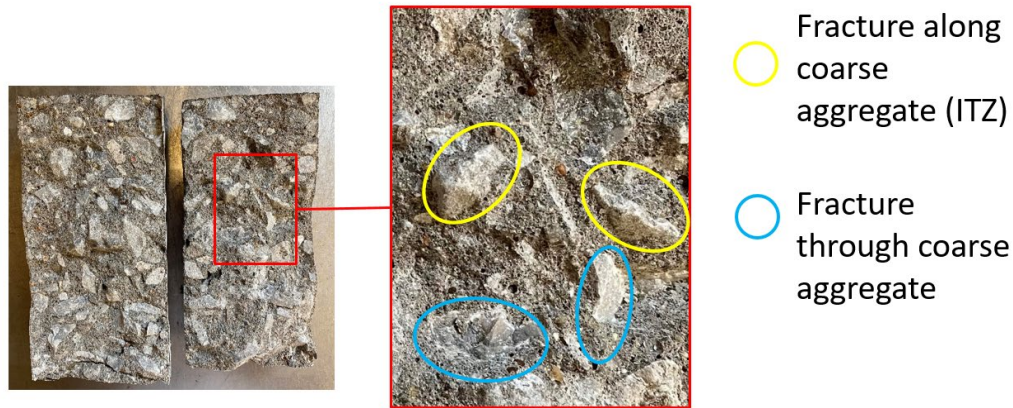


**Figure 60 Example of visual examination of fractured surface.**

**Table 37 Estimated % of fractured aggregates along the fracture surface**

Mix ID	Estimated % of fractured coarse aggregates
DWR	100
DVR	100
55NE LS-45RS 0.120	73
45NE HW1-55RS 0.120	100
45NE CT2-55RS 0.120	100
45NC AP1-55RS 0.120	85
45NC HW1-55RS 0.120	92
50NC CT1-50RS 0.120	100

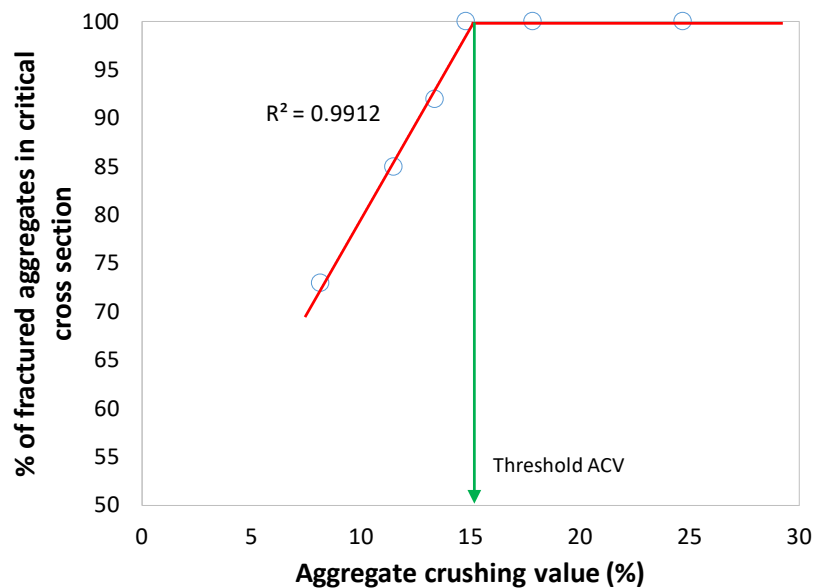


**Figure 61 Relationship between the percentage of fractured aggregates and aggregate ACV**



Modulus of elasticity and Poisson's ratio results are presented in Figure 62. As expected, RAC has a lower elastic modulus and Poisson's ratio due to a softer nature of residual mortar of RCA. Results indicated that when RCA is used in concrete, the rigidity of concrete cannot be predicted from the compressive strength based on the ACI 318 equation as it is commonly done for normal concrete (ACI 318). It is hypothesized that while paste strength might be able to compensate for the effect of weak aggregates and contribute to comparable or higher compressive strength, it might not be the same case for the modulus of elasticity of concrete as aggregates occupy 60-70% of concrete volume and will have more impact on volumetric stability of concrete. In other words, it is believed that while compressive strength is controlled more by paste strength/stiffness, the modulus of elasticity of concrete is controlled more by aggregates' strength/stiffness. Mixtures designed with DWR and DVR methods resulted in a significantly lower elastic modulus and Poisson's ratio. This might be attributed to the high amount of voids in the concrete due to the poorly graded aggregate skeleton and an insufficient amount of paste to fill them.

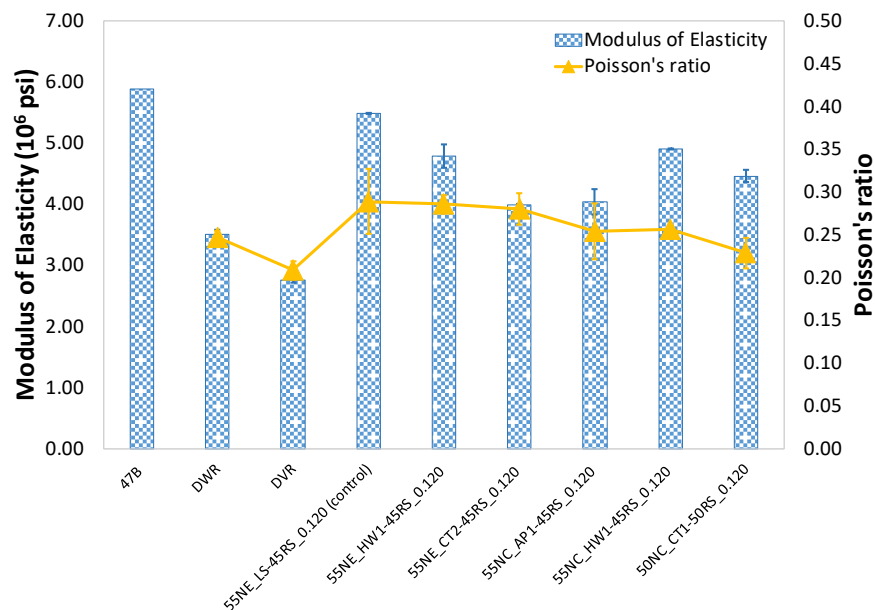
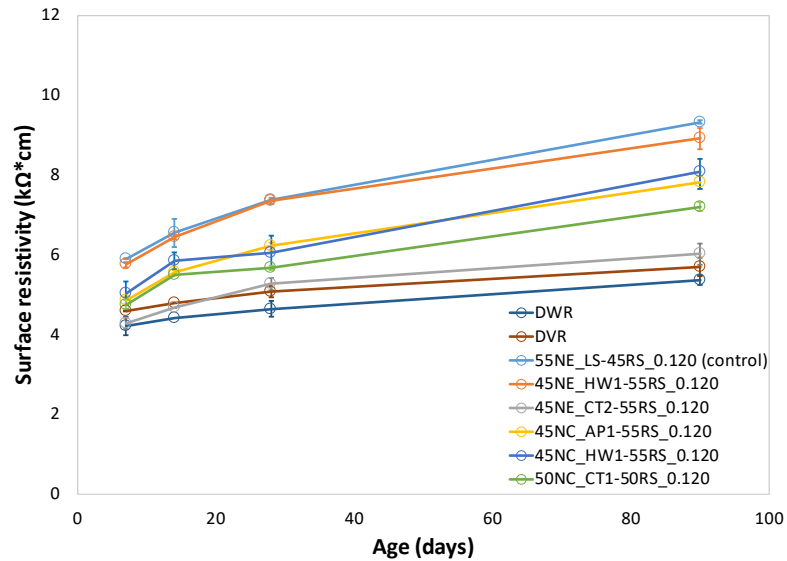


**Figure 62 Elastic modulus and Poisson's ratio results**

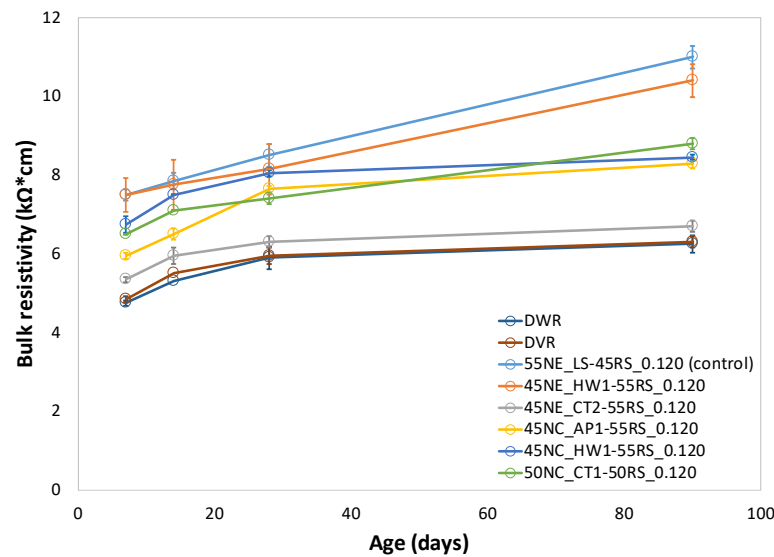
#### *Durability properties*

Surface and bulk resistivity results are shown in Figure 63 showed that RAC mixtures generally exhibited lower resistivity values. However, the mixes obtained with the new proposed

approach resulted in better resistivity properties compared to those designed with DVR and DWR methods. The low resistivity can likely be attributed to the high porosity of RCA, which leads to high water content inside the concrete as specimens were fully saturated during testing. Results indicated that when RCA is introduced into concrete, it may be necessary to compensate for the compromised resistivity by increasing the density of the cement paste matrix by either lowering the w/c or incorporating supplemental cementitious materials (Guo et al. 2018).



a) Surface resistivity



b) Bulk resistivity

**Figure 63 Results from resistivity test**



The property that is expected to be compromised the most in RAC in this study is the shrinkage, because of the higher porosity of RCA and higher cement content needed for the concrete design. Figure 64 illustrates the drying shrinkage results over time, which demonstrated that most of the obtained RAC mixtures pass the criterion for pavement concrete based on the recommended limit of 420 microstrains at 28 days, according to AASHTO PP 84. While the RAC mixtures resulted in a higher shrinkage rate compared to the control mixture, they experienced comparable shrinkage to the 47B mixture. After 28 days, the shrinkage of mixtures with NA (the control mix and 47B) noticeably slowed down, while the RCA mixtures were found to continue to shrink at nearly the same rate. It is worth noting that all of the RAC mixtures experienced initial expansion. Table 38 shows how much each mixture expanded during the curing period. It can be clearly observed that RAC mixtures expanded significantly, while the control mixture with NA experienced no length change. It can also be noticed that DWR and DVR mixtures expanded the most during this stage, which is likely due to the high amount of voids within a concrete matrix that lead to a high amount of water penetration.

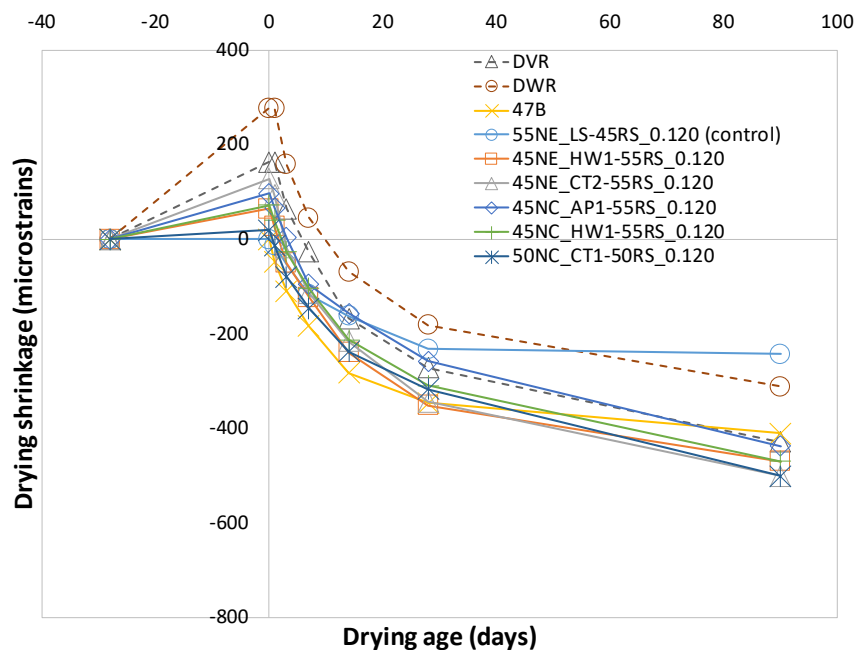


**Figure 64 Results from drying shrinkage tests**

It is worth noting is that the obtained high shrinkage of RAC mixtures is mainly due to the high amount of water absorbed inside concrete during the curing period, which causes expansion. It can be clearly observed that RAC mixtures expanded significantly, while the control mixture

with NA experienced no length change. It can also be noticed that DWR and DVR mixtures expanded the most, which is likely due to the high amount of voids within a concrete matrix that lead to a high amount of water penetration. Once the drying period starts, all the absorbed water starts to evaporate over time, resulting in significant shrinkage. As in-situ concrete generally has a much lower surface area to volume ratio as compared to ASTM C157 specimens, and also does not have a continuous water supply, the concrete structures should not experience initial expansion. Thus, the true shrinkage data can be estimated by accounting for the initial expansion. As shown in Figure 65, the difference between RAC shrinkage and the control mixture is smaller, while the RAC mixes have a comparable shrinkage when compared to the 47B mix.

**Table 38 Expansion of samples during the curing period**

Mix ID	Expansion during curing period (microstrains)
DWR	277
DVR	163
55NE LS-45RS-0.120 (control)	0
45NE HW1-55RS-0.120	64
45NE CT2-55RS-0.120	128
45NC AP1-55RS-0.120	96
45NC HW1-55RS-0.120	72
50NC CT1-50RS-0.120	19

## 5.2 Mixture design nomograph development based on RCA mechanical properties

As the characteristics of aggregate could greatly influence concrete behavior, traditional mixture design methods like the PCA absolute volume method might not be applicable to the design of concrete that incorporates RCA. Mixture design nomographs (MDN) based on specific RCA can be developed and used to better design concrete with RCA (Hu et al. 2013). With the relationship between the mixture design parameters, RAC characteristics, and concrete properties, MDN can be established based on three relationships, which are described by Abram's law, Lyse's law, and Molinari's law (Monteiro et al. 1993, Levy et al. 2004, Hu et al. 2013).

Abram's law describes the relationship between the compressive strength ( $f'_c$ ) of concrete and the water-to-cement ratio ( $w/c$ ) as an exponential function:

$$f'_c = \frac{k_1}{k_2^{w/c}} \quad (\text{Eq. 21})$$

Where  $k_1$  and  $k_2$  are constants, depending on the materials used.

Lyse's law describes the relationship between the w/c and aggregate-to-cement ratio (a/c) as a linear function:

$$a/c = k_3 * (w/c) + k_4 \quad (\text{Eq. 22})$$

Where  $k_3$  and  $k_4$  are constants, depending on the materials used.

Molinari's law describes the relationship between the cement content (C) and a/c as a power function:

$$C = \frac{1000}{k_5 * (a/c) + k_6} \quad (\text{Eq. 23})$$

Where  $k_5$  and  $k_6$  are constants, depending on the materials used.

### 5.2.1 Testing matrix development

One NA and three RCAs with different ACVs were selected to evaluate the effect of ACV on hardened concrete properties at different w/c ratios. Table 39 shows the selected aggregates and corresponding ACVs. Mechanical properties variation with the change of w/c and ACV of coarse aggregate were evaluated. Mechanical properties analyzed were compressive strength, splitting tensile strength, and modulus of elasticity. In addition, surface resistivity was also evaluated.

**Table 39 Selected aggregates for mixture design nomograph development**

Aggregate	ACV (%)
NE LS	8.17
NC AP	11.50
NE HW1	17.85
NE CT2	24.71

### 5.2.2 Mixture proportions

Mixture proportions were obtained using the same mixture design procedure as in section 5.1. The only difference was the water-to-cement ratio which varied from 0.35 to 0.50 with a 0.05 increment. A total of 16 mixtures were prepared in this study, with the information provided in Table 40.

**Table 40 Mixture design for mixture adjustment study**

Mix ID	w/c	C	W	CA	FA	P <sub>t</sub> %	P <sub>c</sub> %/V <sub>B</sub> agg %
55NE_LS-45RS-0.120	0.50	465	232	1769	1436	28.5	0.120
	0.45	495	223	1230	1663	28.5	0.120
	0.40	529	212	1190	1639	28.5	0.120
	0.35	569	199	1404	1515	28.5	0.120
45NE_HW1-55RS-0.120	0.50	542	271	1230	1663	32.3	0.120
	0.45	577	260	1230	1663	32.3	0.120
	0.40	618	247	1230	1663	32.3	0.120
	0.35	664	232	1230	1663	32.3	0.120
45NE_CT2-55RS-0.120	0.50	562	281	1190	1639	33.3	0.120
	0.45	599	269	1190	1639	33.3	0.120
	0.40	641	256	1190	1639	33.3	0.120
	0.35	688	241	1190	1639	33.3	0.120
45NC_AP1-55RS-0.120	0.50	522	261	1368	1687	31.3	0.120
	0.45	556	250	1368	1687	31.3	0.120
	0.40	594	238	1368	1687	31.3	0.120
	0.35	639	224	1368	1687	31.3	0.120

**5.2.3 Results***Fresh concrete properties*

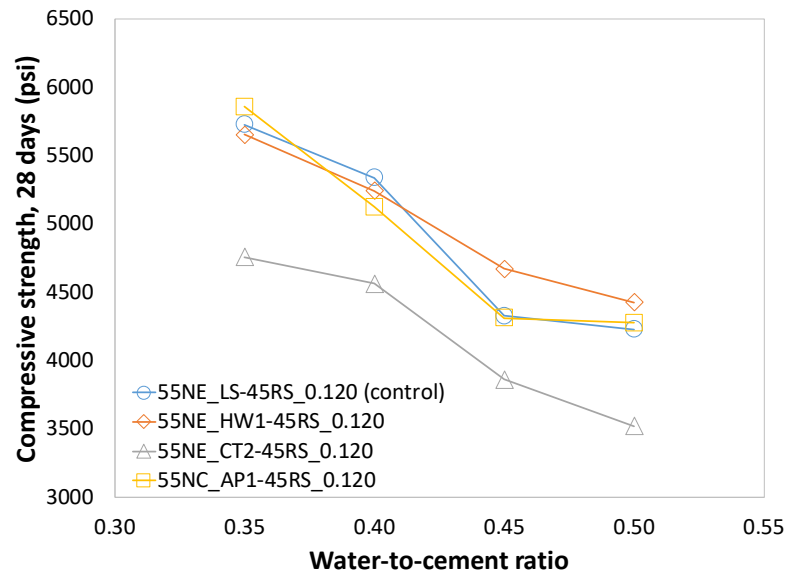
Since the main focus of this part of the study was to evaluate the mechanical properties, fresh concrete tests were performed as a quality control measure (Table 41). The target of 5.0-8.0% air content was maintained consistently throughout most of the mixtures.

**Table 41 Fresh concrete properties of mixtures in mixture adjustment**

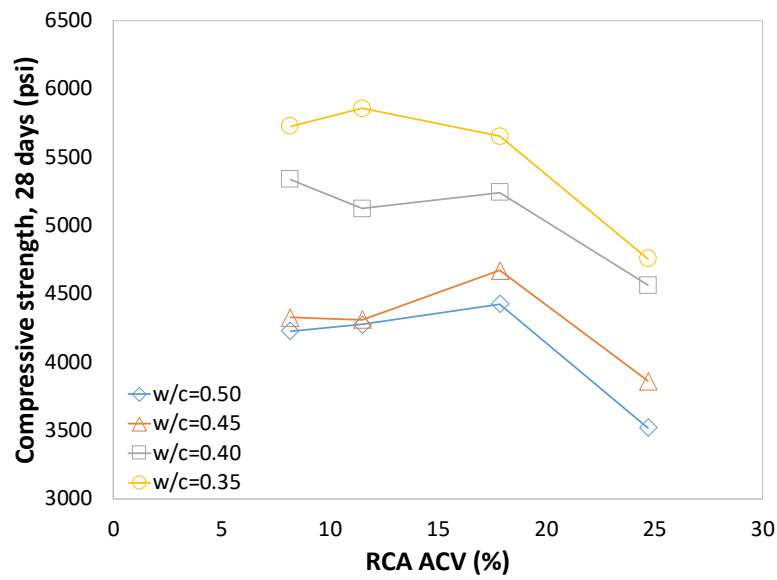
Mix ID	w/c	Slump (in)	Unit weight (pcf)	Air content (%)
55NE_LS-45RS-0.120	0.50	3.00	144.48	6.0
	0.45	2.75	143.76	6.9
	0.40	1.25	146.00	6.1
	0.35	1.00	146.72	6.3
45NE_HW1-55RS-0.120	0.50	4.00	136.32	6.6
	0.45	3.00	135.16	8.0
	0.40	1.25	136.72	7.6
	0.35	0.75	136.92	8.1
45NE_CT2-55RS-0.120	0.50	5.75	138.00	4.5
	0.45	4.50	137.28	5.7
	0.40	2.75	138.00	5.9
	0.35	0.75	138.88	6.0
45NC_AP1-55RS-0.120	0.50	3.00	142.32	5.9
	0.45	1.50	140.08	7.8
	0.40	1.00	142.96	6.4
	0.35	1.00	144.48	6.0

*Hardened concrete properties*

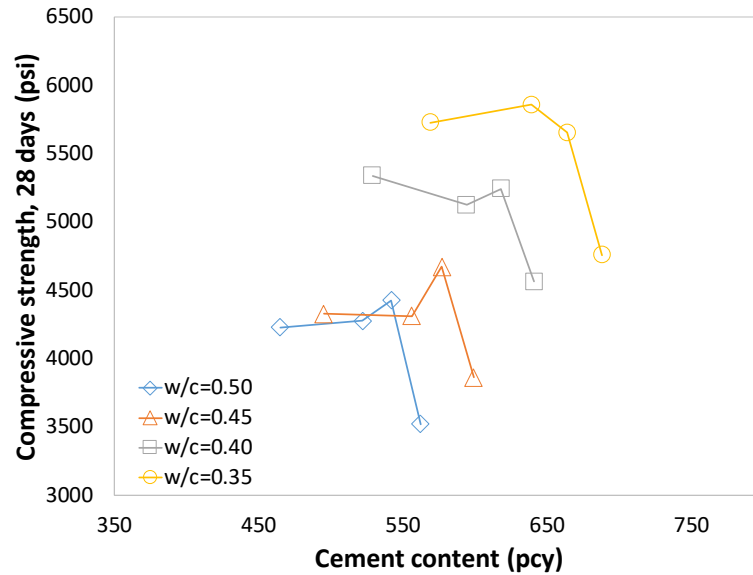
Figure 65 to Figure 68 show the effects of w/c, ACV, and cement content on concrete compressive strength, splitting tensile strength, modulus of elasticity, and surface resistivity, respectively. . As shown in Figure 65a, paste strength appears to have more impact on concrete strength than aggregate strength since there is a consistent compressive strength drop with an increase of w/c. The average compressive strength reduction are approximately 7.5%, 15.2%, and 4.3% for the change in w/c from 0.35 to 0.40, from 0.40 to 0.45, and from 0.45 to 0.50, respectively. Figure 65b demonstrates that ACV does not influence the compressive strength of concrete up to a certain threshold value (18%). It is believed that the proposed mixture design approach is capable of eliminating the effect of weak aggregates.



a) Effect of w/c on compressive strength



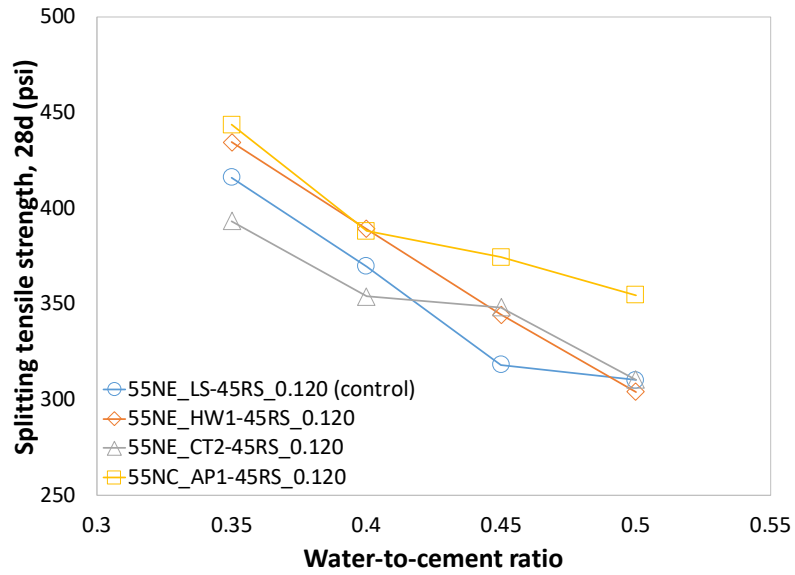
b) Effect of ACV on compressive strength



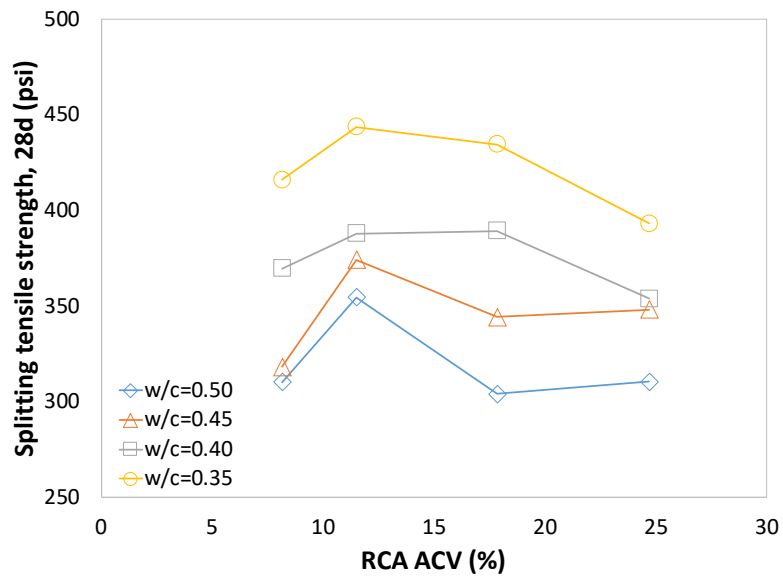
c) Effect of cement content on compressive strength

**Figure 65 Effect of concrete mixture design and RCA ACV on compressive strength of concrete**

There is a similar trend for splitting tensile strength, where it is mostly driven by the paste strength rather than aggregate strength. As shown in Figure 66, the average reductions in splitting tensile strength are 11.0%, 7.6%, and 7.6% for the 0.40, 0.45, and 0.50 w/c, respectively. It is worth noting that the effect of ACV on splitting tensile strength differs from the effect on compressive strength, which implies that aggregates behave differently under different loading conditions.

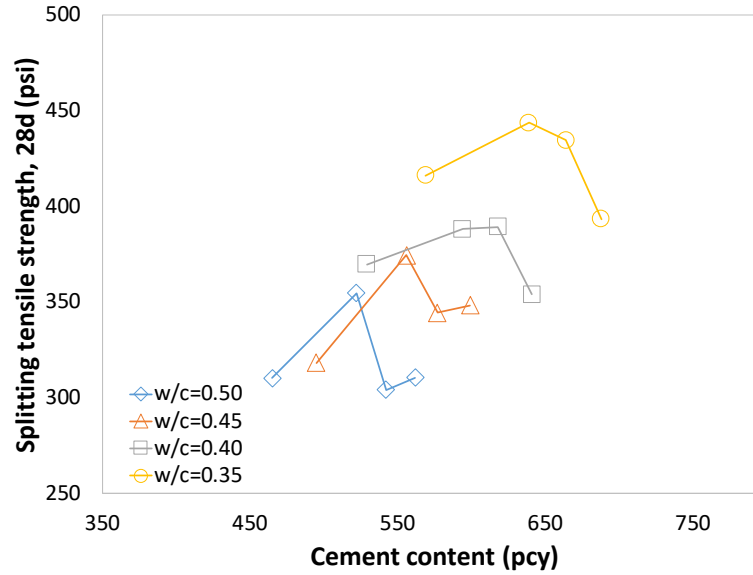


a) Effect of w/c on splitting tensile strength



b) Effect of ACV on splitting tensile strength

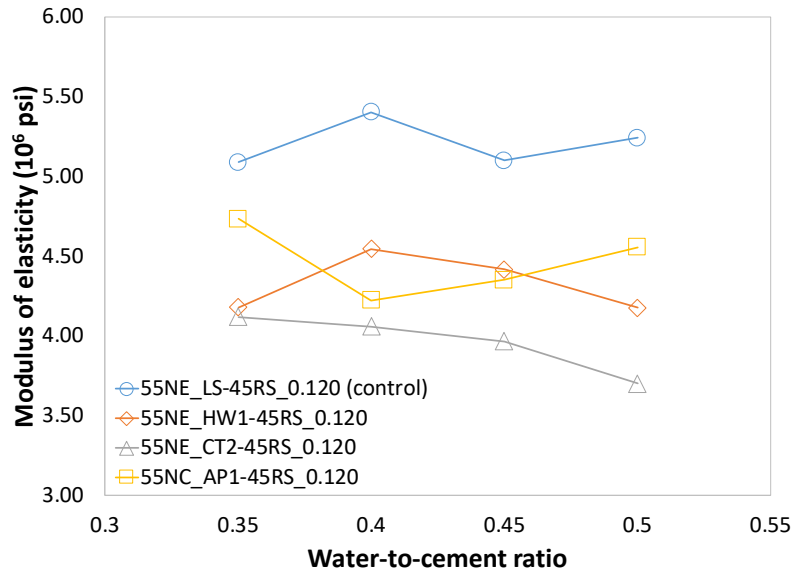




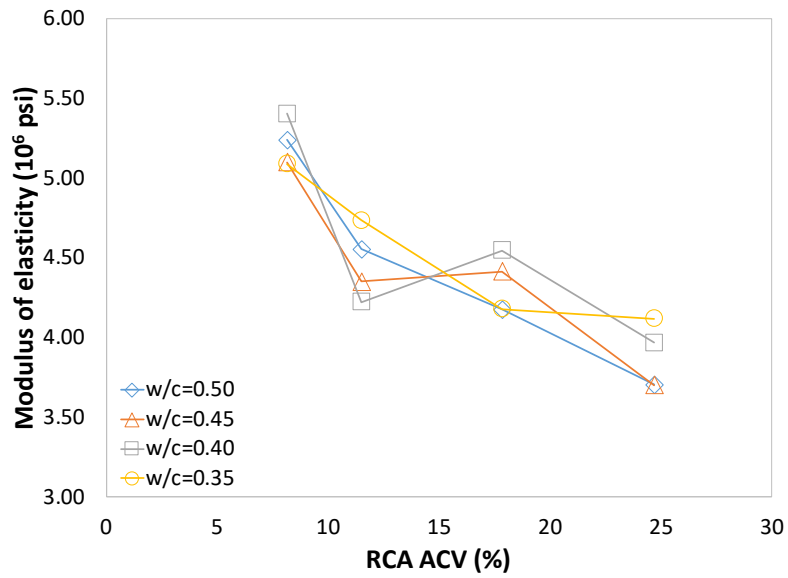
c) Effect of cement content on splitting tensile strength

**Figure 66 Effect of concrete mixture design and RCA ACV on splitting tensile strength of concrete**

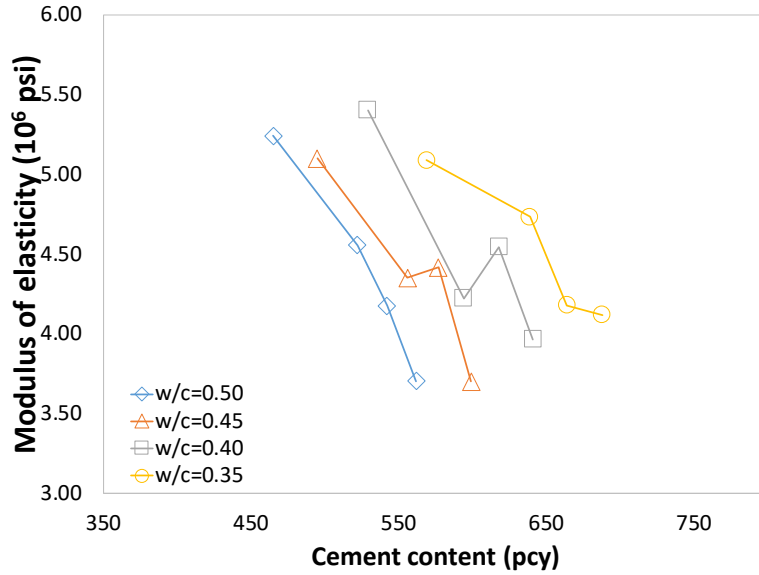
As shown in Figure 67, the paste strength (w/c) was not a significant factor affecting the modulus of elasticity as no clear trend was observed. On the other hand, the ACV of RCA appears to impact the rigidity of concrete, with a higher ACV leading to a lower elastic modulus. These results verify the statement that the modulus of elasticity is driven more by aggregates' stiffness rather than paste stiffness because aggregates occupy most of the concrete volume.



a) Effect of w/c on modulus of elasticity



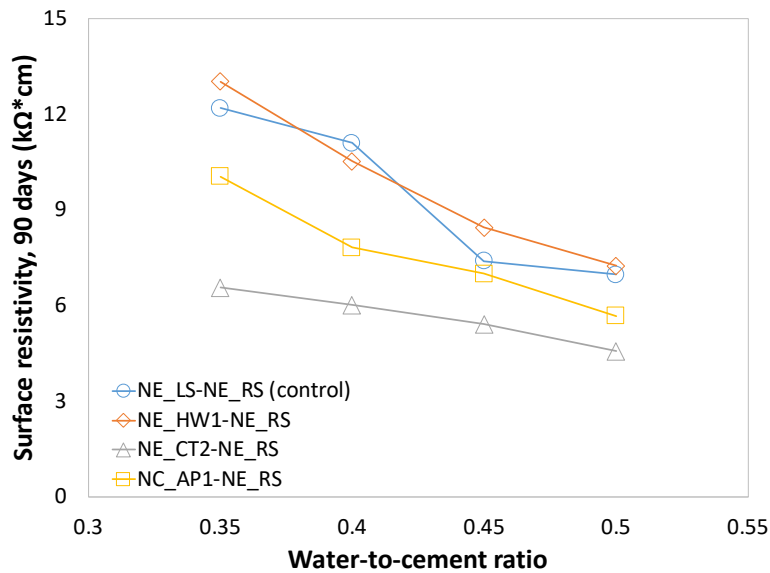
b) Effect of ACV on modulus of elasticity



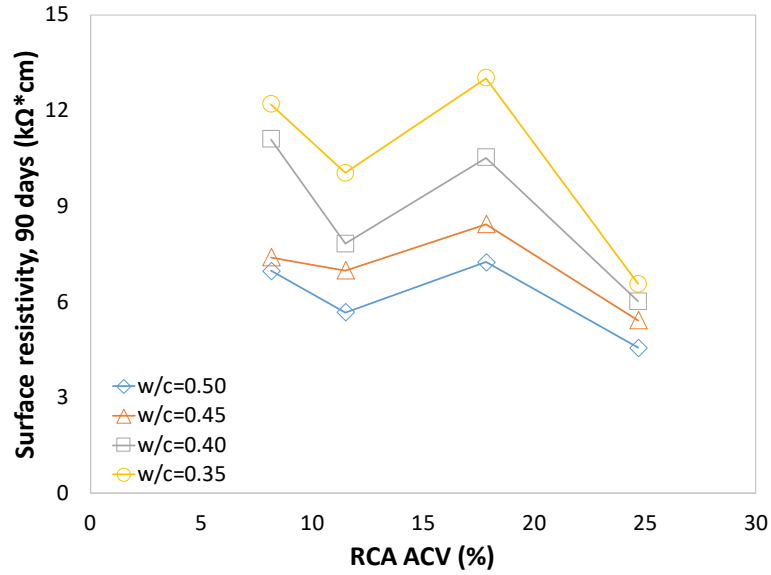
c) Effect of cement content on the modulus of elasticity

**Figure 67 Effect of concrete mixture design and RCA ACV on modulus of elasticity of concrete**

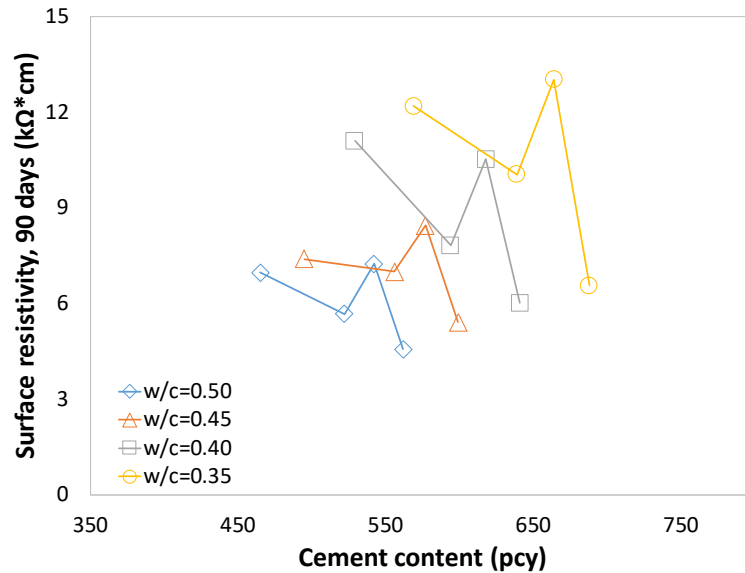
Results, as shown in Figure 69, indicated that the property impacted the most is surface resistivity, as the reduction of the w/c leads to a denser concrete matrix.



a) Effect of w/c on surface resistivity



b) Effect of ACV on surface resistivity



c) Effect of cement content on surface resistivity

**Figure 68 Effect of concrete mixture design and RCA ACV on surface resistivity of concrete**

While no drastic effect of ACV on splitting tensile strength was observed, an interesting trend in regards to compressive strength was found. There is a clear threshold point at approximately 18%, at which the compressive strength starts to decrease with the increase of ACV. The average strength reduction was 16.6% after the threshold value. This finding verifies the

hypothesis that aggregate strength does not significantly affect the concrete strength until it passes a certain limit, at which aggregates are weak enough to play a role in concrete strength. ACV also does not seem to influence surface resistivity. Out of the four properties evaluated, cement content affects the elastic modulus the most. The higher cement content mixes tend to result in a lower modulus of elasticity. Table 42 summarizes the degree of influence of w/c, ACV, and cement content on concrete mechanical properties and surface resistivity, where S and NS stand for significant and non-significant influence, respectively

**Table 42 Influence of w/c, ACV, and cement content on concrete mechanical properties and surface resistivity**

		Compressive strength	Splitting tensile strength	Elastic Modulus	Surface resistivity
Paste quality	w/c	S	S	NS	S
	Cement content	NS	NS	S	NS
Aggregate quality	ACV	S*	NS	S	NS

\* After a certain threshold

With the obtained relationships between strength and design parameters, i.e., w/c, a/c, and cement content, the following nomograph can be obtained (Figure 69). The example of the nomograph used is shown in Appendix D.

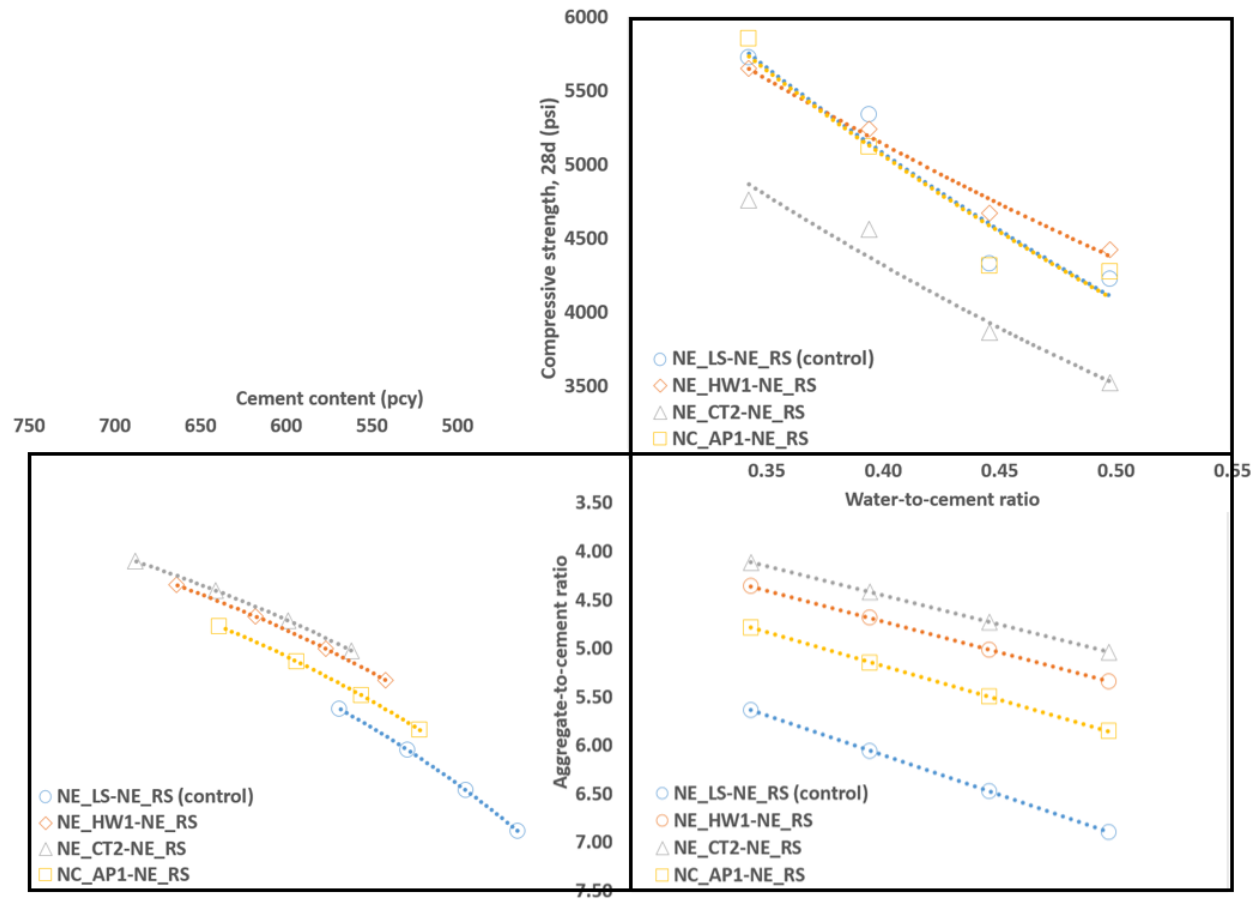


**Figure 69 Developed nomograph with different aggregate**

According to findings from section 5.1, RCA with ACV not higher than 18% can be introduced to concrete at full replacement of NA without compromising concrete strength. A mixture design nomograph of RCA could function as an effective tool to design RAC with different target strengths.

## **CHAPTER 6. CONCLUSIONS AND RECOMMENDATION FOR FUTURE WORK**

### **6.1 Conclusions**

Based on the results from the detailed study of RCA characterization and the use of RCA in pavement concrete, the following conclusions can be made:

- Modified RMC and ACV tests that eliminate potential human error can be effectively used for RCA characterization.
- RCA has a higher absorption capacity and lowers specific gravity due to the porous nature of a residual mortar. However, specific gravity and absorption fail to accurately describe mechanical and physical properties, respectively, as the correlation with the ACV and RMC is not strong.
- Aggregate freeze-thaw test, along with properties such as RMC and ACV, was found to be able to differentiate the air-entrainment level of parent concrete.
- Aggregate angularity and texture have a direct impact on particle packing. With the higher angularity and texture, RCA generally has a higher void content compared to NA.
- The absorption rate test showed that RCA absorbs more than 90% of its capacity within the first two hours of being submerged in water.
- PHXRF shows strong potential for use for the chemical characterization of RCA, as well as for estimating the RMC.
- While DWR and DVR mix design methods fail to design workable pavement concrete mixture, the proposed mix design based on particle packing proved to be efficient in designing pavement concrete with different qualities of RCA at full replacement ratio with comparable or better workability and mechanical properties.
- The shrinkage of RAC is expectedly higher than that of normal concrete. However, the high shrinkage is mostly due to the curing period of the standard test procedure, during which RAC significantly expands because of high absorption.
- With reasonable strength, i.e., ACV higher than 18%, the strength of aggregate is not a significant factor affecting concrete strength.

- With the obtained relationships between strength and design parameters, i.e., w/c, a/c, and cement content, the mix design nomograph can be established and used as an effective tool to design RAC with different target strengths

## **6.2 Recommendations for future studies**

- The standard ASTM C157 might not be a representative test for RAC. More reliable and reasonable test methods should be developed to accurately quantify the drying shrinkage of RAC.
- While the present study demonstrated that coarse RCA of different qualities could fully replace NA without compromising most of the critical properties, further study might be beneficial to investigate the full replacement of both coarse and fine RCA.
- Future research studies that incorporate more RCA samples from a variety of concrete sources will be beneficial in establishing a strength database so as to reduce potential bias due to aggregate sampling for tests such as PHXRF.



## REFERENCES

- [1] AASHTO MP 16-13. (2015). “Standard specification for reclaimed concrete aggregate (RCA) for use as coarse aggregate in hydraulic cement concrete.” American Association of State Highway and Transportation Officials.
- [2] AASHTO M43. (2005). “Standard specification for sizes of aggregates for road and bridge construction.” American Association of State Highway and Transportation Officials.
- [3] AASHTO T 19M/T 19. (2014). “Standard method of test for bulk density (“unit weight”) and voids in aggregate.” American Association of State Highway and Transportation Officials.
- [4] AASHTO TP 33. (1996). “Uncompacted void content of fine aggregate (as influenced by particle shape, surface texture, and grading).” American Association of State Highway and Transportation Officials.
- [5] AASHTO TP 95. (2014). “Standard method of test for surface resistivity indication of concrete’s ability to resist choride ion penetration.” American Association of State Highway and Transportation Officials.
- [6] AASHTO T 96. (2002). “Standard method of test for resistance to degradation of small-size coarse aggregate by abrasion and impact in the Los Angeles machine.” American Association of State Highway and Transportation Officials.
- [7] Abbas, A., Fathifazl, G., Isgor, O.B., Razaqpur, A.G., Fournier, B., Foo, S. (2007). “Proposed method for determining the residual mortar content of recycled concrete aggregates.” Journal of ASTM International.
- [8] Abbas, A., Fathifazl, G., Fournier, B., Isgor, O.B., Zavadil, R., Razaqpur, A.G., Foo, S. (2009). “Quantification of the residual mortar content in recycled concrete aggregates by image analysis.” Materials characterization, 60:716-728.
- [9] ABNT NBR 15116. (2004). “Recycled aggregate of solid residue of building constructions-requirements and methodologies.” Brazilian Technical Standards Association (In Portuguese).
- [10] ACI 318-19. (2019). “Building code requirements for structural concrete.” American Concrete Institute.
- [11] ACI 555R-01. (2001). “Removal and reuse of hardened concrete.” American Concrete Institute.
- [12] ACPA. (2008). “ACPA Concrete Pavement Technology Series: Recycled Concrete in Subbases: A Sustainable Choice.” Skokie, IL.

- [13] Afroughsabet, V., Biolzi, L., Ozbakkaloglu, T. (2017). "Influence of double hooked-end steel fibers and slag on mechanical and durability properties of high performance recycled aggregate concrete." *Composite structures*, 181:273-284.
- [14] "Aggregate Image Measurement System operation manual." (2014). Pine Instrument Company.
- [15] Akbarnezhad, A., Ong, K.C.G., Zhang, M.H., Tam, C.T., Foo, T.W.J. (2011). "Microwave-assisted beneficiation of recycled concrete aggregates." *Construction and Building Materials*, 25:3469-3479.
- [16] Akbarnezhad, A., Ong, K.C.G., Zhang, M.H., Tam, C.T. (2013). "Acid treatment technique for determining the mortar content of recycled concrete aggregates." *Journal of Testing and Evaluation*, 41:441-450.
- [17] Ali, M., Choudhury, T. R., Hossain, B., and Ali, M. P. (2014). "Determination of traces of molybdenum and lead in foods by X-ray fluorescence spectrometry." *SpringerPlus*, 3, 341.
- [18] Alonso, C., Fernandez, L. (2004). "Dehydration and rehydration processes of cement paste exposed to high temperature environments." *Journal of Materials Science*, 39:3015-3024.
- [19] Amario, M., Rangel, C.S., Pepe, M., Filho, R.D.T. (2017). "Optimization of normal and high strength recycled aggregate concrete mixtures by using packing model." *Cement and Concrete Composites*, 84:83-92.
- [20] Angulo, S. C., Ulsen, C., John, V. M., Kahn, H., and Cincotto, M. A. (2009). "Chemical-mineralogical characterization of C&D waste recycled aggregates from Sao Paulo, Brazil." *Waste Management*, 29: 721-730.
- [21] AS1141.6.2. (1996), "Particle density and water absorption of aggregates. Australian Standard.
- [22] ASTM C29. (2016). "Standard test method for bulk density (unit weight) and voids in aggregate." ASTM International.
- [23] ASTM C33. (2018). "Standard specification for concrete aggregates." ASTM International.
- [24] ASTM C39. (2015). "Standard test method for compressive strength of cylindrical concrete specimens." ASTM International.

- [25] ASTM C78. (2015). “Standard test method for flexural strength of concrete (using simple beam with third-point loading).” ASTM International.
- [26] ASTM C127. (2015). “Standard test method for relative density (specific gravity) and absorption of coarse aggregate.” ASTM International.
- [27] ASTM C128. (2015). “Standard test method for relative density (specific gravity) and absorption of fine aggregate.” ASTM International.
- [28] ASTM C136. (2014). “Standard test method for sieve analysis of fine and coarse aggregates.” ASTM International.
- [29] ASTM C143. (2020). “Standard test method for slump of hydraulic-cement concrete.” ASTM International.
- [30] ASTM C157. (2017). “Standard test method for length change of hardened hydraulic-cement mortar and concrete.” ASTM International.
- [31] ASTM C192. (2016). “Standard practice for making and curing concrete test specimens in the laboratory.” ASTM International.
- [32] ASTM C215. (2014). “Standard test method for fundamental transverse, longitudinal, and torsional resonant frequencies of concrete specimens.” ASTM International.
- [33] ASTM C231. (2017). “Standard test method for air content of freshly mixes concrete by the pressure method.” ASTM International.
- [34] ASTM C457. (2016). “Standard test method for microscipical determination of parameters of the air-void system in hardened concrete.” ASTM International.
- [35] ASTM C469. (2014). “Standard test method for static modulus of elasticity and poisson’s ratio of concrete.” ASTM International.
- [36] ASTM C1252. (2017). “Standard test method for uncompacted void content of fine aggregate (as influenced by particle shape, surface texture, and grading.” ASTM International.
- [37] ASTM D3398. (2006). “Standard test method for index of aggregate particle shape and texture (withdrawn 2014).” ASTM International.
- [38] ASTM D4791. (2019). “Standard test method for flat particles, elongated particles, or flat and elongated particles in coarse aggregate.” ASTM International
- [39] ASTM D6928. (2017). “Standard test method for resistance of coarse aggregate to degradation by abrasion in the Micro-Deval apparatus.” ASTM International

- [40] ASTM E1570. (2019). "Standard practice for fan beam computed tomographic (CT) examination." ASTM International
- [41] Barron, A. R., and Raja, P. M. V. (2019). "Physical methods in chemistry and nanoscience."
- [42] Behera, M., Bhattacharyya, S. K., Minocha, A. K., Deoliya, R., and Maiti, S. (2014). "Recycled aggregate from C&D waste & its use in concrete – A breakthrough towards sustainability in construction sector: A review." *Construction and Building Materials*, 68:501-516.
- [43] Bengtsson, L. (1986). "Chemical analysis." *Handbook of Holocene palaeoecology and palaeohydrology*, 423-451.
- [44] Brouwer, P. (2006). "Theory of XRF." Almelo, Netherlands: PANalytical BV.
- [45] Bruker (2010). "Tracer User Guide." <[www.bruker.com/hhxf](http://www.bruker.com/hhxf)>. (25 June, 2019).
- [46] Bruker (2013). "Use of XRF for Mudrock and Ceramic Measurements." [www.bruker.com/hhxf](http://www.bruker.com/hhxf). (15 December, 2019).
- [47] Bruker (2014). "Exploratory GeoChemistry with Tracer XRF." [https://www.bruker.com/fileadmin/user\\_upload/8-PDF-Docs/X-rayDiffraction\\_ElementalAnalysis/HH-XRF/Brochures/Tracer/Tracer\\_GeoChemistry\\_Brochure.pdf](https://www.bruker.com/fileadmin/user_upload/8-PDF-Docs/X-rayDiffraction_ElementalAnalysis/HH-XRF/Brochures/Tracer/Tracer_GeoChemistry_Brochure.pdf)>. (22 May, 2020).
- [48] Bruker (2020). "Periodic Table of Elements and X-ray Energies." <[www.bruker.com/hhxf](http://www.bruker.com/hhxf)>. (20 June, 2020).
- [49] BS 812-105.1. (1989). "Methods for determination of particle shape: flakiness index." British Standard.
- [50] BS 812-105.2. (1990). "Methods for determination of particle shape: elongation index of coarse aggregate." British Standard.
- [51] BS 812-110. (1990). "Methods for determination of aggregate crushing value." British Standard.
- [52] BS 812-111. (1990). "Methods for determination of ten per cent fines value." British Standard.
- [53] BS 812-112. (1990). "Methods for determination of aggregate impact value." British Standard.
- [54] Butler, L., West, J.S., Tighe, S.L. (2011). "Quantification of Recycled Concrete Aggregate (RCA) properties for usage in bridges and pavements: an Ontario study." *Innovative*

Developments in Sustainable Pavements Session, Annual Conference of the Transportation Association of Canada.

- [55] Butler, L. (2012). "Evaluation of recycled concrete aggregate performance in structural concrete." Ph.D. Dissertation, University of Waterloo, Waterloo, ON, Canada.
- [56] Cackler, T. (2018). "Recycled concrete aggregate usage in the US." National Concrete Pavement Technology Center, Iowa State University, Ames, IA.
- [57] Calparsoro, E., Maguregui, M., Morillas, H., Arana, G., and Iñáñez, J. (2019). "Non-destructive screening methodology based on ED-XRF for the classification of medieval and post-medieval archaeological ceramics." *Ceramics International*, 45:10672-10683.
- [58] Cavalline, T.L. (2017). "Concrete pavement recycling – project selection and scoping". Technical Brief, September 2017. National Concrete Pavement Technology Center, Iowa State University, Ames, Iowa. Available at <http://www.cptechcenter.org/>
- [59] Cerato, A. B., Miller, G. A., Ferraro, N., Collins, R., and Center, S. P. T. (2017). "Validating field employed X-Ray fluorescence (XRF) on stabilized subgrade projects to assess impact of extreme precipitation events, improve construction quality control and facilitate geotechnical forensic investigations." Southern Plains Transportation Center, Norman, OK.
- [60] Cerato, A. B. and Miller, G. A. (2013), "Determination of soil stabilizer content using X-Ray fluorescence," *Geotechnical Testing Journal*, 36:1-5,
- [61] Chailapakul, O., Korsrisakul, S., Siangproh, W., and Grudpan, K. (2008). "Fast and simultaneous detection of heavy metals using a simple and reliable microchip-electrochemistry route: An alternative approach to food analysis." *Talanta*, 74:683-689.
- [62] Chen, H.J., Yen, T., and Chen, K.H. (2003). "Use of Building Rubbles as Recycled Aggregates." *Cement and Concrete Research*, 33:125-132.
- [63] Chen, Y., Shi, R., Shu, S., and Gao, W. (2013). "Ensemble and enhanced PM10 concentration forecast model based on stepwise regression and wavelet analysis." *Atmospheric Environment*, 74:346-359.
- [64] Cheremisinoff, N. P. (1996). "Polymer characterization: laboratory techniques and analysis."

- [65] Cook, D., Ghaeezadah, A., and Ley, T. (2013). "Investigation of optimized graded concrete for Oklahoma." Report OTCREOS11.1-39, Oklahoma Transportation Center, Midwest City, OK.
- [66] CSA A23.2-24A. (2009). "Test method for the resistance of unconfined coarse aggregate to freezing and thawing." Canadian Standard Association.
- [67] CSA A23.2-29A. (2014). "Method of test for the resistance of coarse aggregate to degradation by abrasion in the Micro-Deval Apparatus." Canadian Standard Association.
- [68] De Juan, M. S., and Gutiérrez, P. A. (2008). "Study on the influence of attached mortar content on the properties of recycled concrete aggregate." *Construction and Building Materials*, 23: 872-877.
- [69] Dean, W. E. (1974). "Determination of carbonate and organic matter in calcareous sediments and sedimentary rocks by loss on ignition; comparison with other methods." *Journal of Sedimentary Research*, 44:242-248.
- [70] DIN 4226-100. (2002). "Aggregates for concrete and mortar- Part 100: Recycled aggregates." German Institute for Standardization.
- [71] EN 13055-1. (2002). "Lightweight aggregates Part 1: Lightweight aggregates for concrete, mortar and grout."
- [72] EHE-08. (2008). "Structural concrete instruction." (In Spanish).
- [73] Etxeberria, M., Vazquez, E., Mari, A., and Barra, M. (2007). "Influence of amount of recycled coarse aggregates and production process on properties of recycled aggregate concrete." *Cement and Concrete Research*, 37: 735-742.
- [74] Ferraro, N. (2016). "Validation of portable handheld X-ray fluorescence (PHXRF) for construction quality control and forensic geotechnical investigations in stabilized subgrade projects." M.S. Thesis, University of Oklahoma, Norman, OK.
- [75] Fick, G. (2017). "Construction Considerations in Concrete Pavement Recycling." Presentation at Iowa State University, Ames, IA.
- [76] Forster, N., and Grave, P. (2012). "Non-destructive PXRF analysis of museum-curated obsidian from the Near East." *Journal of Archaeological Science*, 39:728-736.
- [77] Garber, S., Rasmussen, R., Cackler, T., Taylor, P., Harrington, D., Fick, G., Snyder, M., Van Dam, T., and Lobo, C. (2011). "Development of a technology deployment plan for the use of recycled concrete aggregate in concrete paving mixtures."

- [78] Gates, L., Masad, E., Pyle, E., Bushee, D. (2011). "Aggregate Imaging Measurement System 2 (AIMS2): Final report", Federal Highway Administration Report FHWA-HIF-11-030.
- [79] Glen, S. (2020). "RMSE: Root Mean Square Error." <<https://www.statisticshowto.com/probability-and-statistics/regression-analysis/rmse-root-mean-square-error/>>. (1 July, 2020).
- [80] Godfrey, L. V., and Glass, J. B. (2011). "The geochemical record of the ancient nitrogen cycle, nitrogen isotopes, and metal cofactors." *Methods in enzymology*, 486:483-506.
- [81] Gokce, A., Nagataki, S., Saeki, T., Hisada, M. (2004). "Freezing and thawing resistance of air-entrained concrete incorporating recycled coarse aggregate: The role of air content in demolished concrete." *Cement and Concrete Research*, 34:799-806.
- [82] Gokce, A., Nagataki, S., Saeki, T., Hisada, M. (2011). "Identification of frost-susceptible recycled concrete aggregates for durability of concrete." *Construction and Building Materials*, 25:2426-2431.
- [83] Gonzalez-Taboada, I., Gonzalez-Fonteboa, B., Martinez-Abella, F., and Carro-Lopez, D. (2016). "Study of recycled concrete aggregate quality and its relationship with recycled concrete compressive strength using database analysis." *Materials of Construction*, 66.
- [84] Guo, H.; Shi, C.; Guan, X.; Zhu, J.; Ding, Y.; Ling, T.-C.; Zhang, H.; Wang, Y. (2018). "Durability of recycled aggregate concrete – A review." *Cement and Concrete Composites*, 89:251-25.
- [85] Gupta, P., Khaudhair, Z., Ahuja. A. (2016) "A new method for proportioning recycled concrete." *Structural Concrete*, 4:677-687.
- [86] Hansen, T.C., Narud, H. (1983). "Strength of recycled concrete made from crushed concrete coarse aggregate." *Concrete International*.
- [87] Hiller, J. E., Deshpande, Y., Qin, Y., and Shorkey, C. J. (2011). "Efficient use of recycled concrete in transportation infrastructure." Michigan Department of Transportation, Lansing, MI.
- [88] Hu, J., Wang, K., Gaunt, J.A. (2012). "Behavior and mix design development of concrete made with recycled aggregate from deconstructed lead-contaminated masonry materials." *Construction and Building Materials*, 40:1184-1192.

- [89] Imanishi, Y., Bando, A., Komatani, S., and Shin-Ichiro Wada, K. (2010). "Experimental parameters for XRF analysis of soils." *International Centre for Diffraction Data*, 53:248-255.
- [90] JIS A 5021. (2018). "Recycled aggregate for concrete- Class H." Japanese Standard Association.
- [91] JIS A 5022. (2018). "Recycled aggregate for concrete- Class M." Japanese Standard Association.
- [92] JIS A 5023. (2018). "Recycled aggregate for concrete- Class L." Japanese Standard Association.
- [93] JGJ52-2006. (2006). "Standard for technical requirements and test method of sand and crushed stone (or gravel) for ordinary concrete." (In Chinese)
- [94] Johnson, R., and Shehata, M. H. (2016). "The efficacy of accelerated test methods to evaluate Alkali Silica Reactivity of Recycled Concrete Aggregates." *Construction and Building Materials*, 112:518-528.
- [95] Kaiser, B., and Wright, A. (2008). "Draft Bruker XRF spectroscopy user guide: Spectral interpretation and sources of interference." BRUKER, Madison, WI.
- [96] Khalaf, F. M., and DeVenny, A. S. (2004). "Recycling of demolished masonry rubble as coarse aggregate in concrete." *Journal of Materials in Civil Engineering*, 16:331-340.
- [97] Knaack, A.M., Kurama, Y.C. (2013). "Design of concrete mixtures with recycled concrete aggregates." *ACI Materials Journal*.
- [98] Koopmans, L. H., Owen, D. B., and Rosenblatt, J. (1964). "Confidence intervals for the coefficient of variation for the normal and log normal distributions." *Biometrika*, 51:25-32.
- [99] Kosmatka, S., Kerkhoff, B., Panarese, W. (2008). "Design and control of concrete mixtures, 14th edition." Portland Cement Association, Skokie, IL.
- [100] KS F 2573. (2014). "Recycled aggregates for concrete." Korean Standards Association (In Korean).
- [101] Kwan, A.K.H., Mora, C.F. (2001). "Effects of various shape parameters on packing of aggregate particles." *Magazine of Concrete Research*.
- [102] Kwan, W.H., Ramli, M., Kan, K.J., Sulieman, M.Z. (2012). "Influence of the amount of recycled coarse aggregate in concrete design and durability properties", *Construction and Building Materials*, 26:565-573.



- [103] Li, Y., Zhang, S., Wang, R., Zhao, Y., Men, C. (2019). "Effects of carbonation treatment on the crushing characteristics of recycled coarse aggregates." *Construction and Building Materials*, 201:408-420.
- [104] Liu, K., Yan, J., Hu, Q., Sun, Y., Zou, C. (2016). "Effects of parent concrete and mixing method on the resistance to freezing and thawing of air-entrained recycled aggregate concrete." *Construction and Building Materials*, 106:264-273.
- [105] Lofty, A., Al-Fayez, M. (2015). "Performance evaluation of structural concrete using controlled quality coarse and fine recycled concrete aggregate." *Cement and Concrete Composites*, 61:36-43.
- [106] Löwemark, L., Bloemsmä, M., Croudace, I., Daly, J. S., Edwards, R. J., Francus, P., Galloway, J. M., Gregory, B. R., Huang, J.-J. S., and Jones, A. F. (2019). "Practical guidelines and recent advances in the Itrax XRF core-scanning procedure." *Quaternary International*, 514:16-29.
- [107] Lopez-Gayarre, F., Serna, P., Domingo-Cabo, A., Serrano-Lopez, M.A., Lopez-Colina, C. (2009). "Influence of recycled aggregate quality and proportioning criteria on recycled concrete properties." *Waste Management*, 29: 3022-3028.
- [108] Mamirov, M., Hu, J., Kim Y. (2021). "Effective reduction of cement content in pavement concrete mixtures based on theoretical and experimental particle packing methods." *Journal of Materials in Civil Engineering*, 10.1061/(ASCE)MT.1943-5533.0003890
- [109] Margui, E., and Van Grieken, R. (2013). "X-ray fluorescence spectrometry and related techniques: an introduction." Momentum Press, New York, NY.
- [110] Martin-Morales, M., Zamorano, M., Ruiz-Moyano, A., Valverde-Espinosa, I. (2010). "Characterization of recycled aggregates construction and demolition waste for concrete production following the Spanish Structural Concrete Code EHE-08". *Construction and Building Materials*, 25:742-748.
- [111] Marucco, A. (2004). "Low-energy ED-XRF spectrometry application in gold assaying." *Nuclear Instruments and Methods in Physics Research Section B: Beam Interactions with Materials and Atoms*, 213:486-490.
- [112] McNeil, K., and Kang, T. H.-K. (2013). "Recycled concrete aggregates: A review." *International Journal of Concrete Structures and Materials*, 7:61-69.

- [113] Mehta, P. K., and Monteiro, P. J. (2006). "Concrete: microstructure, properties, and materials." McGraw-Hill, Berkeley, California.
- [114] Minitab (2019). "Basics of stepwise regression." <<https://support.minitab.com/en-us/minitab/18/help-and-how-to/modeling-statistics/regression/supporting-topics/basics/basics-of-stepwise-regression/#what-is-stepwise-regression>>. (18 July, 2020).
- [115] Molugaram, K., and Rao, G. S. (2017). "ANOVA (Analysis of Variance)." Statistical Techniques for Transportation Engineering, 451-462.
- [116] Monnier, G. F. (2018). "A review of infrared spectroscopy in microarchaeology: Methods, applications, and recent trends." Journal of Archaeological Science: Reports, 18:806-823.
- [117] Murphy, R. V. (2006). "Operator of Portable X-ray fluorescence analyzers examination preparation."
- [118] Nagataki, S., Gokce, A., Saeki, T. (2000). "Effects of recycled aggregate characteristics on performance parameters of recycled aggregate concrete." Special Publication, 192:53-72.
- [119] Nagataki, S., Gokce, A., Saeki, T., Hisada, M. (2004). "Assessment of recycling process induced damage sensitivity of recycled concrete aggregates." Cement and Concrete Research, 34:965-971.
- [120] National Library of Medicine (2019). "Standard Deviation." <[https://www.nlm.nih.gov/nichsr/stats\\_tutorial/section2/mod8\\_sd.html](https://www.nlm.nih.gov/nichsr/stats_tutorial/section2/mod8_sd.html)>. (30 June, 2020).
- [121] Omary, S., Ghorbel, E., and Wardeh, G. (2016). "Relationships between recycled concrete aggregates characteristics and recycled aggregates concretes properties." Construction and Building Materials, 108:163-174.
- [122] Padmini, A. K., Ramamurthy, K., and Mathews, M. S. (2009). "Influence of parent concrete on the properties of recycled aggregate concrete." Construction and Building Materials, 23:829-836.
- [123] PCA (2019). "Cement & Concrete Applications." <<https://www.cement.org/cement-concrete-applications/concrete-materials/aggregates>>. (last accessed July 12, 2020).
- [124] PCA (n.d.). "Recycled Aggregate. <https://www.cement.org/learn/concrete-technology/concrete-design-production/recycled-aggregates>. (last accessed April 25, 2021).
- [125] PennState Eberly College of Science (2020). "Stepwise Regression." <<https://online.stat.psu.edu/stat501/lesson/10/10.2>>. (29 August, 2020).

- [126] Pepe, M., Filho, R.D.T., Koenders, E.A.B., Martinelli, E. (2014). "Alternative processing procedures for recycled aggregates in structural concrete." *Construction and Building Materials*, 69:124-132.
- [127] Pepe, M., Filho, R.D.T., Koenders, E.A.B., Martinelli, E. (2016). "A novel mix design methodology for Recycled Aggregate Concrete." *Construction and Building Materials*, 122:362-372.
- [128] Pradhan, S., Kumar, S., Barai, S.V. (2017). "Recycled aggregate concrete: Particle packing Method (PPM) of mix design approach." *Construction and Building Materials*, 152:269-284.
- [129] Profe, J., and Ohlendorf, C. (2019). "X-ray fluorescence scanning of discrete samples—An economical perspective." *Quaternary International*, 514:68-75.
- [130] Quiroga, P.N. and Fowler, D.W. (2004). "The effects of aggregates characteristics on the performance of Portland Cement Concrete." Report ICAR 104-1F. International Center for Aggregates Research, University of Texas at Austin.
- [131] Ravindrarajah, R.S., Tam, C.T. (1985). "Properties of concrete made with crushed concrete as coarse aggregate." *Magazine of Concrete Research*.
- [132] RILEM TC 121-DRG. (1994). "Specifications for Concrete with Recycled Aggregates."
- [133] Safiuddin, M., Alengaram, U. J., Rahman, M. M., Salam, M. A., and Jumaat, M. Z. (2013). "Use of recycled concrete aggregate in concrete: A review." *Journal of Civil Engineering and Management*, 19:796-810.
- [134] Salas, A., Brand, A.S., Roesler, J.R., Arboleda, C., Lange, D.A. (2013). "Properties of recycled concrete aggregates for airfield rigid pavements." Technical report, Center of Excellence for Airport Technology.
- [135] Sánchez De La Torre, M., Oms, F. X., Le Bourdonnec, F.-X., Aliaga, S., Mercadal, O., Cebrià, A., and Mangado, X. (2018). "Bone or shell? Using ED-XRF to determine the nature of prehistoric ornaments." *Journal of Archaeological Science: Reports*, 21:128-136.
- [136] Saravanakumar, P., Abhiram, K., Manoj, B. (2016). "Properties of treated recycled aggregates and its influence on concrete strength characteristics." *Construction and Building Materials*, 111:611-617.
- [137] Scientific, T. F. (2020). "Inductively Coupled Plasma Mass Spectrometry (ICP-MS) Information." <<https://www.thermofisher.com/us/en/home/industrial/spectroscopy-elemental-isotope-analysis/spectroscopy-elemental-isotope-analysis-learning-center/trace-elemental->

analysis-tea-information/inductively-coupled-plasma-mass-spectrometry-icp-ms-information.html>. (10 May, 2020).

- [138] SGS Group (2021). Whole Rock Analysis. [www.sgsgroup.us.com](http://www.sgsgroup.us.com)
- [139] Shayan, A., and Xu, A. (2003). "Performance and properties of structural concrete made with recycled concrete aggregate." *ACI Materials Journal*, 100:371–380.
- [140] Silva, R.V., de Brito, J., Dhir, R.K. (2014). "Properties and composition of recycled aggregates from construction and demolition waste suitable for concrete production." *Construction and Building Materials*, 65:201-217.
- [141] Shugar, A. N., and Mass, J. L. (2012). "Handheld XRF for art and archaeology." Leuven University Press.
- [142] Smith, D. R., and Nordberg, M. (2015). "General chemistry, sampling, analytical methods, and speciation." *Handbook on the Toxicology of Metals*, 15-44.
- [143] Snyder, M., Cavalline, T., Fick, G., Taylor, P., Klokke, S., and Gross, J. (2018). "Recycling concrete pavement materials: A practitioner's reference guide." National Concrete Pavement Technology Center, Iowa State University, Ames, IA.
- [144] Speakman, S. (2015). "Using the Bruker Tracer III-SD handheld X-ray fluorescence spectrometer using PC software for data collection." Center for Materials Science and Engineering at Massachusetts Institute of Technology, Cambridge, Massachusetts.
- [145] Steiner, K. (2011). "On-site X-ray fluorescence testing for presence of corrosive drywall." *Journal of Materials in Civil Engineering*, 23:1050-1056.
- [146] Tam, V.W.Y., Tam, C.M. Le, K.N. (2006). "Removal of cement mortar remains from recycled aggregate using pre-soaking approaches." *Resources, Conservation and Recycling*, 50:82-101.
- [147] Tam, V.W.Y., Gao, X.F., Tam, C.M., Chan, C.H. (2006). "New approach in measuring water absorption of recycled aggregates." *Construction and Building Materials*, 22:364-369.
- [148] Tavakoli, M., & Soroushian, P. (1996). "Strengths of aggregate concrete made using field-demolished concrete as aggregate." *ACI Materials Journal*, 93:182–190.
- [149] Taylor, P., Yurdakul, E., and Ceylan, H. (2012). "Concrete pavement mixture design and analysis (MDA): Application of a portable X-ray fluorescence technique to assess concrete mix proportions." National Concrete Pavement Technology Center, Iowa State University, Ames, IA.

- [150] Topcu, I.B. (1997). "Physical and mechanical properties of concretes produced with waste concrete." *Cement and Concrete Research*, 27:1817-1823.
- [151] Twelker, E., Wypych, A., Sicard, K. R., Naibert, T. J., Weldon, M. B., Athey, J. E., Willingham, A. L., and Lockett, A. C. (2017). "New geologic investigations of Northeast Tanacross", Alaska Department of Natural Resources Geological & Geophysical Surveys.
- [152] Van Dam, T. J., Harvey, J., Muench, S. T., Smith, K. D., Snyder, M. B., Al-Qadi, I. L., Ozer, H., Meijer, J., Ram, P., and Roesler, J. R. (2015). "Towards sustainable pavement systems: a reference document." United States. Federal Highway Administration, Washington, DC.
- [153] Verian, K. (2012). "Using recycled concrete as coarse aggregate in pavement concrete". M.S. Thesis, Purdue University, West Lafayette, IN.
- [154] Verian, K. P., Whiting, N. M., Olek, J., Jain, J., and Snyder, M. B. (2013). "Using recycled concrete as aggregate in concrete pavements to reduce materials cost." Joint Transportation Research Program, Indiana Department of Transportation and Purdue University, West Lafayette, Indiana.
- [155] Verian, K. P., Ashraf, W., and Cao, Y. (2018). "Properties of recycled concrete aggregate and their influence in new concrete production." *Resources, Conservation and Recycling*, 133:30-49.
- [156] Wang, K., and Hu, J. (2005). "Use of a moisture sensor for monitoring the effect of mixing procedure on uniformity of concrete mixtures." *Journal of Advanced Concrete Technology*, 3:371-383.
- [157] Xing, Z., Beaucour, A.L., Hebert, R., Noumowe, A., Ledesert, B. (2011). "Influence of the nature of aggregates on the behavior of concrete subjected to elevated temperature." *Cement and Concrete Research*, 41:392-402.
- [158] Yrjanson, W. A. (1989). "Recycling of Portland cement concrete pavements." Transportation Research Board, Washington, DC.
- [159] Zhang, Q., Ye, G. (2012). "Dehydration kinetics of Portland cement paste at high temperature." *Journal of Thermal Analysis and Calorimetry*, 110:153-158.
- [160] Zhang, Z., Zhang, Y., Yan, C., Liu, Y. (2017). "Influence of crushing index on properties of recycled aggregates pervious concrete." *Construction and Building Materials*, 135:112-118.

- [161] Zheng, C., Lou, C., Du, G., Li, X., Liu, Z., and Li, L. (2018). "Mechanical properties of recycled concrete with demolished waste concrete aggregate and clay brick aggregate." *Results in Physics*, 9:1317-1322.

## APPENDIX A. DETAILS SUMMARY OF NA AND RCA CHARACTERISTICS

Table 43 Summary of NA and RCA characteristics

	Aggregate ID	SG <sub>OD</sub>	Abs (%)	RMC (%)	Crushing value (%)	Texture	Angularity	F and E>2:1	F and E>3:1	FT mass loss (%)	FT mass loss (% of RM)	% of RM loss-to-CI ratio
NE Limestone	NE_LS_1	2.65	0.91	NA	7.06	160.6	2383.7	57.9%	13.2%			
	NE_LS_0.75	2.65	0.91		7.20	172.4	2489.2	62.0%	6.0%			
	NE_LS_0.5	2.65	0.91		7.63	179.9	2346.5	46.9%	12.2%	2.63	NA	NA
	NE_LS_0.375	2.65	0.91		8.08	192.4	2484.5	51.1%	6.4%			
	NE_LS_0.187	2.65	0.91		10.09	143.5	2535.9	65.0%	15.0%			
NV Gravel	NV_GR_0.75	2.53	2.81	NA	4.73	304.0	2488.2	62.0%	10.0%			
	NV_GR_0.5	2.53	2.81		7.06	350.5	2608.7	57.4%	14.9%	1.51	NA	NA
	NV_GR_0.375	2.53	2.81		6.56	375.0	2866.9	48.0%	8.0%			
	NV_GR_0.187	2.53	2.81		8.34	361.5	3169.0	64.0%	22.0%			
Nebraska Heims	NE_CT1_1	2.20	5.59	68.95	21.59	359.7	2748.3	36.7%	0.0%			
	NE_CT1_0.75	2.18	6.21	70.61	30.51	371.3	3073.1	30.0%	2.0%			
	NE_CT1_0.5	2.15	7.12	66.09	25.66	391.8	3387.9	60.0%	10.0%	28.78	43.55	1.70
	NE_CT1_0.375	2.24	5.64	69.31	24.73	339.6	3257.3	46.0%	2.0%			
	NE_CT1_0.187	2.24	5.84	75.71	25.02	249.6	3462.0	54.0%	6.0%			
Nebraska Fucinaro	NE_CT2_1	2.18	5.98	86.64	26.77	407.2	3189.5	36.7%	6.1%			
	NE_CT2_0.75	2.21	5.62	79.44	26.76	409.6	3181.3	38.0%	6.0%			
	NE_CT2_0.5	2.25	5.32	68.14	22.49	384.5	3312.4	50.0%	8.0%	68.14	48.41	2.15
	NE_CT2_0.375	2.21	5.85	75.70	26.36	381.0	3477.2	34.0%	0.0%			
	NE_CT2_0.187	2.23	6.21	74.40	23.37	268.0	3421.1	26.0%	2.0%			
Nebraska	NE_HW1_1	2.29	4.33	56.05	15.89	322.9	3295.0	32.0%	2.0%			

	NE_HW1_0.75	2.27	4.01	56.92	17.49	313.7	3267.0	32.0%	4.0%			
	NE_HW1_0.5	2.32	4.03	55.93	17.20	321.4	3414.1	36.0%	4.0%	11.59	20.73	1.21
	NE_HW1_0.375	2.31	4.33	62.63	17.79	298.3	3391.8	54.0%	8.0%			
	NE_HW1_0.187	2.30	4.55	71.56	19.29	226.2	3315.0	44.0%	2.0%			
Nebraska HW75	NE_HW2_1	2.22	5.21	74.47	17.37	348.3	2982.7	26.5%	0.0%			
	NE_HW2_0.75	2.26	4.90	69.20	19.35	359.5	3117.1	46.0%	8.0%			
	NE_HW2_0.5	2.26	4.98	61.67	21.44	322.0	3295.7	48.0%	8.0%	11.57	18.77	0.88
	NE_HW2_0.375	2.26	5.31	67.94	21.11	339.4	3609.5	40.0%	0.0%			
	NE_HW2_0.187	2.27	5.46	73.05	21.10	229.4	3450.2	48.0%	10.0%			
Iowa Pavement	IA_CT1_1	2.23	5.58	40.62	15.96	399.4	3196.3	46.0%	6.0%			
	IA_CT1_0.75	2.24	5.78	59.21	15.58	366.6	2853.0	20.0%	4.0%			
	IA_CT1_0.5	2.26	5.47	49.67	15.52	352.0	2999.4	52.0%	10.0%	15.05	30.29	1.95
	IA_CT1_0.375	2.27	5.50	44.80	16.32	325.0	3062.5	52.0%	14.0%			
	IA_CT1_0.187	2.25	5.80	62.66	17.39	257.2	3260.0	54.0%	10.0%			
Texas	TX_CT1_1	2.24	5.55	27.95	15.22	248.2	2986.0	26.0%	4.0%			
	TX_CT1_0.75	2.22	6.33	14.14	19.26	272.8	2794.1	34.0%	0.0%			
	TX_CT1_0.5	2.22	6.86	23.95	17.37	242.1	3000.8	42.0%	4.0%	28.32	118.24	6.81
	TX_CT1_0.375	2.20	7.38	32.60	18.82	237.9	2885.8	34.0%	6.0%			
	TX_CT1_0.187	2.11	9.58	47.71	20.88	193.5	3119.2	42.0%	8.0%			
North Carolina DH Griffin	NC_CT1_1	2.29	5.63	28.44	14.97	253.4	3097.5	39.1%	8.7%			
	NC_CT1_0.75	2.34	5.15	31.29	12.81	285.5	3166.3	52.6%	5.3%			
	NC_CT1_0.5	2.42	4.33	29.03	12.06	294.6	3064.9	32.0%	10.0%	14.55	50.11	4.16
	NC_CT1_0.375	2.31	5.68	39.70	15.53	298.9	3273.0	64.0%	14.0%			
	NC_CT1_0.187	2.24	6.83	54.91	19.74	220.9	3062.1	66.0%	16.0%			
North Carolina Carli Griffin	NC_HW1_1	2.25	5.84	32.08	11.17	360.0	3547.5	17.4%	0.0%			
	NC_HW1_0.75	2.30	5.19	23.56	12.33	328.1	3324.9	63.9%	2.8%			



	NC_HW1_0.5	2.34	4.71	30.60	10.81	371.2	3642.0	40.4%	6.4%	11.39	37.22	3.44
	NC_HW1_0.375	2.26	6.07	34.33	12.41	302.2	3091.7	54.0%	6.0%			
	NC_HW1_0.187	2.12	8.62	64.23	18.59	228.1	3304.6	60.0%	14.0%			
North Carolina Airport CLT	NC_AP1_1	2.53	3.77	35.58	10.44	340.7	3221.2	50.0%	5.0%			
	NC_AP1_0.75	2.56	3.52	21.06	10.35	290.5	3222.7	30.6%	0.0%			
	NC_AP1_0.5	2.57	3.35	26.19	8.48	290.8	2860.3	46.0%	4.0%	9.89	37.74	4.45
	NC_AP1_0.375	2.54	4.12	26.55	12.26	291.8	2806.1	40.0%	4.0%			
	NC_AP1_0.187	2.42	5.74	46.55	15.83	221.5	2950.7	51.0%	8.2%			
North Carolina Coastal	NC_CT2_1	2.18	6.23	50.00	16.05	322.3	2976.8	48.0%	6.0%			
	NC_CT2_0.75	2.21	6.02	50.00	16.05	328.1	3151.8	53.1%	6.1%			
	NC_CT2_0.5	2.23	5.85	47.38	13.96	275.5	3054.9	42.9%	2.0%	14.68	30.98	2.22
	NC_CT2_0.375	2.21	6.20	44.74	17.25	333.0	3012.7	48.0%	8.0%			
	NC_CT2_0.187	2.18	7.08	72.73	20.03	247.8	3066.6	62.0%	14.0%			

## APPENDIX B. DETAILS OF STATISTICAL ANALYSIS FROM PHXRF RESULTS

**Table 44 Standard deviation, COV<sub>STD DEV</sub>, RMSD & COV<sub>RMSD</sub> values for No.4 NC\_AP1 sample**

No.4						
Element	n	Average	Std Dev	COV <sub>STD DEV</sub>	RMSD	COV <sub>RMSD</sub>
Na	12	0.0809	0.0930	1.1503	0.0895	1.1551
MgKa1	12	0.0000	0.0000	0.0000	--	--
AlKa1	12	1.1005	0.5582	0.5072	5.7109	5.4199
Si	12	4.2152	1.5705	0.3726	23.0856	5.7203
P Ka1	12	0.0190	0.0308	1.6210	0.1158	6.3739
S Ka1	12	0.5025	0.0599	0.1192	0.3472	0.7218
K Ka1	12	0.2779	0.1402	0.5046	0.2169	0.8155
CaKa1	12	4.1318	1.5787	0.3821	3.7611	0.9508
BaLa1	12	0.3778	0.4352	1.152	0.5571	1.4747
TiKa1	12	0.2132	0.1193	0.5597	0.5658	2.7716
V Ka1	12	0.0000	0.0000	0.0000	--	--
CrKa1	12	0.0047	0.0015	0.3177	0.0021	0.4630
MnKa1	12	0.0284	0.0054	0.1899	0.0724	2.6587
FeKa1	12	2.0522	1.1233	0.5474	4.3768	2.2276
BaLa1	12	2.4785	1.8903	0.7627	3.0334	1.2783
CoKa1	12	0.0345	0.0206	0.5965	0.0373	1.1297
NiKa1	12	0.0017	0.0022	1.2887	0.0052	3.1411
CuKa1	12	0.0019	0.0020	1.0247	0.0050	2.7261
ZnKa1	12	0.0027	0.0020	0.7716	0.0050	1.9493
AsKa1	12	0.0002	0.0001	0.4267	0.0001	0.5186
PbLa1	12	0.0012	0.0003	0.2345	0.0007	0.5795
ThLa1	12	0.0003	0.0001	0.2216	0.0002	0.4664
RbKa1	12	0.0010	0.0011	1.0666	0.0011	1.0900
U La1	12	0.0044	0.0043	0.9846	0.0060	1.4228
SrKa1	12	0.0374	0.0270	0.7227	0.0453	1.2669
Y Ka1	12	0.0008	0.0009	1.0987	0.0012	1.4401
ZrKa1	12	0.0089	0.0032	0.3646	0.0041	0.4789
NbKa1	12	0.0008	0.0003	0.3222	0.0003	0.3590
MoKa1	12	0.0079	0.0050	0.6364	0.0092	1.2112
RhKa1	12	0.0000	0.0000	--	0.0000	--
SnKa1	12	0.0002	0.0000	0.1447	0.0001	0.5628
SbKa1	12	0.0001	0.0002	1.8232	0.0002	2.0230

**Table 45 Standard deviation, COV<sub>STD DEV</sub>, RMSD & COV<sub>RMSD</sub> Values  
for No.12 NC\_API RCA sample**

<b>No.12</b>						
Element	n	Average	Std Dev	COV <sub>STD DEV</sub>	RMSD	COV <sub>RMSD</sub>
Na	12	0.0000	0.0000	0.0000	--	--
MgKa1	12	0.0000	0.0000	0.0000	--	--
AlKa1	12	1.1205	0.1686	0.1504	5.8414	5.4449
Si	12	4.3376	0.4421	0.1019	22.9181	5.5186
P Ka1	12	0.0040	0.0054	1.3525	0.1270	33.0894
S Ka1	12	0.4984	0.0311	0.0624	0.3397	0.7119
K Ka1	12	0.2708	0.0458	0.1692	0.1828	0.7051
CaKa1	12	4.4303	0.6479	0.1462	3.2061	0.7558
BaLa1	12	0.6236	0.6779	1.0870	0.8697	1.4565
TiKa1	12	0.0970	0.1023	1.0540	0.6775	7.2923
V Ka1	12	0.0000	0.0000	0.0000	--	--
CrKa1	12	0.0063	0.0019	0.2967	0.0018	0.2973
MnKa1	12	0.0275	0.0041	0.1487	0.0732	2.7783
FeKa1	12	1.0289	1.0942	1.0634	5.3692	5.4506
BaLa1	12	0.5785	0.2208	0.3816	0.5747	1.0376
CoKa1	12	0.0061	0.0025	0.4114	0.0040	0.6945
NiKa1	12	0.0036	0.0006	0.1771	0.0029	0.8602
CuKa1	12	0.0072	0.0017	0.2350	0.0018	0.2552
ZnKa1	12	0.0056	0.0008	0.1517	0.0018	0.3441
AsKa1	12	0.0004	0.0000	0.0970	0.0002	0.5949
PbLa1	12	0.0012	0.0003	0.2212	0.0007	0.5819
ThLa1	12	0.0004	0.0000	0.1113	0.0002	0.4575
RbKa1	12	0.0010	0.0004	0.4346	0.0005	0.4954
U La1	12	0.0004	0.0005	1.3302	0.0006	1.5764
SrKa1	12	0.0818	0.0176	0.2157	0.0184	0.2346
Y Ka1	12	0.0025	0.0004	0.1655	0.0010	0.4046
ZrKa1	12	0.0103	0.0026	0.2570	0.0028	0.2846
NbKa1	12	0.0007	0.0001	0.1039	0.0001	0.1094
MoKa1	12	0.0003	0.0004	1.4722	0.0004	1.4722
RhKa1	12	0.0000	0.0000	--	0.0000	--
SnKa1	12	0.0002	0.0000	0.0993	0.0001	0.4050
SbKa1	12	0.0001	0.0001	2.5099	0.0001	2.6029

**Table 46 Standard Deviation, COV<sub>STD DEV</sub>, RMSD & COV<sub>RMSD</sub> Values  
for No.50 NC\_API RCA sample**

<b>No.50</b>						
Element	n	Average	Std Dev	COV <sub>STD DEV</sub>	RMSD	COV <sub>RMSD</sub>
NaKa1	12	0.0516	0.1384	2.6855	1.5713	31.8361
MgKa1	12	0.0000	0.0000	0.0000	--	--
AlKa1	12	1.4142	0.0725	0.0513	5.5459	4.0961
SiKa1	12	5.1253	0.4513	0.0881	22.1307	4.5100
P Ka1	12	0.0109	0.0099	0.9072	0.1204	11.5011
S Ka1	12	0.5051	0.0318	0.0630	0.3664	0.7576
K Ka1	12	0.2967	0.0213	0.0719	0.1530	0.5386
CaKa1	12	4.0024	0.5089	0.1271	3.6065	0.9412
BaLa1	12	0.8227	0.6702	0.8146	1.0085	1.2802
TiKa1	12	0.0812	0.1017	1.2525	0.6930	8.9133
V Ka1	12	0.0000	0.0000	0.0000	--	--
CrKa1	12	0.0066	0.0009	0.1391	0.0010	0.1531
MnKa1	12	0.0282	0.0032	0.1126	0.0725	2.6817
FeKa1	12	0.9035	1.1675	1.2923	5.5061	6.3655
BaLa1	12	0.1371	0.0879	0.6409	0.1255	0.9554
CoKa1	12	0.0012	0.0004	0.3535	0.0017	1.4301
NiKa1	12	0.0031	0.0007	0.2230	0.0035	1.1354
CuKa1	12	0.0083	0.0011	0.1292	0.0020	0.2557
ZnKa1	12	0.0061	0.0012	0.1891	0.0015	0.2633
AsKa1	12	0.0004	0.0001	0.1181	0.0003	0.6459
PbLa1	12	0.0009	0.0003	0.3391	0.0008	0.8794
ThLa1	12	0.0004	0.0000	0.0415	0.0002	0.4909
RbKa1	12	0.0015	0.0004	0.2612	0.0004	0.2949
U La1	12	0.0005	0.0004	0.8069	0.0006	1.2026
SrKa1	12	0.0554	0.0138	0.2496	0.0233	0.4390
Y Ka1	12	0.0026	0.0003	0.1033	0.0010	0.4102
ZrKa1	12	0.0115	0.0017	0.1485	0.0016	0.1485
NbKa1	12	0.0007	0.0001	0.0798	0.0001	0.0922
MoKa1	12	0.0005	0.0009	1.8570	0.0008	1.8570
RhKa1	12	0.0000	0.0000	--	--	--
SnKa1	12	0.0002	0.0000	0.0358	0.0001	0.4686
SbKa1	12	0.0002	0.0003	1.4425	0.0003	1.7207

**Table 47 Standard Deviation, COV<sub>STD DEV</sub>, RMSD & COV<sub>RMSD</sub> Values  
for No.4 NC\_CT1 sample**

<b>No.4</b>						
Element	n	Average	Std Dev	COV <sub>STD DEV</sub>	RMSD	COV <sub>RMSD</sub>
NaKa1	12	0.0008	0.0019	2.4164	1.3716	1806.342
MgKa1	12	0.0000	0.0000	--	--	--
AlKa1	12	0.3400	0.1917	0.5639	5.1145	15.7101
SiKa1	12	3.8349	0.5891	0.1536	25.9939	7.0797
P Ka1	12	0.0069	0.0106	1.5287	0.1375	20.7170
S Ka1	12	0.5628	0.0636	0.1130	0.7004	1.2999
K Ka1	12	0.2366	0.0622	0.2629	1.1374	5.0210
CaKa1	12	6.3559	1.0407	0.1637	1.8355	0.3016
BaLa1	12	0.2238	0.2087	0.9325	0.2744	1.2804
TiKa1	12	0.0246	0.0316	1.2868	0.2888	11.7497
V Ka1	12	0.0013	0.0020	1.5757	0.0094	7.8213
CrKa1	12	0.0045	0.0018	0.4036	0.0018	0.4080
MnKa1	12	0.0223	0.0071	0.3196	0.0327	1.5330
FeKa1	12	0.3143	0.4018	1.2784	2.8869	9.5949
BaLa1	12	0.2702	0.1722	0.6375	0.2886	1.1158
CoKa1	12	0.0027	0.0011	0.3996	0.0017	0.6501
NiKa1	12	0.0026	0.0005	0.1818	0.0007	0.2696
CuKa1	12	0.0042	0.0020	0.4772	0.0019	0.4778
ZnKa1	12	0.0053	0.0030	0.5701	0.0034	0.6846
AsKa1	12	0.0004	0.0002	0.4571	0.0002	0.4648
PbLa1	12	0.0010	0.0004	0.3786	0.0005	0.5098
ThLa1	12	0.0004	0.0001	0.2969	0.0003	0.8345
RbKa1	12	0.0019	0.0014	0.7086	0.0024	1.3348
U La1	12	0.0006	0.0006	1.0247	0.0007	1.1976
SrKa1	12	0.0357	0.0189	0.5281	0.0199	0.5820
Y Ka1	12	0.0023	0.0004	0.1760	0.0010	0.4554
ZrKa1	12	0.0092	0.0016	0.1788	0.0098	1.1159
NbKa1	12	0.0006	0.0001	0.1847	0.0001	0.1862
MoKa1	12	0.0018	0.0015	0.8407	0.0020	1.1373
RhKa1	12	0.0000	0.0000	--	0.0000	--
SnKa1	12	0.0001	0.0000	0.2428	0.0001	0.5047
SbKa1	12	0.0001	0.0001	1.8858	0.0001	1.9135

**Table 48 Standard deviation, COV<sub>STD DEV</sub>, RMSD & COV<sub>RMSD</sub> values  
for No.12 NC\_CT1 RCA sample**

<b>No.12</b>						
Element	n	Average	Std Dev	COV <sub>STD DEV</sub>	RMSD	COV <sub>RMSD</sub>
NaKa1	12	0.0112	0.0266	2.3775	1.3615	127.2895
MgKa1	12	0.0000	0.0000	--	--	--
AlKa1	12	0.4525	0.2228	0.4923	5.0033	11.5485
SiKa1	12	4.2804	0.6406	0.1497	25.5496	6.2344
P Ka1	12	0.0147	0.0138	0.9373	0.0482	3.4315
S Ka1	12	0.5662	0.0479	0.0846	0.3989	0.7358
K Ka1	12	0.3005	0.1103	0.3672	0.7283	2.5317
CaKa1	12	7.3314	1.2733	0.1737	1.3441	0.1915
BaLa1	12	0.0098	0.0275	2.8041	0.0370	3.9444
TiKa1	12	0.1109	0.0304	0.2744	0.2030	1.9125
V Ka1	12	0.0019	0.0023	1.2137	0.0089	5.0174
CrKa1	12	0.0039	0.0009	0.2322	0.0012	0.3238
MnKa1	12	0.0243	0.0023	0.0949	0.0300	1.2896
FeKa1	12	1.5305	0.4231	0.2765	1.6940	1.1560
BaLa1	12	0.2992	0.2874	0.9605	0.3826	1.3357
CoKa1	12	0.0043	0.0039	0.9142	0.0047	1.1549
NiKa1	12	0.0024	0.0007	0.3046	0.0007	0.3291
CuKa1	12	0.0083	0.0038	0.4618	0.0056	0.7048
ZnKa1	12	0.0097	0.0040	0.4150	0.0046	0.4943
AsKa1	12	0.0006	0.0002	0.3635	0.0003	0.4863
PbLa1	12	0.0011	0.0004	0.3429	0.0005	0.4208
ThLa1	12	0.0004	0.0001	0.1489	0.0003	0.8077
RbKa1	12	0.0022	0.0009	0.3928	0.0020	0.9286
U La1	12	0.0007	0.0005	0.7236	0.0007	1.0073
SrKa1	12	0.0354	0.0119	0.3353	0.0143	0.4215
Y Ka1	12	0.0025	0.0003	0.1259	0.0012	0.5029
ZrKa1	12	0.0132	0.0034	0.2548	0.0065	0.5163
NbKa1	12	0.0007	0.0001	0.1252	0.0001	0.1560
MoKa1	12	0.0008	0.0007	0.7992	0.0007	0.9038
RhKa1	12	0.0000	0.0000	--	--	--
SnKa1	12	0.0001	0.0000	0.2152	0.0001	0.6460
SbKa1	12	0.0001	0.0002	1.8468	0.0002	1.9240

**Table 49 Standard deviation, COV<sub>STD DEV</sub>, RMSD & COV<sub>RMSD</sub> values  
for No.50 NC\_CT1 RCA sample**

<b>No.50</b>						
Element	n	Average	Std Dev	COV <sub>STD DEV</sub>	RMSD	COV <sub>RMSD</sub>
NaKa1	12	0.0000	0.0000	--	--	--
MgKa1	12	0.0000	0.0000	--	--	--
AlKa1	12	0.4540	0.0552	0.1215	4.9975	11.4968
SiKa1	12	6.7317	0.4123	0.0612	23.0944	3.5833
P Ka1	12	0.0012	0.0018	1.4621	0.0599	51.3583
S Ka1	12	0.5866	0.0373	0.0636	0.4181	0.7445
K Ka1	12	0.2588	0.0651	0.2517	0.7649	3.0873
CaKa1	12	5.8792	0.9266	0.1576	2.2046	0.3917
BaLa1	12	0.0966	0.1521	1.5748	0.1578	1.7064
TiKa1	12	0.0701	0.0485	0.6923	0.2460	3.6645
V Ka1	12	0.0055	0.0053	0.9630	0.0071	1.3423
CrKa1	12	0.0060	0.0019	0.3164	0.0022	0.3785
MnKa1	12	0.0281	0.0029	0.1017	0.0262	0.9750
FeKa1	12	0.8296	0.5250	0.6328	2.3991	3.0205
BaLa1	12	0.5322	0.4369	0.8210	0.6511	1.2778
CoKa1	12	0.0065	0.0059	0.9100	0.0076	1.2258
NiKa1	12	0.0012	0.0009	0.7356	0.0012	1.0880
CuKa1	12	0.0032	0.0029	0.8987	0.0029	0.9434
ZnKa1	12	0.0025	0.0021	0.8182	0.0051	2.1013
AsKa1	12	0.0002	0.0001	0.4261	0.0002	1.0027
PbLa1	12	0.0011	0.0002	0.1877	0.0003	0.2999
ThLa1	12	0.0003	0.0001	0.1614	0.0004	1.3363
RbKa1	12	0.0007	0.0007	1.0290	0.0033	4.8445
U La1	12	0.0003	0.0003	1.2785	0.0003	1.2823
SrKa1	12	0.0108	0.0074	0.6830	0.0340	3.2950
Y Ka1	12	0.0018	0.0008	0.4520	0.0009	0.5238
ZrKa1	12	0.0072	0.0028	0.3922	0.0120	1.7593
NbKa1	12	0.0005	0.0001	0.1873	0.0001	0.2747
MoKa1	12	0.0082	0.0059	0.7168	0.0096	1.2161
RhKa1	12	0.0000	0.0000	--	0.0000	--
SnKa1	12	0.0002	0.0000	0.1813	0.0000	0.1818
SbKa1	12	0.0005	0.0005	1.0262	0.0006	1.3912

**Table 50 Standard deviation, COV<sub>STD DEV</sub>, RMSD & COV<sub>RMSD</sub> values  
for No.4 NC\_HW1**

No.4						
Element	n	Average	Std Dev	COV <sub>STD DEV</sub>	RMSD	COV <sub>RMSD</sub>
NaKa1	12	0.0000	0.0000	--	--	--
MgKa1	12	0.0000	0.0000	--	--	--
AlKa1	12	0.5891	0.2491	0.4228	5.7140	10.1315
SiKa1	12	4.5482	1.1262	0.2476	24.9239	5.7236
P Ka1	12	0.0117	0.0122	1.0432	0.0381	3.3960
S Ka1	12	0.5608	0.1114	0.1987	0.4341	0.8085
K Ka1	12	0.5808	0.1433	0.2468	2.2045	3.9647
CaKa1	12	4.4733	1.8633	0.4165	3.5171	0.8212
BaLa1	12	0.0480	0.1005	2.0942	0.1016	2.2112
TiKa1	12	0.0519	0.0373	0.7193	0.1100	2.2152
V Ka1	12	0.0033	0.0021	0.6284	0.0022	0.6923
CrKa1	12	0.0043	0.0009	0.2073	0.0013	0.3032
MnKa1	12	0.0248	0.0033	0.1343	0.0143	0.6020
FeKa1	12	0.9243	0.5198	0.5624	1.1602	1.3111
BaLa1	12	0.5153	0.1966	0.3815	0.4758	0.9644
CoKa1	12	0.0057	0.0020	0.3524	0.0057	1.0399
NiKa1	12	0.0012	0.0006	0.4822	0.0010	0.8936
CuKa1	12	0.0006	0.0008	1.3808	0.0010	1.8903
ZnKa1	12	0.0027	0.0018	0.6510	0.0040	1.5435
AsKa1	12	0.0003	0.0002	0.6157	0.0002	0.6309
PbLa1	12	0.0014	0.0004	0.3192	0.0007	0.5450
ThLa1	12	0.0006	0.0001	0.1825	0.0010	1.7279
RbKa1	12	0.0040	0.0022	0.5592	0.0074	1.9470
U La1	12	0.0002	0.0004	2.0780	0.0005	2.4791
SrKa1	12	0.0156	0.0068	0.4343	0.0186	1.2478
Y Ka1	12	0.0037	0.0016	0.4232	0.0018	0.5162
ZrKa1	12	0.0176	0.0083	0.4714	0.0090	0.5330
NbKa1	12	0.0010	0.0002	0.2040	0.0002	0.2174
MoKa1	12	0.0063	0.0028	0.4405	0.0064	1.0596
RhKa1	12	0.0000	0.0000	--	0.0000	--
SnKa1	12	0.0002	0.0000	0.2662	0.0001	0.3803
SbKa1	12	0.0001	0.0002	1.5108	0.0002	1.7459



**Table 51 Standard deviation, COV<sub>STD DEV</sub>, RMSD & COV<sub>RMSD</sub> values  
for No.12 NC\_HW1**

<b>No.12</b>						
Element	n	Average	Std Dev	COV <sub>STD DEV</sub>	RMSD	COV <sub>RMSD</sub>
NaKa1	12	0.0329	0.1140	3.4641	2.2399	71.111
MgKa1	12	0.0000	0.0000	--	--	--
AlKa1	12	0.8335	0.3452	0.4142	5.4746	6.8607
SiKa1	12	4.1852	0.8471	0.2024	25.2765	6.3081
P Ka1	12	0.0014	0.0047	3.4641	0.0469	36.2604
S Ka1	12	0.5012	0.0275	0.0549	0.3621	0.7547
K Ka1	12	0.6666	0.2041	0.3062	2.1235	3.3274
CaKa1	12	4.7039	1.0020	0.2130	2.9603	0.6573
BaLa1	12	0.0769	0.1656	2.1528	0.1585	2.1534
TiKa1	12	0.0645	0.0346	0.5359	0.0972	1.5726
V Ka1	12	0.0042	0.0033	0.7927	0.0032	0.7928
CrKa1	12	0.0054	0.0011	0.1966	0.0023	0.4332
MnKa1	12	0.0239	0.0020	0.0841	0.0150	0.6556
FeKa1	12	0.9277	0.4771	0.5142	1.1402	1.2836
BaLa1	12	0.1396	0.1336	0.9575	0.1419	1.0616
CoKa1	12	0.0008	0.0003	0.3664	0.0005	0.6756
NiKa1	12	0.0022	0.0007	0.3241	0.0007	0.3260
CuKa1	12	0.0043	0.0011	0.2607	0.0032	0.7761
ZnKa1	12	0.0062	0.0018	0.2962	0.0018	0.2974
AsKa1	12	0.0005	0.0001	0.2021	0.0002	0.4589
PbLa1	12	0.0012	0.0006	0.4754	0.0009	0.8537
ThLa1	12	0.0010	0.0001	0.0816	0.0006	0.6321
RbKa1	12	0.0102	0.0016	0.1520	0.0017	0.1772
U La1	12	0.0005	0.0006	1.2472	0.0006	1.2526
SrKa1	12	0.0392	0.0071	0.1819	0.0092	0.2458
Y Ka1	12	0.0023	0.0008	0.3285	0.0008	0.3603
ZrKa1	12	0.0188	0.0019	0.0993	0.0035	0.1924
NbKa1	12	0.0012	0.0001	0.0792	0.0002	0.1643
MoKa1	12	0.0005	0.0005	1.0360	0.0005	1.0380
RhKa1	12	0.0000	0.0000	--	0.0000	--
SnKa1	12	0.0002	0.0000	0.0783	0.0000	0.3132
SbKa1	12	0.0001	0.0002	2.1244	0.0002	2.2780

**Table 52 Standard deviation, COV<sub>STD DEV</sub>, RMSD & COV<sub>RMSD</sub> values  
for No.50 NC\_HW1**

<b>No.50</b>						
Element	n	Average	Std Dev	COV <sub>STD DEV</sub>	RMSD	COV <sub>RMSD</sub>
NaKa1	12	0.0000	0.0000	--	--	--
MgKa1	12	0.0000	0.0000	--	--	--
AlKa1	12	0.9614	0.1504	0.1565	5.3386	5.7999
SiKa1	12	4.8632	0.6149	0.1265	24.5926	5.2818
P Ka1	12	0.0005	0.0018	3.4070	0.0475	91.7218
S Ka1	12	0.5017	0.0218	0.0434	0.3623	0.7542
K Ka1	12	0.9526	0.2054	0.2156	1.8389	2.0162
CaKa1	12	5.1282	0.5817	0.1134	2.4406	0.4971
BaLa1	12	0.0027	0.0051	1.8556	0.0780	29.8666
TiKa1	12	0.0883	0.0132	0.1491	0.0687	0.8129
V Ka1	12	0.0063	0.0038	0.6118	0.0042	0.7013
CrKa1	12	0.0052	0.0008	0.1620	0.0019	0.3889
MnKa1	12	0.0240	0.0009	0.0383	0.0148	0.6446
FeKa1	12	1.3025	0.1909	0.1466	0.6944	0.5568
BaLa1	12	0.5555	0.4205	0.7570	0.6243	1.1739
CoKa1	12	0.0075	0.0060	0.8086	0.0092	1.2815
NiKa1	12	0.0012	0.0008	0.6290	0.0011	0.9683
CuKa1	12	0.0023	0.0029	1.2502	0.0030	1.3356
ZnKa1	12	0.0026	0.0018	0.6891	0.0041	1.6531
AsKa1	12	0.0005	0.0008	1.5650	0.0007	1.6134
PbLa1	12	0.0015	0.0003	0.2331	0.0006	0.4132
ThLa1	12	0.0008	0.0003	0.3258	0.0008	1.0389
RbKa1	12	0.0060	0.0054	0.9016	0.0073	1.2696
U La1	12	0.0004	0.0012	2.8189	0.0011	2.8197
SrKa1	12	0.0240	0.0159	0.6630	0.0177	0.7690
Y Ka1	12	0.0010	0.0011	1.0829	0.0020	1.9905
ZrKa1	12	0.0112	0.0051	0.4529	0.0116	1.0848
NbKa1	12	0.0010	0.0002	0.2449	0.0002	0.2457
MoKa1	12	0.0069	0.0063	0.9085	0.0088	1.3294
RhKa1	12	0.0000	0.0000	--	0.0000	--
SnKa1	12	0.0002	0.0000	0.1648	0.0000	0.1650
SbKa1	12	0.0004	0.0004	0.9470	0.0006	1.3714

**Table 53 Standard deviation, COV<sub>STD DEV</sub>, RMSD & COV<sub>RMSD</sub> values  
for No.4 NC\_CT2**

<b>No.4</b>						
Element	n	Average	Std Dev	COV <sub>STD DEV</sub>	RMSD	COV <sub>RMSD</sub>
NaKa1	12	0.2808	0.2053	0.7309	0.2746	1.0213
MgKa1	12	0.0000	0.0000	--	--	--
AlKa1	12	0.0000	0.0000	--	--	--
SiKa1	12	2.3525	0.6596	0.2804	7.7233	3.4290
P Ka1	12	0.0188	0.0191	1.0134	0.1265	7.0253
S Ka1	12	0.2613	0.0465	0.1780	0.0679	0.2715
K Ka1	12	0.1108	0.0497	0.4487	0.0668	0.6302
CaKa1	12	13.3876	2.2308	0.1666	17.1918	1.3413
BaLa1	12	0.0000	0.0000	--	--	--
TiKa1	12	0.0192	0.0113	0.5858	0.0364	1.9762
V Ka1	12	0.0049	0.0010	0.2074	0.0030	0.6313
CrKa1	12	0.0023	0.0007	0.2875	0.0066	2.9424
MnKa1	12	0.0215	0.0006	0.0284	0.0095	0.4645
FeKa1	12	0.2938	0.2358	0.8024	0.3930	1.3968
BaLa1	12	0.2577	0.2373	0.9207	0.3393	1.3749
CoKa1	12	0.0022	0.0011	0.4712	0.0021	1.0008
NiKa1	12	0.0021	0.0004	0.1780	0.0007	0.3318
CuKa1	12	0.0038	0.0064	1.6916	0.0069	1.9111
ZnKa1	12	0.0031	0.0019	0.6285	0.0037	1.2832
AsKa1	12	0.0003	0.0001	0.3965	0.0001	0.4295
PbLa1	12	0.0010	0.0003	0.2795	0.0006	0.6143
ThLa1	12	0.0003	0.0000	0.0985	0.0001	0.4792
RbKa1	12	0.0005	0.0004	0.7541	0.0004	0.7807
U La1	12	0.0005	0.0004	0.9209	0.0005	1.0197
SrKa1	12	0.0404	0.0089	0.2194	0.0096	0.2476
Y Ka1	12	0.0019	0.0002	0.1212	0.0014	0.7855
ZrKa1	12	0.0097	0.0022	0.2222	0.0022	0.2403
NbKa1	12	0.0004	0.0001	0.2270	0.0003	0.6057
MoKa1	12	0.0013	0.0011	0.8051	0.0016	1.2517
RhKa1	12	0.0000	0.0000	--	0.0000	--
SnKa1	12	0.0002	0.0000	0.1489		0.0000
SbKa1	12	0.0002	0.0003	1.2734	0.0003	1.5587

**Table 54 Standard deviation, COV<sub>STD DEV</sub>, RMSD & COV<sub>RMSD</sub> values for No.12 NC\_CT2**

No.12						
Element	n	Average	Std Dev	COV <sub>STD DEV</sub>	RMSD	COV <sub>RMSD</sub>
NaKa1	12	0.2490	0.1717	0.6894	0.2294	0.9621
MgKa1	12	0.0000	0.0000	--	--	--
AlKa1	12	0.0042	0.0146	3.4641	0.5517	136.7464
SiKa1	12	2.2261	0.2591	0.1164	7.8278	3.6727
P Ka1	12	0.0091	0.0156	1.7084	0.1357	15.5643
S Ka1	12	0.2855	0.0969	0.3394	0.1196	0.4376
K Ka1	12	0.1468	0.0352	0.2395	0.0354	0.2517
CaKa1	12	14.0301	2.8714	0.2047	16.6448	1.2391
BaLa1	12	0.0287	0.0828	2.8895	0.0817	2.9774
TiKa1	12	0.0198	0.0132	0.6648	0.0364	1.9208
V Ka1	12	0.0038	0.0015	0.3983	0.0022	0.6082
CrKa1	12	0.0025	0.0006	0.2536	0.0064	2.7024
MnKa1	12	0.0226	0.0022	0.0976	0.0086	0.3968
FeKa1	12	0.3408	0.2304	0.6759	0.3523	1.0797
BaLa1	12	0.3253	0.2937	0.9029	0.4256	1.3667
CoKa1	12	0.0029	0.0009	0.3207	0.0027	0.9759
NiKa1	12	0.0026	0.0009	0.3370	0.0013	0.5389
CuKa1	12	0.0049	0.0024	0.4900	0.0049	1.0466
ZnKa1	12	0.0006	0.0007	1.1718	0.0057	9.6229
AsKa1	12	0.0002	0.0000	0.1964	0.0002	0.9974
PbLa1	12	0.0010	0.0004	0.3417	0.0007	0.6559
ThLa1	12	0.0003	0.0000	0.1218	0.0001	0.5276
RbKa1	12	0.0004	0.0005	1.0493	0.0005	1.1681
U La1	12	0.0004	0.0004	0.9619	0.0004	1.0308
SrKa1	12	0.0358	0.0093	0.2589	0.0089	0.2590
Y Ka1	12	0.0020	0.0003	0.1676	0.0015	0.8108
ZrKa1	12	0.0136	0.0050	0.3647	0.0056	0.4321
NbKa1	12	0.0005	0.0001	0.1951	0.0003	0.6728
MoKa1	12	0.0022	0.0019	0.8829	0.0028	1.3282
RhKa1	12	0.0000	0.0000	--	0.0000	--
SnKa1	12	0.0002	0.0000	0.1387	--	0.0000
SbKa1	12	0.0000	0.0001	3.0968	0.0001	3.1229

**Table 55 Standard deviation, COV<sub>STD DEV</sub>, RMSD & COV<sub>RMSD</sub> values  
for No.50 NC\_CT2**

<b>No.50</b>						
Element	n	Average	Std Dev	COV <sub>STD DEV</sub>	RMSD	COV <sub>RMSD</sub>
NaKa1	12	0.1556	0.0473	0.3038	0.0805	0.5404
MgKa1	12	0.0000	0.0000	--	--	--
AlKa1	12	0.0084	0.0290	3.4641	0.5480	68.2674
SiKa1	12	3.0400	0.4598	0.1513	7.0237	2.4131
P Ka1	12	0.0000	0.0000	--	--	--
S Ka1	12	0.3591	0.0523	0.1456	0.1573	0.4574
K Ka1	12	0.1474	0.0232	0.1572	0.0245	0.1732
CaKa1	12	13.0233	1.2125	0.0931	17.4615	1.4004
BaLa1	12	0.0103	0.0358	3.4641	0.0343	3.4669
TiKa1	12	0.0325	0.0152	0.4664	0.0259	0.8329
V Ka1	12	0.0054	0.0023	0.4194	0.0039	0.7617
CrKa1	12	0.0034	0.0007	0.2123	0.0055	1.6675
MnKa1	12	0.0224	0.0005	0.0220	0.0086	0.4007
FeKa1	12	0.4266	0.1867	0.4375	0.2600	0.6366
BaLa1	12	0.1658	0.0936	0.5648	0.1834	1.1557
CoKa1	12	0.0028	0.0017	0.6246	0.0029	1.1071
NiKa1	12	0.0018	0.0005	0.2933	0.0006	0.3434
CuKa1	12	0.0011	0.0010	0.8631	0.0011	1.0096
ZnKa1	12	0.0025	0.0031	1.2294	0.0048	1.9956
AsKa1	12	0.0002	0.0001	0.5851	0.0002	0.7347
PbLa1	12	0.0011	0.0003	0.2890	0.0007	0.6505
ThLa1	12	0.0003	0.0000	0.0891	0.0002	0.5695
RbKa1	12	0.0005	0.0006	1.1031	0.0006	1.1245
U La1	12	0.0005	0.0006	1.1231	0.0006	1.2138
SrKa1	12	0.0290	0.0065	0.2251	0.0094	0.3387
Y Ka1	12	0.0017	0.0004	0.2281	0.0013	0.7891
ZrKa1	12	0.0093	0.0021	0.2204	0.0023	0.2619
NbKa1	12	0.0005	0.0001	0.1174	0.0004	0.6735
MoKa1	12	0.0031	0.0032	1.0465	0.0043	1.4523
RhKa1	12	0.0000	0.0000	--	0.0000	--
SnKa1	12	0.0002	0.0000	0.1163		0.0000
SbKa1	12	0.0003	0.0004	1.4284	0.0005	1.7143

## **APPENDIX C. RECOMMENDED TEST METHOD WITH PHXRF**

### **I. Scope**

This test method determines the chemical characteristics of recycled concrete aggregates (RCA) using PHXRF. The test method includes a series of procedures for sampling, determination of physical properties and chemical characterization of the aggregates, and estimation of the mortar content and potential contaminant contents using the PHXRF measurements.

### **II. Sampling**

Care should be taken during sampling to ensure that representative RCA material is selected from the stockpile. The sampling procedure should ensure the sample selected for testing is representative of the total material to be represented by the testing. To obtain samples, the ASTM D75, “Standard Practice for Sampling Aggregates” standard can be followed for guidance. This standard describes the procedure to obtain samples from different sources such as (1) stockpiles, (2) conveyor belts, (3) bins or belt discharges, and (4) roadway.

### **III. Physical Characterization tests**

The RCA samples obtained should undergo physical characterization tests, including sieve analysis (ASTM C136/C136M-14), density, relative density (specific gravity), absorption (ASTM C 127), and bulk density and voids in aggregates (ASTM C 29/C 29 M). These preliminary tests of the RCA assist in mixture design and proportioning so that workable, durable concrete with adequate mechanical properties can be produced (PCA 2019).

### **IV. Determination of mortar content using the Thermal Shock Method**

*Apparatus-* The apparatus required for this test includes:

- standard sieves of sizes 1 inch,  $\frac{3}{4}$  inch,  $\frac{1}{2}$  inch,  $\frac{3}{8}$  inch, and No. 4
- a furnace (with a minimum volume of 0.115 cubic feet and capable of heating to 1200°F
- a jar mill with cylindrical alumina grinding media of sizes 13/16” x 13/16”.

A representative sample of coarse RCA weighing 500g, retained on the No. 4 sieve and above, shall be prepared after the removal of any contaminants like brick, metal, wood, and asphalt from the sample.

The residual mortar content of the bulk sample of RCA should be determined using the Thermal Shock Method as described in Section 3.3.4 to separate the mortar and aggregate and calculate the RMC % for No. 67 gradation.

The RMC % can be calculated using the equation as follows:

$$RMC (\%) = \frac{\text{Mass of material passed \#4 sieve}}{\text{Total mass}} \times 100\% \quad (\text{Eq. 24})$$

The grinding time and heating temperature should be carefully evaluated for the sample under consideration. The objective behind the selection of both the parameters should be based on selecting the optimal temperature and grinding time which results in the complete removal of residual mortar.

#### V. PHXRF sample preparation and testing procedure

*Apparatus-* The apparatus for this test procedure includes:

- a PHXRF
- vacuum pump
- desktop stand
- sample cups
- mylar film
- desktop computer

A representative sample weighing 10 kgs shall be sieved through sieve sizes 1 inch, ¾ inch, ½ inch, 3/8 inch, No. 4, No. 12, and No. 50. The portion of the sample retained on sieve sizes No. 4, No. 12, and No. 50 should be set aside for PHXRF analysis.

The selected samples shall be placed in sample cups that have a depth of at least 10 mm to mitigate the inaccuracies caused due to the surface thickness phenomenon.

Secure the sample cups with a mylar film and divide the sample cup into four quadrants. Place the sample cup upside down on the sample table such that it rests on the nose of the PHXRF device. Following the PHXRF manufacturer's instructions, select an appropriate calibration file (such as 'Mudrock' for the Bruker Tracer device) that is capable of detecting and quantifying elements present in concrete aggregates.

If an appropriate PHXRF manufacturer's calibration file is unavailable, develop your own calibration file by preparing a fresh reference sample or augment an existing calibration file by adding additional reference samples relevant to the existing file. The Artax software can be used for augmenting or building a new calibration file. Once the device is set up and the calibration file is ready, take three measurements for each sample quadrant using the quadrant scanning technique (described in Section 4.3.3). Calculate the average of 12 readings for each elemental concentration.

The scanning duration for the major & trace element analysis should be as per the calibration file provided by the manufacturer. For Bruker's Mudrock calibration, the recommended scan duration is 180 and 60 seconds for major and trace elements, respectively. Use a vacuum for major element analysis if recommended by the manufacturer.

## 6. Whole Rock Analysis

The purpose of this section is to provide instructions for developing a reference sample for the validation and assessment of the accuracy of the PHXRF results. The control sample must be prepared for each individual RCA sample under consideration. To prepare the reference sample, the mortar and aggregate should be separated, and the RMC by percent weight should be determined using the Thermal Shock Method.

Once separated, a composite sample should be developed according to the computed RMC percent weight value. The weight distribution of the reference sample should be: X% of the total weight of the sample + (100-X)% of total weight of the sample.

Use the whole rock analysis technique to obtain measurements of major and trace elements present in the sample. Also, test the separated mortar and aggregate from the Thermal Shock Method separately using the PHXRF.

## 7. Statistical Analysis

7.1 After obtaining the measurements from PHXRF and whole-rock analysis, run the ANOVA test to test statistical significance between the particle sizes of the same sample and across samples of the same size. Compute statistical parameters including standard deviation, COV, RMSD &  $COV_{RMSD}$ .



Plot the RMSD vs. size graph to observe a trend between both the parameters. The goal should be to identify a decreasing trend of RMSD value with a decrease in particle size. The particle size with the lowest RMSD indicates high accuracy.

To make an accuracy comparison, use regression analysis and create a size-based regression model for each element of all the samples tested with whole rock analysis values and PHXRF values. Observe the  $R^2$  values for each size. An  $R^2$  value closer to 1 would suggest a stronger correlation between the whole rock analysis and PHXRF results, thereby showing higher accuracy. Based on the  $r^2$  values for all the major and trace elements, select the best particle size and use the regression equation for that particle size to compute the predicted values for all elements.

#### VIII. Mortar Content

To predict the mortar content of the samples, using stepwise regression analysis.

Take the mortar content computed from the Thermal Shock Method as the response variables and the major and trace elements as the predictor variables. Use statistical software to perform a stepwise regression and obtain the model equation for each size.

Input the values of variables in the model equation to get the predicted values of mortar for each size. Compare the % difference between the true values of mortar and the predicted ones to determine the best predictor of mortar content based on size.

## APPENDIX D. USE OF THE MIXTURE DESIGN NOMOGRAPH

Figure 71 below presents an example of using the developed nomograph to determine the concrete mixture design with RCA of NE\_CT2-NE\_RS, with the target strength of 4,500 psi. As shown in the figure, the first nomograph can be used to determine  $w/c$ , which in this case is 0.38, then the second nomograph can be used to obtain  $a/c$ , which in this case is 4.30, and finally, the third nomograph can be used to detect cement content, which in this case is 655 pcy.

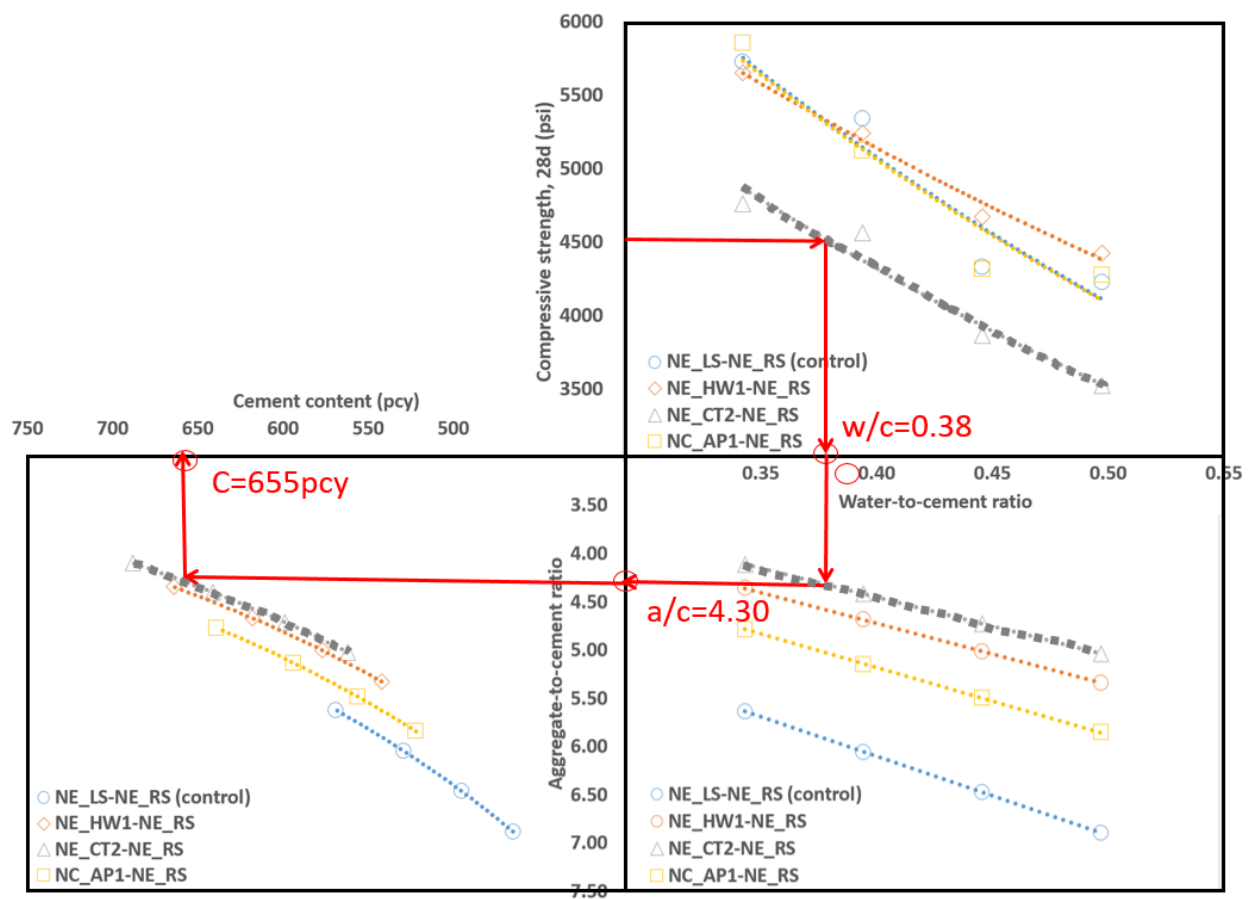


Figure 70 Example of utilizing the developed nomograph